

Using NOMOS measurements to assess improvements of ECAC Doc. 29 aircraft noise calculations

by R.P.F. Koster



Using NOMOS measurements to assess improvements of ECAC Doc. 29 aircraft noise calculations

by

R.P.F. Koster

to obtain the degree of Master of Science
at the Delft University of Technology,
to be defended publicly on Friday January 24, 2020 at 14:00.

Student number: 4147847
Project duration: September 1, 2018 – January 24, 2020
Thesis committee: Prof. dr. D.G. Simons, TU Delft
Dr. ir. M. Snellen, TU Delft, supervisor
Dr. ir. J. Ellerbroek, TU Delft

An electronic version of this thesis is available at <http://repository.tudelft.nl/>.

Abstract

The amount of air traffic worldwide is increasing, with an adverse effect on aircraft noise in the vicinity of airports as a result. Measurements and calculations have complementary benefits and limitations for the assessment of aircraft noise. A common method for the calculation of aircraft noise is ECAC Doc. 29. Various improvements of this method have been developed and studied in the past. However, research often lacks large numbers of measurements to validate these findings. The current study examined the effect of ECAC Doc. 29 model improvements on the differences between measured and calculated aircraft noise levels. The two improvements addressed in this research are: (1) The use of actual instead of standard meteorological conditions and (2) the use of derived flight performance instead of standard flight performance profiles. The calculated results have been compared with NOMOS measurements, the network of unattended microphones around Amsterdam Airport Schiphol. Using 151,108 flights and 385,001 NOMOS measurements, it was found that the difference between measurement and calculation depends on type of operation, aircraft type, and position of the microphone. The use of actual meteorological conditions showed the ability to reduce variability due to temperature, relative humidity, and pressure. The use of derived flight performance showed the ability to reduce variability due to wind up to 8 m/s. However, the absolute difference between measurements and calculations did not decrease for both improvements. Additionally, the aircraft substitution corrections were assessed. The substitution corrections based on ICAO type code showed smaller differences between measurements and calculations compared to the corrections based on aircraft configuration. It is suggested to study the substitution corrections further in the future. Moreover, it is advised to make use of the advancements in air traffic operations research for noise calculations based on derived flight performance.

Keywords

aircraft noise, noise modelling, noise calculations, noise monitoring, noise measurements, uncertainty, flight performance estimation

Preface

Back in 2017, Eric Dammeijer and I founded AerLabs, a software development company with a focus on the aviation industry. The first product that we built was Echo, our ECAC Doc. 29 model. During the development of Echo, I had the opportunity to speak to many industry experts and their challenges related to aircraft noise modelling. One of the key challenges was the societal and political debate about the use of measurements and the differences between calculations and measurements. Knowing the challenges that would lie ahead, I was convinced that it is possible to contribute to this discussion in a positive way. This belief drove the research that resulted in this report.

This report addresses the differences between measurements and calculations of aircraft noise. Despite the fact that a societal debate triggered the research, this report focuses on readers with a technical background and a basic knowledge of aviation and acoustics. By including a brief explanation of ECAC Doc. 29, prior knowledge is not required, but it is safe to say that it will make the read easier.

A wide range of people contributed to my research in one way or another. Above all, I would like to thank my TU Delft supervisor Mirjam Snellen for her scientific knowledge on aircraft noise and her guidance throughout the project. During regular meetings she was always open to my ideas, while using her expertise and critical thinking to provide me with the feedback to improve my research. In that light I would also like to thank Dick Simons for his contribution to my scientific understanding of aircraft noise with the courses he thought, in addition to the critical reviews on my work.

A special thanks is there for Wouter Dalmeijer, who opened up Amsterdam Airport Schiphol to me. Not only did he make it possible to use their data, he also organized so-called Schiphol Tuesdays for all students working with NOMOS data. During these Tuesdays, I had access to their expertise in noise and policy assessments. I look back at a lot of informative and fun Tuesdays. Besides all the colleagues at Amsterdam Airport Schiphol, I would also like to thank Davey Hooijmeijer, a fellow thesis student. All the hours we spent talking about aircraft noise (among other things) really contributed to my enthusiasm for the topic.

I would also like to thank To70 for making their ADS-B data available for me during this research. In particular, I would like to thank Maarten Tielrooij in his assistance with the ADS-B data, providing me with a head start on ADS-B data usage and interpretation. Furthermore, I would like to thank Kjeld Vinkx from To70 for sharing his expertise and insights on aircraft noise with me, his ideas were used as the starting point of my research.

I would like to thank Junzi Sun (TU Delft) for his effort of applying his weight estimation method to my data. Although it was not used in this research eventually, through this effort we both gained the insight that his research could be used for aircraft noise modelling in the future.

Because AerLabs introduced me to the topic of aircraft noise modelling, I would like to thank everyone that contributed to the successes we have booked so far with AerLabs. It is with great pride and joy that I am able to continue this adventurous journey.

Thanks to my family and friends for supporting me during my thesis. Their support really provided me with positive energy and the necessary distraction from time to time. In particular, I would like to thank my friend and colleague Richard Janssen, with whom I could discuss literally all aspects of my research. Besides that he was particularly helpful by reviewing my work. Furthermore, I would also like to thank my friend Joost Remmers for his review of the statistics. Last, but certainly not least, I would like to thank Soudry Staats, the love of my life, for both the mental support during the project and her contribution to my academic writing. It is very much appreciated that she has always been there for me to discuss the challenges I encountered during my research.

*R.P.F. Koster
Delft, January 2020*

Contents

1	Introduction	1
1.1	Calculations and measurements of aircraft noise	1
1.2	Factors influencing aircraft noise	2
1.3	Current state-of-art of long-term average aircraft noise modelling	2
1.4	Research gap	3
1.5	Research objective	3
1.6	Thesis outline	5
2	Model setup	7
2.1	ECAC Doc. 29	7
2.1.1	Framework.	7
2.1.2	Flight path segments.	9
2.1.3	Basic segment noise level	9
2.1.4	Engine installation effect.	10
2.1.5	Lateral attenuation correction	11
2.1.6	Duration correction	12
2.1.7	Noise fraction correction.	12
2.1.8	Start of roll correction	12
2.1.9	Verification of ECAC Doc. 29.	13
2.2	Meteorological adjustment	14
2.2.1	Acoustic impedance correction	14
2.2.2	Correction for non-reference atmospheric absorption	16
2.2.3	Verification of meteorological adjustment	17
2.3	Aircraft substitution.	18
2.3.1	Substitution used for this research	18
2.3.2	The effect of the aircraft substitution correction	19
2.4	Flight performance	20
2.4.1	Aircraft weight	20
2.4.2	Standard flight performance	20
2.4.3	Derived flight performance	23
2.4.4	Verification of derived flight performance	24
3	Description of data used	25
3.1	NOMOS noise measurement	25
3.1.1	NOMOS characteristics	25
3.1.2	Properties of available NOMOS data	27
3.1.3	Measurement data used for this research	29
3.2	ADS-B flight path data	30
3.2.1	Ground track.	30
3.2.2	Altitude and ground speed.	30
3.2.3	Missing & ignored data.	32
3.3	Meteorological data.	32
3.4	Data processing.	33
3.4.1	Correlation of flight data	33
4	Results	35
4.1	The baseline method	35
4.1.1	Definition of long-term average noise	37
4.1.2	Uncertainty of long-term average noise	38
4.1.3	Separated by aircraft type	38
4.1.4	Separated by NMT	40

4.2	Effect of meteorological adjustment	42
4.2.1	Pure-tone absorption calculation	43
4.2.2	Statistics and pattern.	49
4.3	Effect of speed and thrust adjustment.	50
4.4	Effect of aircraft substitution correction.	53
5	Discussion	57
5.1	Comparisons within baseline method results	57
5.2	Effect of meteorological adjustment	60
5.3	Effect of speed and thrust adjustment.	60
5.4	Effect of aircraft substitution	64
6	Conclusions & Recommendations	65
6.1	Conclusions.	65
6.2	Recommendations	65
A	The challenge of comparing measurements and aircraft noise calculations	67
B	Calculation procedure	69
C	Statistic description of the dataset	71
D	AerLabs Echo verification	77
D.1	Receptor results.	77
D.2	Grid results	77
E	Distribution of the noise levels	79
F	Meteorological adjustment	85
F1	Actual meteorological conditions	85
F2	Wind	85
G	Derivation of BADA force balance equation	91
H	Uncertainty quantification of long-term average noise levels	93
	Bibliography	95

Nomenclature

List of Acronyms

ADS-B	Automatic dependent surveillance-broadcast
AEDT	Aviation Environmental Design Tool
ANOMS	Aircraft Noise Monitoring and Management
ANP	Aircraft noise and performance
BADA	Base of Aircraft Data
ECAC	European Civil Aviation Conference
ICAO	International Civil Aviation Organization
INM	Integrated Noise Model
KNMI	Royal Netherlands Meteorological Institute
NLR	Royal Netherlands Aerospace Centre
NMT	Noise monitoring terminal
NOMOS	Noise monitoring system
NPD	Noise-power-distance
SAE	Society of Automotive Engineers
SEL	Sound exposure level

List of Symbols

α	atmospheric attenuation coefficient	$\frac{dB}{m}$
$\Delta L_{AE,c-m} = L_{AE,calculation} - L_{AE,measurement}$	see also L_{AE} and ΔL_{c-m}	dB
$\Delta L_{Amax,c-m} = L_{Amax,calculation} - L_{Amax,measurement}$	see also $L_{A,max}$ and ΔL_{c-m}	dB
ΔL_{c-m}	difference between aircraft noise calculation and noise measurement	dB
δ	atmospheric attenuation	dB
ϵ	bank angle	°
$\epsilon_{calculation}$	calculation error	dB
$\epsilon_{measurement}$	measurement error	dB
d	distance	$\frac{dB}{m}$
L_E	exposure noise level	dB
$L_{A,max}$	maximum A-weighted noise level	dB
$L_{AE,calculation}$	calculated sound exposure level	dB
$L_{AE,measurement}$	measured sound exposure level	dB

L_{AE}	sound exposure level		$dB(A)$
$L_{aircraft}$	aircraft noise		$dB(A)$
$L_{Amax,calculation}$	calculated maximum A-weighted noise level		$dB(A)$
$L_{Amax,measurement}$	measured maximum A-weighted noise level		$dB(A)$
L_{DEN}	day-evening-night level		$dB(A)$
L_{eq}	equivalent exposure noise level		dB
L_{max}	maximum noise level		dB
$L_{measurement}$	measured noise		$dB(A)$
P	thrust setting	unit depending on aircraft type	
V	ground speed		m/s
x	x-coordinate		m
y	y-coordinate		m
z	z-coordinate		m



Introduction

The amount of air traffic worldwide has been increasing over the last decades, with an adverse effect on aircraft noise in the vicinity of airports as a result [3]. Both measurements and calculations can be used to determine how much noise is produced by aircraft. However, both methods have restrictions, making it difficult to determine which approach best represents the real aircraft noise and should therefore be used to assess aircraft noise.

1.1. Calculations and measurements of aircraft noise

From the resident's point of view, measurements are often considered to be the best means to show the noise produced by aircraft [27]. Measurements are perceived as simple, transparent, and more objective compared to calculations. From an acoustic perspective this is correct¹. Measuring is a trustworthy way to determine the total noise level with a known uncertainty at a specific location at a certain moment in time. In contrast, the steps to undertake for a noise calculation might be so complex that it leaves people wondering how noise levels came to be. Furthermore, human factors (such as errors in the implementation) might also contribute to errors in results. This is also why measurements are often used to validate the results of calculations. Thus, measuring has many beneficial properties, though stating that measurements are always better than calculations is overly simplified.

Although measuring has its benefits, it is definitely not perfect for the assessment of aircraft noise. In this regard, three limitations can be identified. First, measurements can only take place on locations where there is a microphone. When assessments in a large geographical area need to be made, it can be very expensive to sufficiently cover the area of interest. Second, measurements can only be used to evaluate current and historic noise. This is a problem because the industry is also interested in aircraft noise predictions, such as to study the effect of a new route or changing policy regarding aircraft noise management. An example of such an effort can be found in the yearly utilization forecast of Schiphol [8]. The last - but certainly not the least - downside of measuring is the fact that a single microphone will detect the total noise, which also includes the noise from other sources [29]. These limitations do not apply to noise calculations. Thousands of geographical locations can be assessed with calculations, at the cost of computational resources only. Furthermore, the use of models allows us to make predictions of future noise levels, which are valuable for the design of noise abatement procedures. Lastly, with calculations we are certain that only aircraft noise is assessed and no additional sources.

So, for the assessment of aircraft noise both measurements and calculations have complementary benefits and limitations. In an ideal situation, there would be a perfect aircraft noise model and a sound level meter able to detect aircraft noise only. But since this does not exist, in practice we want both methods to be close enough to each other such that the differences are acceptable. This implies that on an individual flight level, the sound levels of both methods should be within the range where there is no perceived 'hearable' difference. For long-term average sound levels there is no established definition of acceptable. It has been identified before that there is a need for validation standards in the field of aircraft noise modelling [15].

¹when a certified sound level meter is used

1.2. Factors influencing aircraft noise

In order to understand and in the end reduce differences between measurements and calculations of aircraft noise, it is important to take into account several factors influencing aircraft noise. Factors to consider are: aircraft configuration, aircraft operation (e.g. flight path, speed, and thrust setting), and meteorological conditions.

Aircraft noise is strongly related to the characteristics of the aircraft itself. Larger aircraft often make more noise, because they require larger engines, larger wings and larger landing gears, all important noise sources of the aircraft. Furthermore, the noise characteristics of the aircraft are also affected by the type and location of engine(s).

The noise produced is also related to how the aircraft operates. Where and when the aircraft flies is important for the amount of noise produced by an aircraft. When the aircraft is closer, the received sound levels are higher. When the aircraft flies faster, the sound is emitted for a shorter period of time leading to lower received exposure sound levels. Next to aircraft speed, thrust² is also related to the noise production. Thrust is related to rotational speeds of the turbofan and jet exhaust speeds, which both produce noise. Using higher thrust settings will result in higher noise levels. Other operational factors influencing the noise of the aircraft range from the moment of gear-down at arrival, to the flap setting used for take-off.

Meteorological conditions also affect the performance of the aircraft. Accelerating an aircraft at take-off with tailwind requires more thrust, resulting in higher noise levels. Moreover, meteorological conditions impact how the noise travels through the atmosphere. For instance, the amount of noise absorbed by the atmosphere depends on the temperature, relative humidity, and pressure. Additionally, measurements of aircraft noise can be heavily influenced by meteorological conditions. For example, atmospheric turbulence caused by natural sources might induce pressure differences which can be observed as noise.

1.3. Current state-of-art of long-term average aircraft noise modelling

In the European Union, ECAC Doc. 29 is the legislated method for airport noise assessments [7]. ECAC Doc. 29 is a fully empirical method based on best-practices for the calculation of long-term average aircraft noise in the vicinity of airports. The 4th edition of ECAC Doc. 29 [13] is the current version of the method. ECAC Doc. 29 is not only used for legal compliance. Often, research regarding long-term average noise levels in the vicinity of airports is also based on ECAC Doc. 29 or similar methods such as ICAO Doc 9911 [21] or SAE AIR1845 [31].

In research, there have been efforts to improve the acoustic models used in ECAC Doc. 29 and similar methods. For example, Lau et al. developed a new start of takeoff-roll directivity pattern in 2015 [24], which was adopted in the last edition of ECAC Doc. 29. Furthermore, a new method for atmospheric absorption (SAE ARP5534 [33]) was adopted in the latest edition of ECAC Doc. 29. In this method, the absorption coefficient also depends on pressure, while the older method (SAE ARP866A) only included temperature and relative humidity. Before the introduction of SAE ARP5534, Arntzen et al. [4] researched the impact of meteorological adjustments and concluded that it has a significant effect on event noise levels, but no significant effect on long-term average noise levels. However, these results were not validated with measurements, therefore it is still unknown what the differences are between measurements and calculations. When models are compared with measurements, they often use a limited range of meteorological conditions. Examples of such research can be found in studies by Filippone et al. [16] and Hooijmeijer [19]. Both use only measurements close to meteorological conditions utilized for noise certification. This reduces the ability to generalise such studies, since the meteorological conditions at most airports are typically not close these certification conditions.

Not all research regarding ECAC Doc. 29 is meant to improve the acoustic components used in the method. Since the results of a calculation are often as good as the input, the construction of the flight path as input for the noise model has been studied by Op de Woert, a master of science student of Delft University of Technology in [28]. Op de Woert concluded that using equations of motion gives the best modelling results compared with other flight path construction methods. Unfortunately, the modelling results were only validated using a small sample size of 32 sound level measurements. Additionally, using fan rotational speed as input has been examined by Merino-Martínez et al. in [25]. In this research, the fan rotational speed was used to obtain the thrust setting of the aircraft along the flight path. It was found that for two aircraft types, the fan rotational speed explains up to 45% of the variability in the noise levels. However, in order to obtain

²“the force which moves an aircraft through the air” NASA Glenn Research Center

the fan rotational speed, audio recordings or flight recorder data are required, which are not always available or do not provide information along the whole trajectory.

Besides academic research on improving the model itself or the input, many airports perform noise assessments using both measurements and models because they are complementary. Unlike model validation studies, the measurements for long-term average noise level assessments are often obtained using unattended microphones. Using unattended microphones introduces the risk of falsely relating detected noise events to aircraft operations [5]. Examples of research using long-term average aircraft noise models and unattended microphones can be found in [9, 36, 41]. A limitation of the research by Veerbeek et al. [41] is the fact that not all measurement stations were used and only a limited number of aircraft types were assessed. Moreover, the studies by DeKoninck et al. [9] and Sari et al. [36] were based on long-term average noise levels only instead of single flight-events. This is useful to quantify the differences between the long-term average noise calculations and measurements, but makes it difficult to gain a better understanding of where these differences come from. Eventually, this understanding is required to improve the model.

1.4. Research gap

In spite of the fact that research on ECAC Doc. 29 has been performed in the past, it remains relevant for both academia and society to study ways to improve this best-practice. Previous research on differences between measurements and calculations of aircraft noise has several limitations. First, analyses are often based on small samples of sound level measurements only [28], a limited range of meteorological conditions [16, 19], and a limited number of aircraft types and measurement stations [41]. These characteristics restrict the ability to generalise the findings across different meteorological conditions, aircraft types, and locations. Second, other research that assessed the effect of meteorological conditions on noise levels did not even use measurements at all [4]. Third, most studies used long-term average noise levels instead of single flight events to assess differences between measurements and calculations [9, 36]. The analysis of individual noise events is necessary to get a better understanding of where the long-term average noise level differences between calculations and measurements come from. This is relevant for further improvement of calculations in order to create a more accurate estimation of aircraft noise. Therefore, the current study will investigate differences between measurements and calculations by using a large dataset of individual flight events as well as long-term average noise levels. The noise modelling of individual flights will address both the use of actual meteorological conditions as well as the path construction methods. In addition, all available microphones and aircraft types will be taken into account in the analyses.

1.5. Research objective

It is expected that ECAC Doc. 29 will remain the most important model for long-term average noise levels in the nearby future in Europe, therefore it is worth improving. The objective of this thesis is thus to make recommendations on how to improve calculations based on the difference between measurements and calculations of long-term aircraft noise, by analysing noise measurements and ECAC Doc. 29 calculations of a large number of single flight-events.

On the one hand side, this is done by evaluating the current best-practice with a model-measurement comparison, to gain a better understanding of the current modelling performance. The current practice is illustrated in Figure 1.1. On the other side, a selection of alterations are implemented and evaluated to make specific suggestions for improvement.

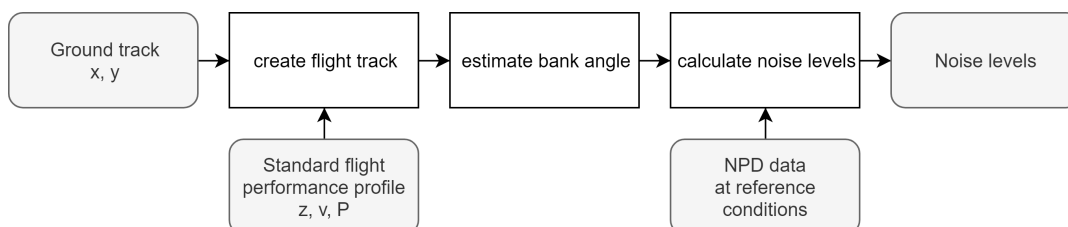


Figure 1.1: The calculation steps of the current practice.

The first improvement is made to the meteorological conditions used. The suggested practice for Amsterdam Airport Schiphol uses standard meteorological conditions in combination with SAE ARP5534 [18], while

this method could also be used to correct for the actual meteorological conditions as well. Additionally, in other studies the flyover noise measurements were conducted for meteorological conditions close to those defined for aircraft noise certification [16, 19], while this limits the amount of measurements that can be used and the ability to generalise the conclusions. In contrast, we will assess measurements at all meteorological conditions, because we want to get a better understanding of all the errors that remain present in the model when compared to measurements. Therefore it is key to use as many observations as possible to cover a wide range of meteorological conditions. The differences compared to the current practice are illustrated in bold in Figure 1.2.

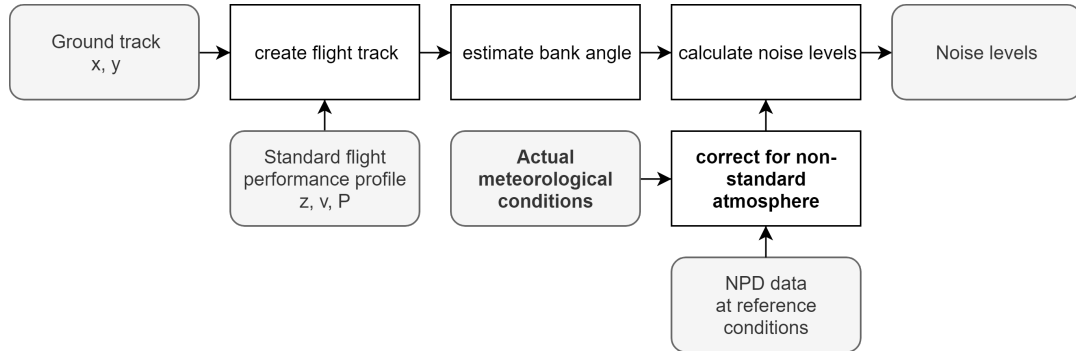


Figure 1.2: The calculation steps using actual meteorological conditions.

The second improvement is made to the flight performance used as input for the model. The effect of using flight performance derived from observed flight data has been researched before [28] using a limited set of measurements to validate the calculations. To overcome this limitation, this research will use a dataset with thousands of flights and even more measurements to compare with. This method is visualised in Figure 1.3, indicating the differences compared to the figure above in boldface.

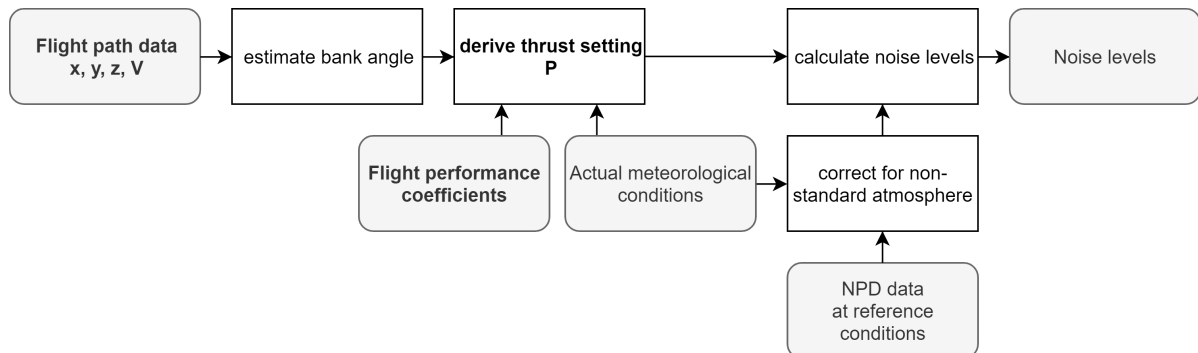


Figure 1.3: The calculation steps using derived flight performance.

Additionally, to make this research reproducible and to address the issue of transparency, ADS-B data and other publicly available data sources will be used as primary data source for this research.

To summarize, the following research question is defined: *What is the effect of ECAC Doc. 29 model improvements on the differences between measured and calculated aircraft noise levels?* How this research question will be answered is visualised in the flow diagram that can be found in Figure 1.4. Here it is shown that there are three sets of results, all making use of the same measurements but using a different combination of meteorological conditions and flight performance estimation method.

To our knowledge, this is the first study that strives to bridge the gap between calculations and measurements of aircraft noise by using a large number of single-event ECAC Doc. 29 calculations based on ADS-B data and measurements from all available unattended microphones around the airport. More specifically, NOMOS, the unattended network of microphones around Amsterdam Airport Schiphol was used for this research.

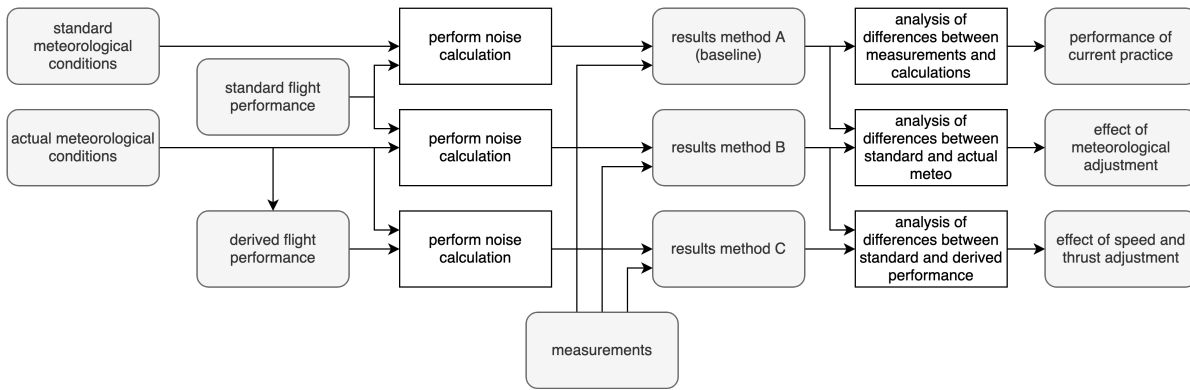


Figure 1.4: A flow diagram of the main steps performed within this research.

1.6. Thesis outline

Chapter 2 describes the calculation method. A number of relevant components of ECAC Doc. 29 will be addressed, in addition to a description of how the flight performance parameters are selected for each aircraft. Furthermore, the chapter also addresses the verification efforts of the model.

In chapter 3 it is described which data was available for this research and how it was used. In particular, it explains which measurement data were available and how they were used in the study. The limitations of the data and the assumptions made to conduct valuable comparisons are also addressed in this chapter.

In chapter 4, the results of this research are listed. The results will be further discussed in chapter 5. Finally, the study is concluded in chapter 6, highlighting the importance of this research. Additionally, this chapter provides recommendations for further research and future use of the model.

Accompanying this work is a detailed description of the calculation procedure, a derivation of the force-balance equation, a description of the long-term average uncertainty quantification, and various additional intersections of the results. These can be found in the appendices.

2

Model setup

The goal of this research is to study the differences between calculations and measurements of aircraft noise. In order to do this, a model is required to perform the aircraft noise calculations. The model used for this research is based on the 4th Edition of ECAC Doc. 29 - *Report on Standard Method of Computing Noise Contours around Civil Airports* [13].

This chapter provides a brief overview of this model and how it is implemented for this study in section 2.1. A number of relevant acoustic components of ECAC Doc. 29 will be addressed. In addition, a detailed description of the adjustment for non-standard meteorological conditions will be provided in section 2.2. How the aircraft noise performance data is selected is described in section 2.3. Finally, this chapter ends with how the flight performance is determined in section 2.4, addressing the two different methods used within this research.

2.1. ECAC Doc. 29

ECAC Doc. 29 is a fully empirical harmonized method, thus primarily based on measurements and reflecting the best-practice in aircraft noise modelling across ECAC member states. The first edition of ECAC Doc. 29 was published in 1986, while the current and 4th edition - the edition used in this research - was published in December 2016. Although the method describes the best-practices of the ECAC member states, the method is also adopted by ICAO in the second edition of ICAO Doc 9911 - *Recommended Method for Computing Noise Contours around Airports* [21, 30].

To prevent this report from being a direct copy of ECAC Doc. 29, only the high-level methodology and the various acoustic elements will be addressed. For detailed information, e.g. about the distances used for the NPD interpolation or a description of the segmentation method, one is referred to ECAC Doc. 29 [13].

To illustrate the concept of the method, all calculations are explained for a single observer. One can regard this observer as a microphone in three dimensional space, which we use to observe the noise induced by the aircraft. When calculating noise contours, one would typically include thousands of observers around the airport.

2.1.1. Framework

The calculation framework of ECAC Doc. 29 is based on SAE AIR1845 [31]. Within this framework, the noise of a flight is calculated as the cumulative effect of multiple straight segments, for which the noise levels are determined individually. The basic noise level of a segment is based on noise-power-distance (NPD) data. NPD data contains reference noise levels for a given noise level metric at tabulated power and distance combinations. How the NPD data is used is described in subsection 2.1.3.

There are two types of metrics identified in ECAC Doc. 29: exposure based metrics L_E (such as the sound exposure level and the effective perceived noise level) and maximum based metrics L_{max} (such as maximum A-weighted noise level and maximum tone corrected perceived noise level). Throughout this research, only the A-weighted noise levels will be used, because they are most commonly used for noise assessments around Amsterdam Airport Schiphol [8] and other metrics are not widely available in the measurement data (see also subsection 3.1.1). Therefore the maximum noise level L_{max} in this document is synonym for maximum A-weighted noise level $L_{A,max}$ and the exposure noise level L_E is synonym for the sound exposure level L_{AE} .

Both metrics use the unit dBA instead of dB to indicate the applied A-weighting. For maximum noise level metrics, the maximum noise level of the event $L_{A,max}$ is determined by the largest noise level of all segments as can be seen in Equation 2.1. For exposure noise level metrics, the event noise level L_{AE} is determined by calculating the energetic sum of all segment noise levels $L_{AE,seg}$, as can be seen in Equation 2.2.

$$L_{max} = \max\{L_{max,1}, \dots, L_{max,i}, \dots, L_{max,n_{segments}}\} \quad (2.1)$$

$$L_E = 10 \log_{10} \left(\sum_{i=1}^{n_{segments}} 10^{L_{E,i}/10} \right) \quad (2.2)$$

where i indicates the result of an individual segment, $L_{max,i}$ is the maximum noise level of a segment in dBA, $L_{E,i}$ is the exposure noise level of a segment in dBA, and $n_{segments}$ is the number of segments.

The segment noise level does not only depend on the aforementioned basic segment noise level. Additional corrections are applied based on aircraft and flight characteristics. These additional corrections are listed below, including a reference to the section with more information.

- Engine installation correction Δ_I (subsection 2.1.4) to account for the directivity due to engine location.
- Lateral attenuation correction Λ (see subsection 2.1.5) to account for ground surface reflections.
- Duration correction Δ_V (see subsection 2.1.6) to account for non-reference aircraft speeds.
- Noise fraction correction Δ_F (subsection 2.1.7): is applied to account for the finiteness of the segment.
- Start of roll correction Δ_{SOR} (see subsection 2.1.8) is applied to account for the directivity during the take-off ground roll.
- Acoustic impedance correction $\Delta_{impedance}$ (subsection 2.2.1) is applied to correct for non-reference characteristic acoustic impedance.
- Atmospheric absorption correction (see subsection 2.2.2) is applied to correct for non-reference noise level absorption in the atmosphere.

How segments determine the noise level of an individual flight, depends on the type of metric calculated. Besides the metric, the segment type also influences the acoustic corrections that should be applied. Two segment types are identified: airborne and ground roll segments. The equations for the airborne segment noise levels are shown in Equation 2.3 and Equation 2.4.

$$L_{max,seg} = L_{max,\infty}(P, d) + \Delta_I(\phi) - \Lambda(\beta, l) \quad (2.3)$$

$$L_{E,seg} = L_{E,\infty}(P, d) + \Delta_V + \Delta_I(\phi) - \Lambda(\beta, l) + \Delta_F \quad (2.4)$$

where $L_{max,\infty}(P, d)$ is the basic segment maximum noise level in dBA, $L_{E,\infty}(P, d)$ is the basic segment exposure noise level in dBA, $\Delta_I(\phi)$ is the engine installation correction in dBA, $\Lambda(\beta, l)$ is the lateral attenuation correction in dBA, Δ_V is the duration correction in dBA, and Δ_F is the noise fraction correction in dBA. Additionally there is also the start-of-roll correction Δ_{SOR} , however, this correction is only applied to ground-roll segments. To illustrate the effect the various corrections might have on the segment noise levels, the theoretical limits and typical values are provided in Table 2.1.

Table 2.1: Value ranges of the various exposure level corrections in ECAC Doc. 29 with the theoretical upper and lower limits and the typical values from ECAC Doc. 29 Volume 3 [13], also indicated with the minimum and maximum value. The results are based on sound exposure level calculations.

Correction	Theoretical Limits (dBA)	Typical Values (dBA)
$L_{E,\infty}(P, d)$	depending on NPD data	(40.62, 115.28)
$\Delta_I(\phi)$	(-3.0, 0.4)	(-3.0, 0.4)
$\Lambda(\beta, l)$	(0, 10.857)	(0, 10.849)
Δ_V	($-\infty$, ∞)	(-2.69, 12.40)
Δ_F	(-150, 0)	(-98.88, -0.03)
Δ_{SOR}	(-13.52, 1.96)	(-13.48, 1.09)
$\Delta_{impedance}$	($-\infty$, ∞)	0.0741

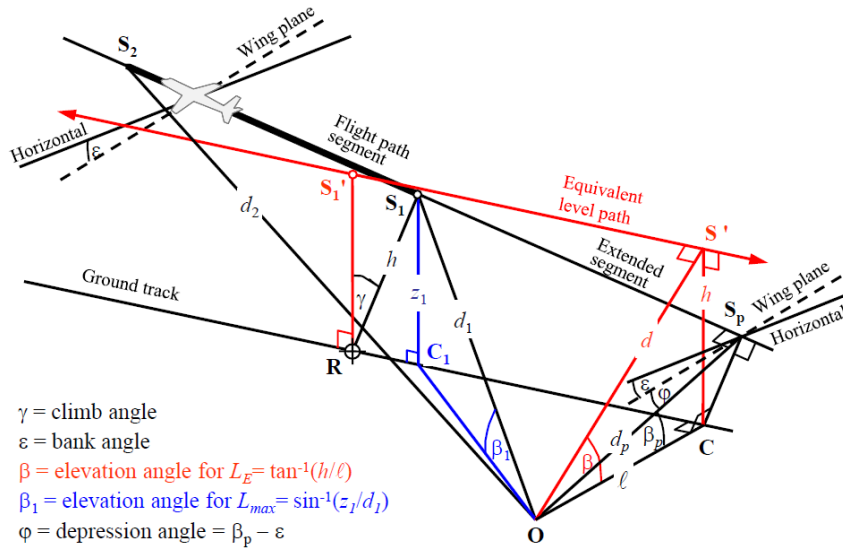


Figure 2.1: The geometry for observers (indicated in the figure with O) behind the segment, obtained from ECAC Doc. 29 [13].

2.1.2. Flight path segments

Flight path segments provide the basis for the noise calculations using ECAC Doc. 29 and are constructed from the flight path. A flight path is described by a number (n) of consecutive points. These points include x, y, z, V, P , and ε where x, y, z is the position of the aircraft, V is the ground speed of the aircraft, P is the thrust setting of the aircraft, and ε is the bank angle of the aircraft. From these points, $n - 1$ straight line segments can be made.

Although all segments are described with the aforementioned parameters, not all segments contribute to the event noise levels in the same way. A differentiation should be made between airborne segments and ground roll segments. These segment types have an effect on how geometry is defined, which acoustic corrections should be applied, and how acoustic corrections are defined. This report will only address the acoustic corrections, referring to [13] for more information about the geometric definitions and how they depend on the type of segments.

To illustrate the definition of a flight path segment and the complexity of the geometry definitions in three dimensional space, Figure 2.1 is included to show a number of parameter definitions. For example, the elevation angle β has three variants: the elevation angle for exposure-based noise levels β , the elevation angle for maximum-based noise levels β_1 , and the elevation angle for the depression angle β_p .

2.1.3. Basic segment noise level

The basic noise level of a segment is determined by interpolating the NPD data of the aircraft. An example of such NPD data can be found in Table 2.2. The noise levels are tabulated for each combination of power setting and distance. The NPD data represents the noise levels directly below a continuous, straight, steady, and level flight in reference atmosphere flying at 160 knots.

Table 2.2: The noise-power-distance (NPD) data for aircraft type A320-211 containing the reference sound exposure levels in dBA that should be used for arrivals. The noise levels L are provided for a combination of power setting P and distance d .

Power Setting P	L_{200ft}	L_{400ft}	L_{630ft}	L_{1000ft}	L_{2000ft}	L_{4000ft}	L_{6300ft}	$L_{10000ft}$	$L_{16000ft}$	$L_{25000ft}$
2700.0	96.6	90.5	87.5	84.2	78.9	72.8	68.2	62.9	56.8	50.3
6000.0	97.4	91.6	88.2	84.8	79.3	73.1	68.5	63.3	57.1	50.6

The value at a specific power setting and distance combination can be determined using a bilinear interpolation of the tabulated noise levels at neighbouring power settings and distances. A visualisation of this method can be found in in Figure 2.2. The equations for this procedure can be found in Equation 2.5 and Equation 2.6.

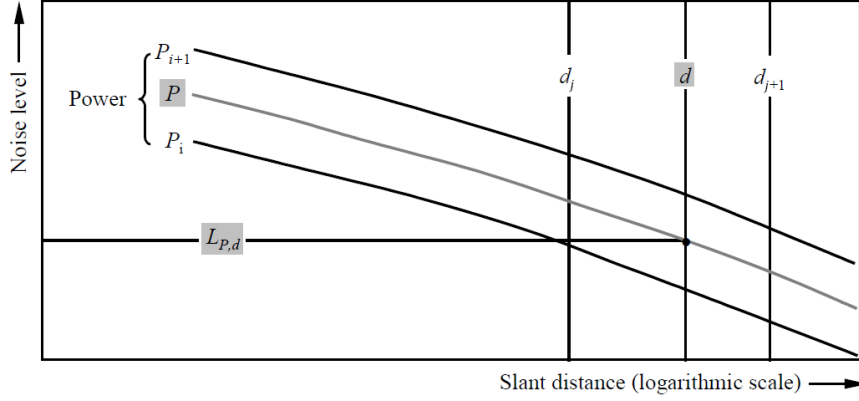


Figure 2.2: The interpolation of noise-power-distance data. The original was obtained from ECAC Doc. 29 [13], but modified for consistency within this report.

$$L_{\infty}(P, d) = \frac{1}{(P_{i+1} - P_i)(y_2 - y_1)} \begin{bmatrix} P_{i+1} - P & P - P_i \end{bmatrix} \begin{bmatrix} L_{P_i, d_j} & L_{P_i, d_{j+1}} \\ L_{P_{i+1}, d_j} & L_{P_{i+1}, d_{j+1}} \end{bmatrix} \begin{bmatrix} y_2 - y \\ y - y_1 \end{bmatrix} \quad (2.5)$$

$$y = \log_{10}(d), \quad y_1 = \log_{10}(d_j), \quad y_2 = \log_{10}(d_{j+1}) \quad \text{and} \quad P_i \leq P \leq P_{i+1} \quad \text{and} \quad d_j \leq d \leq d_{j+1} \quad (2.6)$$

where P and d are the power setting and distance for which the noise level should be determined, P_i and P_{i+1} are the tabulated power settings at i and $i + 1$, d_j and d_{j+1} are the tabulated distances at j and $j + 1$, $L_{\infty}(P, d)$ is the desired basic segment noise level in dBA, and L_{P_i, d_j} , $L_{P_i, d_{j+1}}$, L_{P_{i+1}, d_j} , and $L_{P_{i+1}, d_{j+1}}$ are the tabulated noise levels at the specified power settings and distances in dBA. For power-distance combinations beyond the range of the provided NPD table, the data can similarly be extrapolated [13].

2.1.4. Engine installation effect

An aircraft is not an acoustic point source. Aircraft noise is caused by multiple noise sources, which can be attributed to parts of the aircraft such as the airframe and the engines [26]. The noise of the aircraft is not the sum of its parts, because the noise radiated by individual parts interact with each other and with the many solid surfaces and aerodynamic flow fields of the aircraft, causing distinct noise radiation patterns [13]. To account for these effects, ECAC Doc. 29 includes a directivity correction in the plane perpendicular to the roll axis of the aircraft. Since the directivity in this plane is primarily attributed to the engine location, the correction is named the *engine installation effect*. It is assumed that these effects take place in two dimensions, although it probably has a three dimensional effect.

There are three type of engine installations identified in ECAC Doc. 29 (originally SAE AIR 5662 [34]) with distinct radiation patterns: one for propeller aircraft and two for jet aircraft to separate wing-mounted from fuselage-mounted engine installations. The three radiation patterns induced by the engine installation effect are visualised in Figure 2.3. Although mentioned as a distinctive radiation pattern, the engine installation correction for propeller aircraft is actually the lack of a radiation pattern. Therefore no correction is applied for propeller aircraft. This can be explained by the fact that the propeller noise is often produced in front of the wings or even in front of the fuselage, therefore it does not benefit from possible shielding effects by the wings.

For fuselage-mounted engines, the highest noise levels can be found directly beneath the aircraft. The noise levels decrease with increasing depression angle, which is explained by blocking by the fuselage. The noise levels of wing-mounted engines show a lobed pattern. This is explained by the fact that sound of two sources will interact with each other, creating lower noise levels directly below the aircraft and maxima slightly towards the sides around 45 degrees. Ultimately, some shielding by the fuselage will take place at depression angles of 90 degrees and higher.

Within ECAC Doc. 29, the engine installation effect is only defined below the aircraft, since no measurements have been performed above the wings. Therefore it is assumed that the power above the wing is equal to power in the plane of the wing.

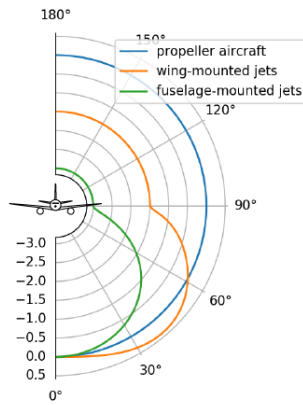


Figure 2.3: The engine installation effect $\Delta_I(\phi)$ used in ECAC Doc. 29 noise calculations in dBA. The indicated angle is the depression angle ϕ , the angle between the wing plane and the vector from the aircraft to the observer in degrees. The directivity pattern is symmetrical in the vector pointing from the aircraft down (i.e. $\phi = 0$)

2.1.5. Lateral attenuation correction

The lateral attenuation correction in ECAC Doc. 29 is adopted from SAE AIR 5662 [31] and accounts for standard surface reflections on soft level ground, while assuming a straight line from noise source to receiver. In reality, many factors such as temperature gradients, wind gradients, atmospheric irregularities and surface irregularities cause the sound to travel differently. Although mentioned as an area of improvement in ECAC Doc. 29 [13], an improved lateral attenuation correction such as developed by Arntzen et al. in [4] has not yet been adopted in the latest version of ECAC Doc. 29.

The lateral attenuation correction is visualised in Figure 2.4. As is shown, the lateral attenuation correction increases with increasing distance and decreasing elevation. Referring to Equation 2.3 and Equation 2.4, the lateral attenuation is the only correction that should be subtracted from the segment noise level. Consequently, the lateral attenuation correction can decrease the segment noise levels up to 10.857dBA for observers far away from the flight path with the aircraft at a low elevation angle.

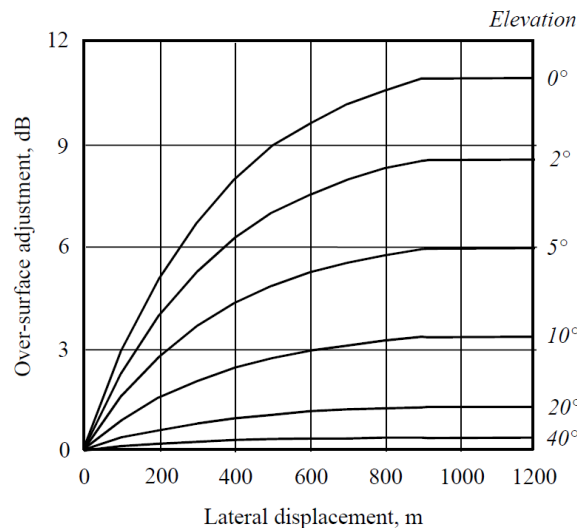


Figure 2.4: The lateral attenuation correction used in ECAC Doc. 29 noise calculations, obtained from [13].

The lateral attenuation correction can be calculated using Equation 2.7 to Equation 2.9.

$$\Lambda(\beta, l) = \Gamma(l)\Lambda(\beta) \tag{2.7}$$

$$\Gamma(l) = \begin{cases} 1.089(1 - e^{-0.00274l}) & \text{for } 0 \leq l \leq 914m \\ 1 & \text{for } l > 914m \end{cases} \quad (2.8)$$

$$\Lambda(\beta) = \begin{cases} 10.857 & \text{for } \beta < 0^\circ \\ 1.137 - 0.0229\beta + 9.72e^{-0.142\beta} & \text{for } 0^\circ \leq \beta < 50^\circ \\ 0 & \text{for } 50^\circ \leq \beta \leq 90^\circ \end{cases} \quad (2.9)$$

where β is the elevation angle in degrees, l is the lateral distance between the ground track of the flight and the receiver in meters, $\Lambda(\beta, l)$ is the lateral attenuation correction in dBA, $\Gamma(l)$ is the distance factor of the lateral attenuation correction without unit, $\Lambda(\beta)$ is the long-range air-to-ground lateral attenuation in dBA, and e is a mathematical constant. A visualisation of the elevation angle and the lateral distance can be found in Figure 2.1.

2.1.6. Duration correction

NPD data is provided at a reference speed of 160 knots. Flying faster or slower might expose the receiver shorter or longer to the noise, respectively increasing or decreasing the exposed sound. It is therefore only relevant for the calculation of exposure level noise levels.

The equation for the duration correction is provided in Equation 2.10.

$$\Delta_V = 10 \log_{10} \left(\frac{V_{ref}}{V_{seg}} \right) \quad (2.10)$$

where Δ_V is the duration correction in dBA, V_{ref} is the NPD reference speed of 160 knots, and V_{seg} is the segment speed in knots. Because the start and end speed of the segment might be different, a definition for the segment speed is required. How the segment speed is defined can be found in [13].

2.1.7. Noise fraction correction

Basic segment noise levels obtained from NPD tables represent the noise levels for continuous (i.e. infinite), straight, steady, and level flight. To account for the fact that the segment has a finite length, the noise fraction correction is calculated. The correction is also referred to as finite segment correction in ECAC Doc. 29 [13]. The correction calculates how much energy is emitted by the segment relative to the total acoustic energy for which the NPD data is provided. The noise fraction calculation is based on the geometry of the segment and the receiver. The noise fraction correction is a theoretical method based on a dipole sound source travelling an infinite path. More information including the derivation of this method can be found in [13].

The equation to calculate the finite segment correction for the sound exposure level is given in Equation 2.11 and Equation 2.12.

$$\Delta_F = 10 \log_{10} \left(\frac{\alpha_2}{1 + \alpha_2^2} + \tan^{-1} \alpha_2 - \frac{\alpha_1}{1 + \alpha_1^2} - \tan^{-1} \alpha_1 \right) - 10 \log_{10} \pi \quad (2.11)$$

$$\alpha_1 = \frac{-q}{d_\lambda}, \quad \alpha_2 = \frac{\lambda - q}{d_\lambda}, \quad d_\lambda = \frac{2V_{ref} t_0}{\pi} 10^{\frac{L_{E,\infty}(P,d_p) - L_{max,\infty}(P,d_p)}{10}} \quad (2.12)$$

where Δ_F is the finite segment correction in dBA, α_1 and α_2 are helper variables without unit, q is the length of the vector going from segment start to the receiver, projected on the segment in meters, λ is the length of the segment in meters, d_λ is the scaled distance in meters, V_{ref} is the NPD reference speed of 82.31 meters per second (160 knots), t_0 is the SEL reference time equal to 1 second, $L_{E,\infty}$ is the basic segment exposure noise level obtained from the NPD table in dBA, $L_{max,\infty}$ is the basic segment maximum noise level obtained from the NPD table in dBA, P is the power setting with units matching the NPD data, and d_p is the distance of the receiver perpendicular to the extended segment in meters.

2.1.8. Start of roll correction

It is observed that departing aircraft radiate in a lobed pattern behind the aircraft when on the ground [24]. This is primarily pronounced for jet aircraft, but also observable for turboprop aircraft, leading to two variations identified for the start of roll correction: one for turbofan-powered jet aircraft and one for turboprop-powered aircraft. The directivity patterns for both start of roll corrections can be found in Figure 2.5. Since

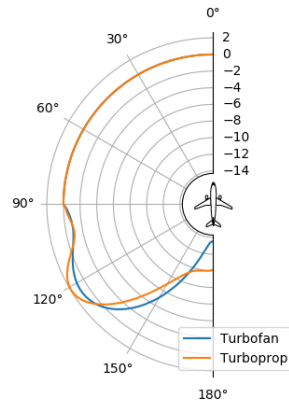


Figure 2.5: The start-of-roll directivity correction $\Delta_{SOR}(\Psi)$ used in ECAC Doc. 29 noise calculations in dBA. The indicated angle is the azimuth angle Ψ , the angle between the flight path vector and the vector from the aircraft to the observer in degrees. The directivity pattern is symmetrical around the flight path vector (i.e. $\Psi = 0$).

this effect is only observed for departing aircraft on the ground, this correction should only be applied to combinations of departures, ground roll segments and observers behind the segments.

Start of roll is normalised with distance to make the directivity less pronounced further away from the aircraft. The normalisation equation is given in Equation 2.13.

$$\Delta_{SOR}(\Psi, d_{SOR}) = \begin{cases} \Delta_{SOR}(\Psi) & \text{if } d_{SOR} \leq 762 \text{ m} \\ \Delta_{SOR}(\Psi) \frac{762}{d_{SOR}} & \text{if } d_{SOR} > 762 \text{ m} \end{cases} \quad (2.13)$$

where $\Delta_{SOR}(\Psi, d_{SOR})$ is the start of roll correction in dBA, $\Delta_{SOR}(\Psi)$ is the start of roll directivity in dBA, Ψ is the azimuth angle, the angle between the flight path vector and the vector from the aircraft to the observer in degrees, and d_{SOR} is the distance of the observer to the start of the segment in meters. Since the start of roll correction is only applied to receivers behind the departure ground roll segments, Δ_{SOR} thus only applies to receivers where $90^\circ \leq \Psi \leq 180^\circ$.

2.1.9. Verification of ECAC Doc. 29

The latest version of ECAC Doc. 29 is provided with verification cases and verification data in volume 3 [13]. Although the verification cases are flawed, e.g. not taking bank angles into account, not providing verification data for $L_{A,max}$ calculations and not providing verification data for NPD corrections for non-standard atmospheric conditions, it provides a decent starting point to determine if a model is implemented correctly.

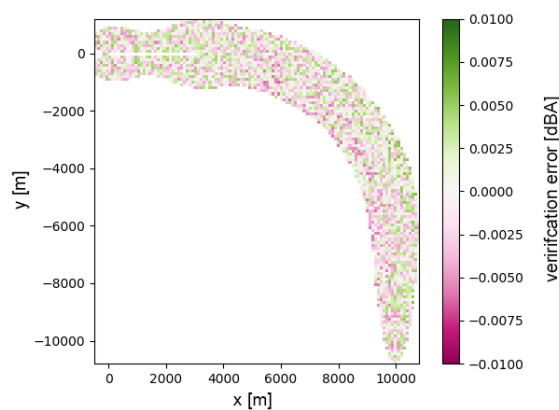


Figure 2.6: The verification results of Echo for the JETFDC case: a curved departure of a jet aircraft with fuselage mounted engines.

For this study, the ECAC Doc. 29 implementation of AerLabs called Echo has been used. In the past,

Echo has been verified using ECAC Doc. 29 volume 3 as well as some additional cases provided by industry partners. Echo has been used in production for many projects.

An example of the verification results for one of the ECAC Doc. 29 verification cases is shown in Figure 2.6. In this figure, the reference results from ECAC Doc. 29 volume 3 are subtracted from the calculated noise levels using Echo to determine the error of the implementation over a wide range of observer locations. In ECAC Doc. 29, it is suggested to aim for a root mean squared error of 0.01dBA or less [13] for all verification cases. As can be seen in Figure 2.6, all errors have an absolute value equal to or below 0.01dBA. This corresponds with an overall root mean squared error of 0.003dBA, meeting the suggested accuracy requirements from ECAC Doc. 29. For the other verification cases, similar results have been found as can be seen in the summary of Echo's verification report in Appendix D.

2.2. Meteorological adjustment

In this research it is tested what the effect is of applying actual meteorological conditions instead of standard meteorological conditions. Meteorological conditions affect the way acoustic waves travel through the air. So, at non-standard atmospheric conditions, the noise levels observed are expected to be different from the ones calculated using standard atmospheric conditions. ECAC Doc. 29 provides two supplementary methods that can be applied to the NPD data for the meteorological adjustment: the acoustic impedance correction and the correction for atmospheric absorption in a non-standard atmosphere. How they are applied in this research is shown in Figure 2.7. The steps that have to be performed to obtain NPD data at either standard or actual meteorological conditions are the same. This is because the NPD data is provided with a different atmospheric absorption model than the one used in this research, which will be addressed in more detail in subsection 2.2.2. Furthermore, the NPD data is provided at $T=25^{\circ}\text{C}$ [12, 13], while the advised standard temperature for Amsterdam Airport Schiphol is $T=15^{\circ}\text{C}$ [18].

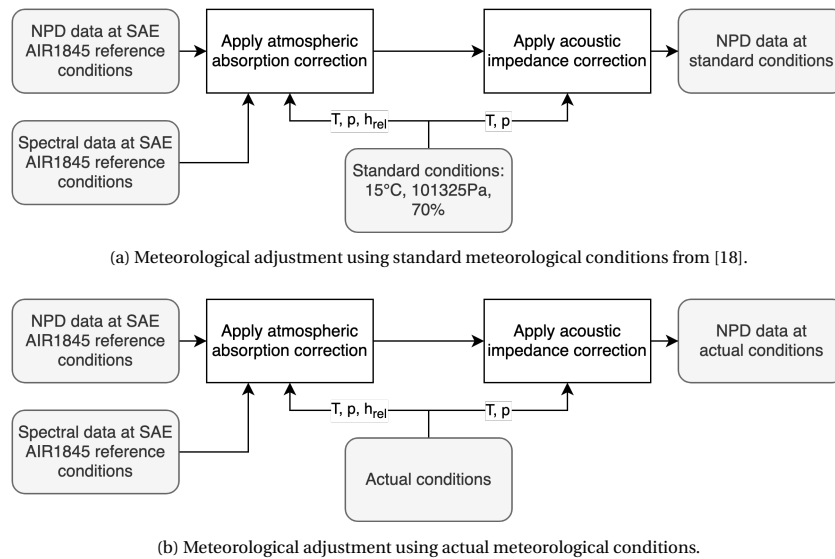


Figure 2.7: The two meteorological adjustments used in this research.

2.2.1. Acoustic impedance correction

The acoustic impedance correction is applied to account for the difference between the sound intensity level and the sound pressure level. The sound intensity is related to the energy of the sound (per unit time and unit area), whereas the sound pressure is the quantity used to describe the pressure change caused by the acoustic wave travelling to the air.

To illustrate the difference, an example will be provided. Suppose there are two identical acoustic point sources, each in a separate environment with different acoustic mediums e.g. hot and cold air. Assume both acoustic mediums to be both non-viscous and causing very weak motion of air. The energy observed at a certain distance from the source will be the same for both environments because of the conservation of energy. However, the observed sound pressure level might be different, because a particle of one medium

might be easier to excite compared to a particle of the other medium. This causes the sound pressure levels to be different, while the same energy is being applied by the acoustic sources.

Although the NPD data provides sound pressure levels in reference atmospheric conditions, the NPD data essentially encapsulates the amount of energy that the aircraft produces in the form of sound (i.e. the sound intensity) at a given thrust setting. Therefore, the sound pressure level included in the NPD data should be corrected for the use of non-reference atmospheric conditions to ensure conservation of energy.

In free field condition¹ the sound intensity has the following relation with the sound pressure, due to the conservation of energy, momentum and mass.

$$I = \frac{p_e^2}{\rho_\infty c} \quad (2.14)$$

where I is the sound intensity in W/m^2 , p_e is the acoustic pressure in Pa, ρ_∞ is the free field density of the air in kg/m^3 , and c is the speed of sound in m/s . This is directly related to the characteristic acoustic impedance, which is given in the following equation:

$$Z_0 = \frac{p'}{u} = \rho_\infty c \quad (2.15)$$

where Z_0 is the characteristic acoustic impedance in $\frac{Pa \cdot s}{m}$, p' is the pressure difference due to the sound wave in Pa, u is the particle velocity in m/s , ρ_∞ is the ambient air density in kg/m^3 , and c is the speed of sound in m/s .

Using this relation and the definition of the sound intensity level and the sound pressure level, the following relation between the sound pressure level and the sound intensity level could be obtained.

$$SPL = SIL + 10 \log_{10} \left(\frac{I_0 \rho_\infty c}{p_{e_0}^2} \right) \quad (2.16)$$

where SPL is the sound pressure level in dB, SIL is the sound intensity level in dB, $I_0 = 10^{-12} W/m^2$ is the reference sound intensity, and $p_{e_0} = 2 \cdot 10^{-5} Pa$ is the reference sound pressure.

The NPD data in the ANP database is normalized with the following reference conditions: $p_{npd} = 101325 Pa$ and $T_{npd} = 25^\circ C$ [12, 13, 31]. Using the ideal gas law $p = \rho RT$ and the equation for the speed of sound $c = \sqrt{\gamma RT}$, the following values can be obtained: $\rho_{\infty, npd} = 1.1839 kg/m^3$ and $c_{npd} = 346.13 m/s$.

These values can be used in Equation 2.16, leading to the following relation between sound intensity level and sound pressure level.

$$SPL_{npd} = SIL + 0.105 \quad (2.17)$$

As mentioned before, the NPD data contains the SPL values from Equation 2.17, while the sound intensity levels corresponding to these values are the levels that are actually constant regardless of the meteorological conditions. Therefore, if the free field air density and speed of sound are not equal to the reference conditions, different values must be used in Equation 2.16 leading to a different relation between SPL and SIL. Fortunately, Equation 2.16 can be rewritten such that it includes SPL_{npd} . The last term in this equation contains the adjustment of the sound pressure level for non-standard acoustic impedance. Therefore it is referred to as the *impedance adjustment of standard NPD data* in ECAC Doc. 29.

$$SPL = SIL + 10 \log_{10} \left(\frac{I_0 (\rho_\infty c)_{npd}}{p_{e_0}^2} \frac{\rho_\infty c}{(\rho_\infty c)_{npd}} \right) = SPL_{npd} + 10 \log_{10} \left(\frac{\rho_\infty c}{(\rho_\infty c)_{npd}} \right) = SPL_{npd} + \Delta_{impedance} \quad (2.18)$$

where ρ_∞ is the free field density of the air in kg/m^3 at the observer, c is the speed of sound in m/s at the observer, $(\rho_\infty c)_{npd}$ is the product of the density and the speed of sound in $kg/m^2/s$ at NPD reference conditions, SPL_{npd} is the tabulated sound pressure level in the NPD data in dBA, and $\Delta_{impedance}$ is the acoustic impedance correction in dBA.

¹condition where there are no acoustic reflections, i.e. the sound wave travels directly from the source to the observer and is observed only once by the observer.

Rewritten using the pressure and temperature ratio with respect to international standard atmospheric (ISA) conditions at mean sea level, in combination with the ideal gas law and the equation for the speed of sound, the following definition of the acoustic impedance correction is given in ECAC Doc. 29 [13]:

$$\Delta_{\text{impedance}} = 10 \log_{10} \left(\frac{416.86}{409.81} \frac{\delta}{\theta^{1/2}} \right) \quad (2.19)$$

where $\delta = \frac{p}{p_0}$ is the pressure ratio of the ambient air pressure p (in Pa) at the observer to the standard air pressure at mean sea level $p_0 = 101325 \text{ Pa}$ and $\theta = \frac{T+273.15}{T_0+273.15}$ is the temperature ratio of the ambient air temperature at the observer T (in °C) to the air temperature constant $T_0 = 15^\circ \text{C}$. The constants provided in this function correspond to the characteristic acoustic impedance for NPD reference conditions ($Z_{0,\text{npd}} = 409.81 \frac{\text{Pa}\cdot\text{s}}{\text{m}}$) and for ISA mean sea level conditions ($Z_{0,\text{ISA}} = 416.86 \frac{\text{Pa}\cdot\text{s}}{\text{m}}$). This allows to use the pressure and temperature ratios with respect to ISA mean sea level conditions.

2.2.2. Correction for non-reference atmospheric absorption

Part of the acoustic energy is absorbed by the air. Similar to the acoustic impedance correction, the amount of acoustic energy absorbed by the air depends on the atmospheric conditions.

Basic method

Although explained in detail in [13], it is essential to have a basic understanding of the correction for non-reference atmospheric absorption to understand the design choices to be taken. As mentioned before, the NPD data is normalised at reference atmospheric conditions. In the case of atmospheric attenuation, the reference atmospheric condition means the SAE AIR1845 reference atmosphere.

For the adjustment of the NPD data, the influence of the attenuation in the reference atmosphere should be removed first, before adding the attenuation from the corrected atmosphere. Because the attenuation depends on the frequency, the spectral data provided in the ANP database are used. In aviation, one-third octave band frequencies are commonly used as spectral data. Similar to the NPD data, spectral data is also provided for each ANP aircraft for each type of operation. In the ANP database, the spectral data is provided at a reference distance of 1000 feet in reference atmosphere SAE AIR1845 [31].

In order to correct the NPD data for a non-standard atmosphere (hereafter called specified atmosphere), a number of steps have to be performed. First, the 1000ft attenuation in the reference atmosphere is removed from the spectral data. Second, the attenuation is added to the spectral data for each distance in the noise-power-distance table. This step is performed twice on the unattended data: once to apply the reference atmosphere and once to apply the the specified atmosphere. Third, the A-weighted sound pressure levels at each distance are calculated for both atmospheres. Finally, the correction at each distance is determined by subtracting the specified atmosphere levels from the reference atmosphere levels.

To conclude, the correction of the NPD data depends on the specified atmosphere, the spectral data and the distances. In contrast, it does not depend on the actual noise level values of the NPD data itself nor the thrust setting.

Unlike the acoustic impedance correction, ECAC Doc. 29 provides multiple methods to define the specified atmosphere. When talking about specified atmosphere, we are actually talking about how the absorption coefficients change due to the change in atmospheric conditions in combination with the distance the sound wave has travelled (and thus how much noise is absorbed along the path). The reference atmosphere used is SAE AIR1845 [31], which does not depend on actual meteorological conditions because it is meant as a generic average attenuation model for aviation noise as is shown below. If one wants to use a different attenuation that actually depends on meteorological conditions, there are two possibilities: SAE ARP866B [32] and SAE ARP5534 [33]. The differences will be explained in the following sections.

SAE AIR1845

SAE AIR1845 has a single absorption coefficient for each one-third octave frequency band. The absorption of each frequency band is a simple multiplication of the absorption coefficient of the mid-frequency and the distance, as can be seen in Equation 2.20. Detailed information about this method can be found in [31].

$$\delta_{1845}^{i,d} = \alpha_{1845}(f_{m_i})d \quad (2.20)$$

where i is the index of the one-third octave-band, d is the distance from the source to the observer in meters, f_{m_i} is the mid-band frequency of one-third octave-band i , $\alpha_{1845}(f_{m_i})$ is the pure-tone absorption

coefficient of the mid-band frequency f_{m_i} in decibels per meter, and $\delta_{1845}^{i,d}$ is the absorption at one-third octave band i over a distance d in decibels.

SAE ARP866B

Absorption using SAE ARP866B is also calculated using the absorption coefficient multiplied by the distance. However, the SAE ARP866B absorption coefficient depends on temperature, humidity and frequency. Depending on the mid-band frequency of the one-third octave band, the pure-tone absorption coefficient should be calculated using the mid-band frequency or the lower frequency of the one-third octave band as can be seen in Equation 2.21. Detailed information about this method can be found in [32].

$$\delta_{866B}^{i,d}(T, h_{rel}) = \begin{cases} \alpha_{866B}(f_{m_i}, T, h_{rel})d & \text{if } f_{m_i} \text{ is at or below 4000Hz} \\ \alpha_{866B}(f_{l_i}, T, h_{rel})d & \text{if } f_{m_i} \text{ is above 4000Hz} \end{cases} \quad (2.21)$$

where i is the index of the one-third octave-band, d is the distance from the source to the observer in meters, T is the ambient atmospheric temperature in Kelvin, h_{rel} is the relative humidity in percent, f_{m_i} is the mid-band frequency of one-third octave-band i in hertz, $\alpha_{866B}(f_{m_i})$ is the pure-tone absorption coefficient of the mid-band frequency f_{m_i} in decibels per meter, $\alpha_{866B}(f_{l_i})$ is the pure-tone absorption coefficient of the lower-limiting frequency f_{l_i} of frequency band i in decibels per meter, and $\delta_{866B}^{i,d}$ is the absorption at one-third octave band i over a distance d in decibels.

SAE ARP5534

The SAE ARP5534 absorption coefficient depends on temperature, humidity, pressure and frequency. The final frequency band absorption is a multiplication of the mid-frequency pure-tone absorption coefficient and distance Equation 2.22. However, it is normalised using a regression function as can be seen in Equation 2.23. The regression function has been fitted to the results of a higher-order model to ensure a correct representation of the attenuation over various noise levels. Detailed information about this method can be found in [33].

$$\delta_{5534}^{m_i,d}(T, h_{rel}, p) = \alpha_{5534}(f_{m_i}, T, h_{rel}, p)d \quad (2.22)$$

$$\delta_{5534}^{i,d}(T, h_{rel}, p) = \begin{cases} A(1 + B(C - D\delta_{5534}^{m_i,d})^E)\delta_{5534}^{m_i,d} & \text{if } \delta_{5534}^{m_i,d} \text{ is below 150dB} \\ F + G\delta_{5534}^{m_i,d} & \text{if } \delta_{5534}^{m_i,d} \text{ is at or above 150dB} \end{cases} \quad (2.23)$$

where i is the index of the one-third octave-band, d is the distance from the source to the observer in meters, T is the ambient atmospheric temperature in Kelvin, h_{rel} is the relative humidity in percent, p is the ambient atmospheric pressure in Pascal, f_{m_i} is the mid-band frequency of one-third octave-band i in hertz, $\delta_{m_i,d}$ is the pure-tone absorption of the mid-band frequency of one-third octave-band i over distance d in decibels, $\alpha(f_{m_i})$ is the pure-tone absorption coefficient of the mid-band frequency f_{m_i} in decibels per meter, A through G are constants from SAE ARP5534 derived using statistical regression, and $\delta_{5534}^{i,d}$ is the absorption at one-third octave band i over a distance d in decibels.

Applied atmospheric absorption model

ECAC Doc. 29 suggests to use SAE ARP5534, because it is the most recent standard for non-standard atmospheric absorption. Since the effects of meteorological conditions are an important aspect of this research, it is desired to use the atmospheric absorption model that is the most accurate and includes the most effects on the atmospheric attenuation. Therefore SAE ARP5534 was selected for this research, since it is the most recent and includes the ambient pressure unlike the other models. Furthermore SAE ARP5534 is also advised in [18] for calculations around Amsterdam Airport Schiphol.

2.2.3. Verification of meteorological adjustment

Although it is suggested to use SAE ARP5534 for meteorological conditions in ECAC Doc. 29, no verification data is provided besides the calculation example. Therefore, a number of case studies had to be performed to verify that the implementation is correct.

In these case studies, the standard flight performance calculations using both standard and actual meteorological conditions were compared. Both to each other as well as to the pure-tone absorption results obtained directly from both SAE ARP5534 and SAE ARP866B. Although differences have been found, they could

all be attributed to the use of single frequencies in the back-of-the-envelope calculation. More information about the case studies and their results can be found in subsection 4.2.1.

2.3. Aircraft substitution

To perform a noise calculation, aircraft performance and aircraft noise data is required. A data collection suited for aircraft noise calculations is provided by Eurocontrol in the ANP database [12]. Since both performance and noise depend on the aircraft configuration, it is impractical to acquire noise and performance data for all possible aircraft configurations, because one aircraft type can have thousands of configurations. Therefore, reference aircraft are used for noise calculations, which can be corrected with information about the certified noise levels. The ANP database published by Eurocontrol [12] contains 154 different aircraft types and 110 different NPD tables.

Selecting the best matching reference aircraft from the ANP database is not a trivial task. ECAC Doc. 29 [13] prescribes that the following criteria should be used:

- engine category (jet, turboprop or piston)
- number of engines
- engine installation (wing or fuselage)
- aircraft maximum take-off weight (MTOW)
- thrust-to-weight ratio
- certified noise levels
- airframe manufacturer
- engine manufacturer

However, using these criteria in itself might lead to ambiguous results, because it does not explicitly state how to cope with a double match (or without a match at all) for a given criterion. In the past, multiple solutions have been developed for this problem. The following three methods could be used for substitution:

- **substitution table by ICAO type code:** provided by Eurocontrol in addition to the ANP database [12], requires both ICAO type code and engine manufacturer.
- **substitution table by aircraft configuration:** also provided by Eurocontrol in addition to the ANP database [12], requires the EASA record number (used for aircraft noise certification).
- **substitution using scoring system developed for Amsterdam Airport Schiphol:** developed by NLR [18], requires the EASA record number and ICAO engine emissions number.

Since ADS-B data is being used as the primary source for flight data upon which the noise calculations are based, only the ICAO type code is known for all aircraft. All substitution protocols require some information regarding the engine type, causing none of the methods to provide unambiguous results. However, where the ANP substitution by ICAO type code only provides two alternatives, the method developed by NLR provides more choices, which is harder to generalize when only ICAO type code is available. Furthermore, the substitution protocol by NLR is developed specifically for Amsterdam Airport Schiphol, which limits the applicability to other airports since it is based on requirements specific to Amsterdam Airport Schiphol.

2.3.1. Substitution used for this research

Because none of the substitution methods can be used directly, a new substitution method was developed based on the substitution table by ICAO type code. The substitution table was adopted such that only one aircraft type would be possible for a single ICAO type code. To do this, a number of records were removed from the original substitution table. A new parameter Δ was created to select the records to be removed. Δ is calculated for each record in the table using Equation 2.24.

$$\Delta = \sqrt{\Delta_{app}^2 + \Delta_{dep}^2} \quad (2.24)$$

where Δ is the combined correction in dBA, Δ_{app} is the listed correction for arrivals in dBA, and Δ_{dep} is the listed correction for departures in dBA.

For each ICAO aircraft type, only the lowest record with the lowest Δ was kept, the others were removed from the substitution table. The lowest Δ was used for the final substitution, because a small value for Δ indicates that the noise levels after correction of the NPD data are closest to the original measurements used to obtain the NPD data. The result is a substitution table that has only one ANP aircraft type substitution for each ICAO type code.

2.3.2. The effect of the aircraft substitution correction

Initially, no correction will be applied to the NPD data, because it can also be applied afterwards. Additionally, it is shown in Figure 2.8 that the suggested ICAO type code correction will tend to overestimate the noise level correction by always taking the largest corrections of all possible aircraft configurations. Although the figure only shows one aircraft type, the same pattern could be found for other aircraft types.

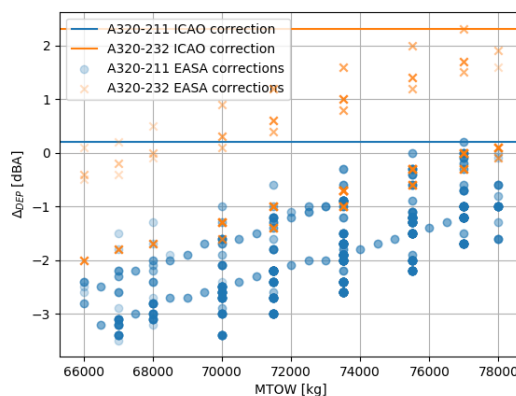


Figure 2.8: The two possible aircraft type substitutions for aircraft with ICAO type code A320 and the suggested noise level corrections based on ICAO type code only (ICAO correction) or aircraft configuration (EASA correction). The results are visualised versus the maximum takeoff weight (MTOW) to illustrate the relation between aircraft weight and aircraft noise [12].

In Figure 2.8, all the substitution options of the Airbus A320 (ICAO type code A320) are illustrated. The two horizontal lines indicate the two corrections obtained from the lookup table by ICAO type code. The A320-211 is the suggested reference aircraft for A320's with CFM² engines. The A320-232 is the suggested reference aircraft for A320's with IAE³ engines. Although it is not used for the substitution by ICAO type, the figure also illustrates the EASA recordnumber corrections with the orange crosses and the blue dots. It can be observed that the ICAO type code correction for a reference aircraft is equal to the largest EASA recordnumber correction for this reference aircraft. Thus the ICAO type code correction is an overestimation of the most accurate correction that should be applied based on certified noise levels. In this case, the ANP aircraft A320-211 is selected for substitution, since the combined correction Δ (obtained using Equation 2.24) is closest to zero for this ANP aircraft type.

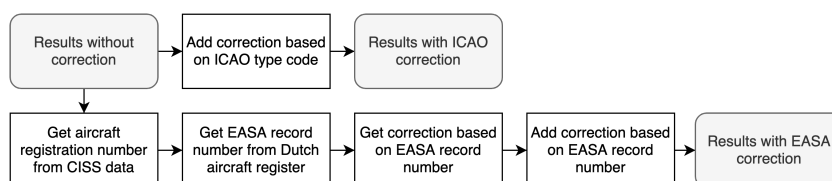


Figure 2.9: Applying corrections based on ICAO type code and EASA record number.

When comparing the substitution tables by ICAO type code and EASA record number, it can also be concluded that in many cases, the substitution using ICAO aircraft type and EASA record number results in the same aircraft type. Therefore, the impact of both corrections can be compared to each other. For these aircraft, the calculated noise levels will be corrected with both the EASA and ICAO correction, such that both methods for substitution correction can be compared with each other. However, in order to determine the

²<https://www.cfmaeroengines.com>

³<http://i-a-e.com>

EASA record number correction, the EASA record number must be known. As can be seen in Figure 2.9, this can be done by using the aircraft's registration number and the Dutch aircraft register. Since a lookup in the Dutch aircraft register is required, only a selection of all the flights can be analysed.

2.4. Flight performance

As an input of the noise calculation, the flight path is very important. To construct the flight path, information about the aircraft's flight performance and how the aircraft is operated must be known. Aircraft weight is one of the factors influencing the flight performance. Because the heavier the aircraft is, the more thrust is required to propel the aircraft. Furthermore, weight also has an influence on the flight path, because the rate of climb is also limited by the aircraft's weight.

In contrast with the derived flight performance, the standard flight performance does not use the aircraft weight directly as will be further explained in subsection 2.4.1. However, an estimation of the weight still has to be made. How the aircraft's weight is determined will be addressed in the following section.

2.4.1. Aircraft weight

For aircraft noise calculations using standard flight performance profiles (see also subsection 2.4.2), thrust is already defined within the profile, implying that weight should also be known. To account for the weight variability, standard performance profiles are thus constructed for multiple weights. For the standard performance profiles, the weights are related to stage lengths. Essentially, the stage length of a departing aircraft indicates how far the aircraft will fly and thus how heavy it will probably be. The default weights for each stage length are provided in the ANP database [12].

Ideally, one would use the actual weight to select the stage length for the noise calculation. Actual weight is data that is not readily available and airlines are reluctant to share this data. So, other methods have to be used to determine the weight. In the past, Sun et al. [40] have been able to successfully determine the aircraft weight based on ADS-B data. With the help of Sun, the weight estimation method of Sun et al. was applied to a selection of the data used in this research. Assuming zero wind and ISA temperature, the mass estimation for a collection of 49 flights with the same aircraft type provided an estimated weight of 60 ± 3 ton. Based on these results a number of limitations were identified:

- 49 flight tracks returned a single mass estimation. Ideally, the mass would be estimated for each flight track separately.
- The ADS-B data from To70 is not well-suited for the mass-estimation, because it is rounded at each whole second. Additional assumptions are required to overcome this limitation.
- The model has only been validated for a single aircraft type (i.e. Cessna Citation II).
- The model could not be used without Sun.

Because the mass estimation model by Sun et al. has its limitations as well, the proposed method in ECAC Doc. 29 [13] (and also suggested in the implementation for Amsterdam Airport Schiphol [18]) to determine aircraft weight based on stage length was used. By using the great-circle distance between the origin and destination airport to determine the stage length. The data provided by Schiphol also included the origin and destination, so stage lengths and therefore aircraft weight could be determined for all flights.

2.4.2. Standard flight performance

As described in subsection 2.1.2, the flight path is an important input for an aircraft noise calculation. In general, the flight path will depend on the aircraft's performance and on how the aircraft is operated, e.g. which procedure it is flying and how heavy the aircraft is. Using radar data or ADS-B data, the 4D trajectory (x, y, z, t) of the aircraft is known, providing the basis for most of the parameters (V, ϵ) needed for a noise calculation, except for the thrust setting P . The current practice is to use standard flight performance profiles to determine the altitude, ground speed and thrust setting of the aircraft along its flight path. This section will discuss how this method works and how these standard flight performance profiles are assigned.

Standard flight performance profiles - or fixed point profiles as they are called in ECAC Doc. 29 - are a collection of points providing performance parameters for consecutive travelled distances from the runway. The performance parameters included in a standard flight performance profile are the altitude z , the groundspeed V , and thrust setting P of the aircraft. As can be seen in Figure 2.10, these performance profiles are combined with ground tracks (described with x, y) using alignment of the travelled distance s . The

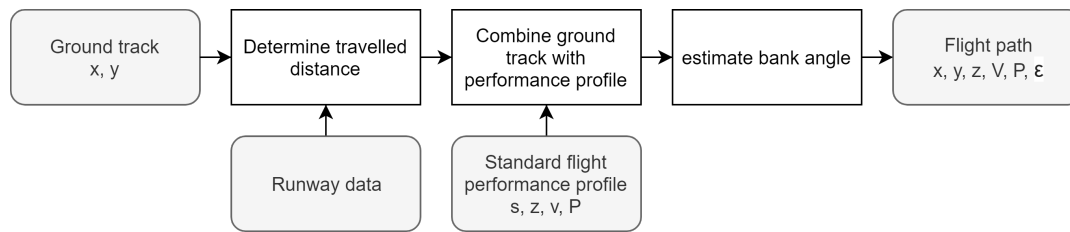


Figure 2.10: The steps to obtain the flight path using a ground track and a standard flight performance profile.

travelled distance is the path length of the ground track, relative to the start of the runway. For a departure this is the point where the aircraft starts the take-off ground roll. For an arrival, the start of the runway is the point where the flare procedure starts. After the ground track and flight performance profile are combined, the bank angle can be estimated and the flight path segments suitable for ECAC Doc. 29 calculations as described in subsection 2.1.2 can be determined.

Performance profiles are especially useful for predicting aircraft noise, because once they have been constructed, only the lateral movement has to be estimated. Lateral movement (i.e. the projection of the flight path on the Earth's surface, also referred to as the ground track) can be taken from many sources, including ADS-B and radar, but it can also be theoretical such as routes from the aeronautical information package (AIP) or a completely new route e.g. one that has been constructed for noise abatement and for which the impact must be assessed.

The performance profiles can be constructed in two ways: using (theoretical) procedural steps or by analysing historic flight paths in a similar fashion to the method described in subsection 2.4.3. An example of these procedural steps can be found in Table 2.3. However, for this research, pre-defined standard performance profiles are used. This includes the default fixed point profiles from Eurocontrol's ANP database [12] as well as the fixed point profiles created specifically for Amsterdam Airport Schiphol by the Netherlands Aerospace Center (NLR) [18]. The best results are expected with the fixed point profiles developed by NLR, since they were specifically developed for Amsterdam Airport Schiphol. However, to get the most results, the standard flight performance profiles from the ANP database were also included. Examples of various flight performance profiles for Amsterdam Airport Schiphol can be found in Figure 2.11.

Table 2.3: Procedural steps for profile ICAO A profile of aircraft type A320-211 with stage length 1 [12]. The step types are related to equations in [13], the thrust rating and flap ID are related to coefficients in the ANP database [12].

Step Number	Step Type	Thrust Rating	Flap ID	End Point Altitude (ft)	Rate Of Climb (ft/min)	End Point CAS (kt)
1	Takeoff	MaxTakeoff	1+F			
2	Climb	MaxTakeoff	1+F	1500		
3	Climb	MaxClimb	1+F	3000		
4	Accelerate	MaxClimb	1+F		812.1	186.1
5	Accelerate	MaxClimb	1		933.5	201.2
6	Accelerate	MaxClimb	ZERO		1119.7	228.2
7	Accelerate	MaxClimb	ZERO		1240.5	250
8	Climb	MaxClimb	ZERO	5500		
9	Climb	MaxClimb	ZERO	7500		
10	Climb	MaxClimb	ZERO	10000		

Selecting profiles

Within ECAC Doc. 29 [13], it is not prescribed how to select the flight performance profiles. However, the flight performance profiles for a given aircraft type can be selected using a profile identifier and stage length. The profile identifier is related to procedures, such as ICAO noise abatement departure procedure (NADP1, NADP2, etc.) and continuous descent approaches. As discussed before in subsection 2.4.1, the stage length is related to the aircraft's weight. So in order to use standard flight performance profiles, aircraft type, procedure and weight must be known. Similar to determining the ANP aircraft type, this is not trivial, because procedure and weight are not confined within ADS-B data.

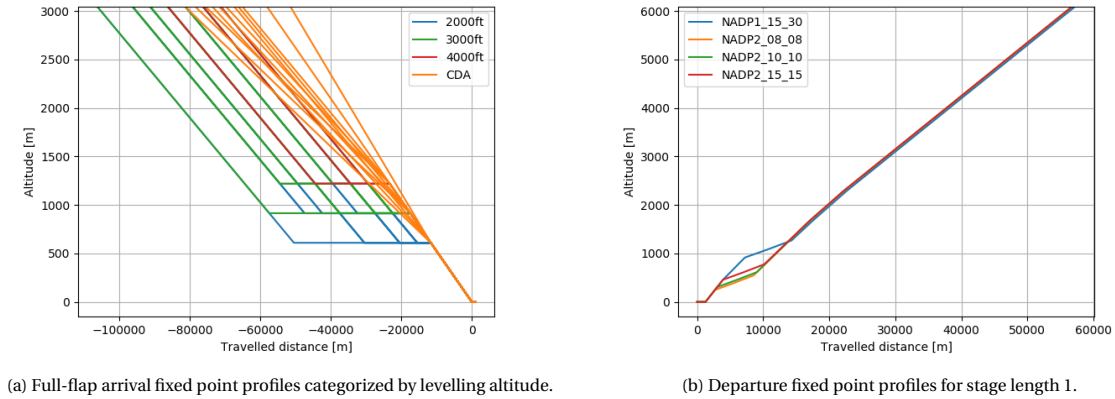


Figure 2.11: Example fixed point profiles created by NLR for ANP aircraft type A320-211.

Together with the standard flight performance profiles for Amsterdam Airport Schiphol, a procedure to select the best matching performance profile is provided in [18]. This method uses selection based on the altitude of the profile and the actual altitude. For this method it is assumed that stage length and aircraft type are known. This method uses a scoring method, based on how good the altitude matches over various travelled distances. The score used is the altitude error (actual altitude minus altitude of standard profile) squared, weighted with the inverse of actual height squared. So altitude errors at lower altitudes are more important than errors at higher altitudes.

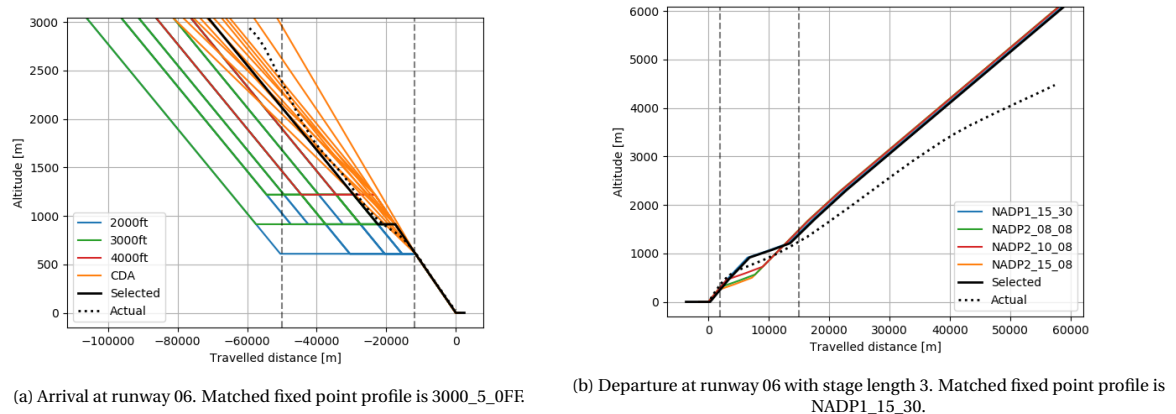


Figure 2.12: Examples of the actual altitude and the available and fitted fixed point profile altitudes for aircraft type A320-211. The fixed point profile is matched using the altitudes within the range of travelled distances indicated by the grey dashed lines.

The locations included in this analysis are at travelled distance from 50 km to 12 km before the touchdown point for arrivals. With a suggested spacing of 200 meter per point, this leads to 191 locations. The last 12 kilometers are fixed for all profiles, because this phase is strongly related to the use of the instrument landing system (ILS). An example of a fitted arrival altitude profile can be found in Figure 2.12a.

For departures it is stated that the procedure (and thus profile) used depends on the airline [18]. However, since this information is not known, a method similar to the one used for arrivals is used to assign departure profiles. Based on the typical differences between the available departure flight performance profiles, the travelled distance range of interested was determined to be from 2 km to 15 km after lift-off. Using the same spacing as the arrivals, 66 points are used to determine the best matching standard performance profile. An example of a fitted departure altitude profile can be found in Figure 2.12b. Because the liftoff location was used as the point of reference, the travelled distance of the ADS-B data had to be adjusted accordingly, such that the liftoff locations using the fixed point profile would be approximately equal to the derived flight performance flight path. Since ADS-B ground roll data was removed, the initial airborne altitudes were ex-

trapolated to obtain the travelled distance with $s = 0m$ at the liftoff location.

For some aircraft types, the Schiphol specific arrival profiles are available for both full flap setting as well as reduced flap setting. Because the altitude profiles for both reduced and full flap settings were the same, this study only considered the default flap setting (i.e. full flap setting) in this study.

2.4.3. Derived flight performance

The thrust setting is related to the corrected net thrust for all aircraft types used in this research. With a known flight path (including altitude and groundspeed), the thrust setting can also be derived instead of using a standard flight performance profile. There are two documented options, the force balance equation (or equations of motion) from ECAC Doc. 29 [13] and the Total-Energy Model from BADA [11], which are almost equal, except for the use of bank angle and flight path angle. Since the equations were not provided in the same format or with the same units, a derivation was performed to ensure that they would be the same. The derivation of the equations can be found in Appendix G. The force balance equation provided in ECAC Doc. 29 [13] can be found in Equation 2.25, whereas the force balance equation derived from BADA [11] can be found in Equation 2.26.

$$\frac{F_n}{\delta} = W \frac{R \cos \gamma + \sin \gamma + \frac{a}{g}}{N\delta} \quad (2.25)$$

$$\frac{F_n}{\delta} = W \frac{R \frac{1}{\cos \phi} + \sin \gamma + \frac{a}{g}}{N\delta} \quad (2.26)$$

where F_n is net thrust per engine in lbf, W is the aircraft weight in lb, R is the drag-to-lift ratio C_D/C_L , γ is the flight path angle, ϕ is the bank angle, g is the gravitational acceleration of 9.81 m/s^2 , a is the average acceleration in m/s^2 , N is the number of engines supplying thrust, and δ is the ratio of ambient air pressure at the aircraft to the standard air pressure at mean sea level. It can be seen that Equation 2.26 uses the bank angle while Equation 2.25 uses the flight path angle. For this research, a combination of these two methods was used, since it included both the effect of the bank angle ϕ and the flight path angle γ . The resulting force balance equation to determine the corrected net thrust of the engine is shown in Equation 2.27.

$$\frac{F_n}{\delta} = W \frac{R \frac{\cos \gamma}{\cos \phi} + \sin \gamma + \frac{a}{g}}{N\delta} \quad (2.27)$$

A number of parameters of the force-balance equation are related to aircraft configuration and performance. The number of engines, weight and drag-to-lift ratio could be obtained from the ANP database. The weight could be determined using tables with various stage lengths and their default weight. Thus the same stage length as used for the selection of the fixed point profiles is used. How the stage length is determined is described in subsection 2.4.2.

The drag-to-lift ratio is also available in the ANP database. The drag-over-lift ratio normally changes over various flight phases, e.g. due to changing control surface settings. So ideally, one would detect the flight phase and select the appropriate drag-over-lift ratio for that specific flight phase. However, the various flight phases and aerodynamic configurations are coded differently for each aircraft type, therefore it is not a straightforward exercise to determine the correct aerodynamic configuration using a pre-programmed procedure. Therefore average of available drag-to-lift ratios was used for a specific aircraft type at a specific type of operation. When drag-to-lift ratio was not known for a specific type of operation, the average of all drag-to-lift ratios was used.

Bank angle is determined using the same method as with fixed point profile, using three smoothed points (x,y) to determine the turn radius. The bank angle can be calculated using the turn radius and the ground speed [13]. Flight path angle (or climb/descent angle) is determined using the derivative of the smoothed altitude and the smoothed ground speed. Acceleration is determined using the derivative of the smoothed ground speed.

Lastly, because the corrected net thrust is used in the NPD data, the pressure ratio δ must be determined. Since the pressure ratio changes with the altitude, both the actual meteorological conditions and the flight path must be known. To determine the pressure ratio the corrected GNSS altitude and a lapse rate model (-6.5 K/km) were used. The lapse rate model was calculated using the observed conditions at sea level as described in section 3.3 as a basis.

After all the input parameters are determined, the corrected net thrust could be determined. The calculation procedure is described in detail in Appendix B.

The force-balance equation discussed before only holds for airborne flights. Because there is a different force balance, a different method to obtain the thrust setting on the runway is required. Although there are methods to estimate the thrust setting at take-off ground roll or reduced thrust at landing ground roll, this research focuses on NOMOS noise monitoring terminals only, which are not located nearby the runway. Thus, it is expected that the part on the runway would not be detected by the noise monitoring terminals, making the phase on the ground less relevant to model. It was therefore decided to only take the airborne flight phases into account for this research.

2.4.4. Verification of derived flight performance

To assure that the derived flight performance was implemented correctly, some of the individual results have been analysed. Since it is not a standardized method, verification data is not readily available. Therefore the method is verified by comparing the results to the available flight performance data, such as the maximum sea level static thrust.

An example of a visualisation used for verification can be found in Figure 2.13. First, the smoothing of flight path has been evaluated, as can be seen in Figure 2.13a. Visually, it was checked if the smoothed ground tracks were close to the original ground track. It was expected that the distance to the noise monitoring terminal points would not change significantly. Furthermore, the smoothing coefficient (residual) was also shown as an indication of the smoothing performance. A similar procedure was performed on the altitude. Here, the point of reference was zero altitude, because that is approximately where the NMTs are located.

After the altitude, the derivation was assessed. First the bank angle. Based on this figure it can be concluded that the bank angles are noisy and quite large, both indicating that more smoothing might be applied. As will be explained in section 3.2, bank angles passing 35° will be removed due to stability issues. Furthermore, the thrust setting is assessed in Figure 2.13d. It is investigated how the thrust setting changes over time and how this relates to the maximum sea level static thrust.

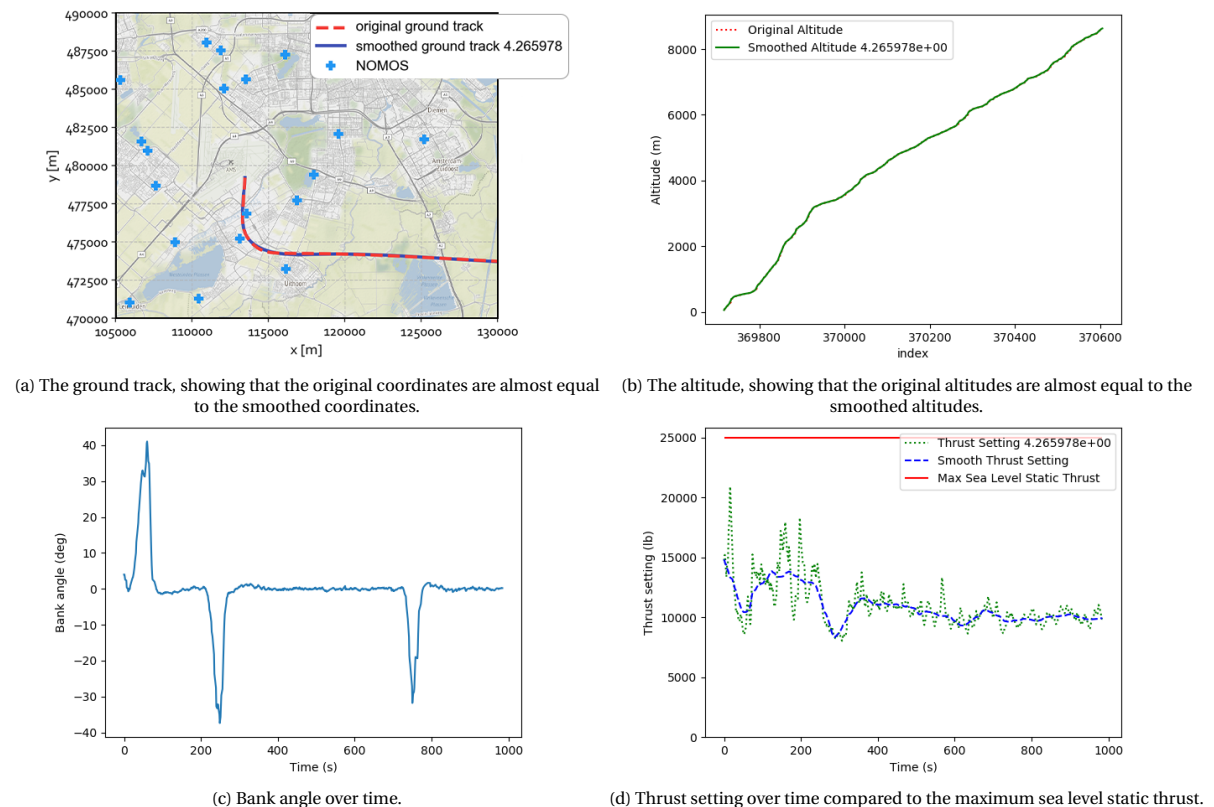


Figure 2.13: Collection of some verification results for an A320 departure from runway 18L.

For many flights, such an effort has been performed, leading to some minor improvements in terms of numerical stability for the smoothing algorithms. However, from this effort it could be concluded that the method was implemented correctly providing feasible results.

3

Description of data used

For a comparison between measured and calculated aircraft noise, multiple data sources are required. Measurements, flight paths, meteorological data, and data about the flight (e.g. aircraft type) are required. To obtain a comparison between the measurements and calculations that covers a wide range of meteorological corrections, the data must cover a full year to investigate the impact of various seasons. Additionally, a large number of flights are required to analyse the results of a wide range of aircraft types. Therefore, this study focuses on all the available data from July 2018 up to June 2019.

This chapter addresses the data used in the study, starting with the noise measurement from NOMOS in section 3.1. Additionally, the flight path data will be addressed in section 3.2, which includes a description of how this data is processed and the limitations of the used ADS-B data. The chapter is concluded with a section on the meteorological data in section 3.3 and a description of how the datasets from various sources are linked to each other in section 3.4.

3.1. NOMOS noise measurement

The measurements used for this research come from NOMOS. NOMOS, which is an acronym of noise monitoring system, is a network of microphones around Amsterdam Airport Schiphol that measures aircraft noise [37]. The system has been active since 1993 and expanded a number of times since the beginning. Currently, NOMOS consists of 41 microphones (or noise monitoring terminals - NMTs). The locations of the various noise monitoring terminals can be found in Figure 3.1.

3.1.1. NOMOS characteristics

The hardware and accompanying software is provided by Brüel & Kjær [37]. The software used for managing and post-analysis of the noise measurements is called ANOMS [10]. All NMTs have the following characteristics [10, 37]:

- they consist of a microphone, analyzer and pole,
- they use an ISO Class-I microphone with an accuracy of 0.7-0.9 dBA,
- they measure the sound levels continuously, and
- they detect aircraft noise events based on sound levels measured and flight path information.

While the measurement accuracy tolerance for an ISO Class-I microphone is +/- 1.9dB [23], NOMOS has a measurement accuracy between 0.7 and 0.9 dBA [35, 37]. Although NOMOS measures all the time, NOMOS is designed to detect the amount of noise that can be attributed to flights. It does this by detecting noise events: a period of time where the sound levels measured deviate from the 'normal' conditions, which are commonly referred to as background noise. Noise events are detected using fixed thresholds. A noise event in ANOMS starts once a threshold is met and ends when the maximum time has passed (2 minutes) or when the event noise levels drop below the threshold. These thresholds are determined based on long-term measurements and might be different for each NMT. After the noise event detection, the system correlates noise events to flights, based on flight path geometry. In order to do this, the system checks if there is a flight nearby to which the noise event can be related.

Although many characteristics of the different NMTs are the same, there might be differences between the NMTs. Those differences between NMTs include:

- the location (see Figure 3.1),
- the type of location (ground or rooftop, see Figure 3.2),
- the type of hardware,
- the hardware to protect against the environment (e.g. fences),
- the noise level threshold (based on background noise), and
- the frequency range (normal or low-frequency).



Figure 3.2: Example of ground and rooftop monitoring terminals of NOMOS, the visible part of the pole and microphone indicated in the red box. Obtained using Google Maps [17].

Because NOMOS has increased in size since its origins, hardware has been added and/or changed over time. Therefore the hardware for each location might be different. As mentioned before, the accuracy for all NMTs is equal, so although the acoustic components for each NMT might be different, they are all equivalent in terms of measuring accuracy.

As explained before, the noise level thresholds that are used to detect noise events, might be different for each NMT. This is because these thresholds are based on the background noise, which is related to the location itself. For instance, an NMT located near a busy street will typically detect more background noise compared to an NMT located in a quiet rural area.

Important for this research is the frequency range which the NMT analyses. A typical NMT uses the range that is perceived by the human ear, based on perceived loudness. As will be explained in the next section, these NMTs typically make use of A-weighting to account for the loudness that is perceived by a human. However, it was found that particularly low-frequency noise might cause a number of the adverse effects caused by aircraft noise, including reduced speech intelligibility and increased annoyance [6]. Therefore, NOMOS also contains two noise monitoring terminals (NMT 78 and NMT 80) to monitor low-frequency noise. For these NMTs, a different frequency range is used and C-weighting is applied instead of A-weighting. Although low-frequency noise is interesting due to its relation with potential adverse effects on humans, analysing low-frequency noise is beyond the scope of this research.

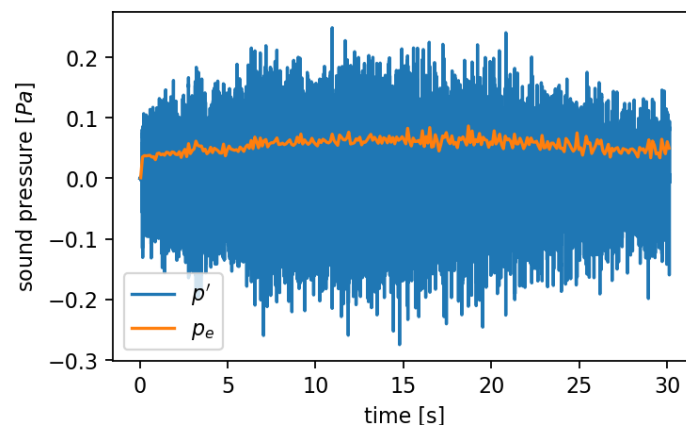
3.1.2. Properties of available NOMOS data

For this research the exact coordinates of the noise monitoring terminals were provided by Schiphol. Next to the position, this data also included the type of installation (roof or ground). Additionally, access to ANOMS was provided. As explained in the previous section, NOMOS is measuring all the time, but one of the main features of NOMOS is the ability to identify noise events that can be attributed to aircraft noise. ANOMS provides a variety of data for each noise event, as can be seen in Table 3.1.

Table 3.1: The available noise data in ANOMS.

Description	File format	Data included	Sampling Frequency
Audio files	MP3	$p'_{normalised}(t)$	8kHz
Event samples	xlsx/csv	$L_{A,eq}[t]$	1Hz
Event spectra	xlsx/csv	$L[f]$	per event
Event records	xlsx/csv	$SEL, L_{A,max}, t_{start}, t_{max}, \Delta t$, class, implausible, confirmed	per event

The NOMOS audio files are a normalised copy of what is measured by the microphone: the sound pressure p' over time t . However, the measurements have been compressed to optimise storage, ending up with the availability of MP3 data. To store the data using the MP3 format, the measurements are sub-sampled using a lower frequency and the sound pressure is normalised. So high-frequency data is lost and absolute sound levels cannot be deduced from the data. Due to the limited amount of storage available on the NMT, MP3 files are only available for a limited time (up to 4 months) after the event. An example of the normalized sound pressure $p'_{normalised}$ contained in an audio file is shown in Figure 3.3. Additionally, the corresponding effective sound pressure p_e is shown from which the (normalised) sound pressure level $SPL(t)$ can be determined. The sound pressure can also be visualised using a spectrogram. The spectrogram in Figure 3.4 shows how the noise contribution of each frequency changes over time, which helps to determine the dominant tones of an aircraft flyover. Ultimately, this is valuable information because this can be used to determine the fan rotational speed, such as described in [25].

Figure 3.3: The normalised sound pressure $p'_{normalised}(t)$ of a NOMOS measurement with the corresponding effective pressure p_e .

The event sample contains the equivalent A-weighted noise levels $L_{A,eq}$ as a time series for each noise event. The time series $L_{A,eq}[t]$ provides values for each second, therefore square brackets are used to indicate that the time series is considered in discrete time. In contrast with the audio files, the event samples are not normalized. This is verified by recalculating the SEL values for a number of flights. A maximum difference of 0.1 dBA was found which could be attributed to rounding errors, since $L_{A,eq}[t]$ values are provided with a single decimal value. An example of $L_{A,eq}[t]$ can be found in Figure 3.5. It also shows the overall sound pressure level (OSPL) and the overall A-weighted sound pressure level (OASPL) that could be obtained from the audio sample, to illustrate the fact that the audio sample is normalized. Note that the time range of the OASPL and $L_{A,eq}$ curves are not perfectly the same because the OSPL and OASPL use a different time window.

A one-third octave band spectrum is also available for each noise event. Since this does not provide us with information about the absolute noise levels of the event, spectrum event data was not considered.

Ultimately, event data is also provided, which contains accumulated data for the whole event. Among the properties is SEL, $L_{A,max}$, duration of event, etc. Normal NMTs are A-weighted, low-frequency NMTs are C-weighted. As can be seen in Figure 3.5, the results of the event data can be different from the audio file, since the audio file has been scaled and therefore does not represent the actual sound pressure level.

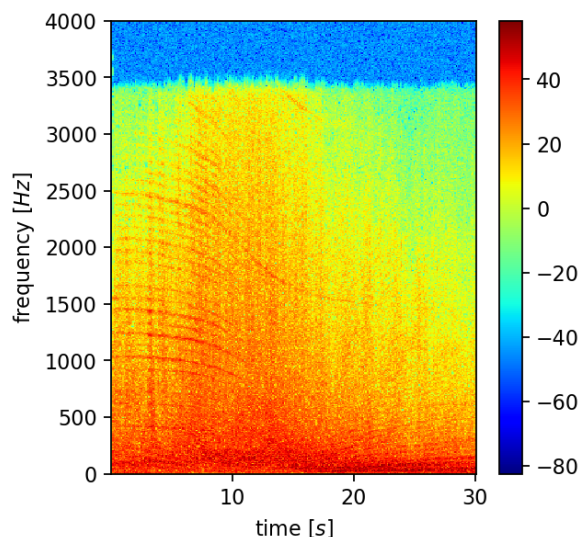


Figure 3.4: A spectrogram of a NOMOS measurement with the measurement sampled at $f_s = 8000\text{Hz}$. The spectrogram is obtained using a Fast Fourier Transform without overlapping windows and a window size of $n_{fft} = 838$.

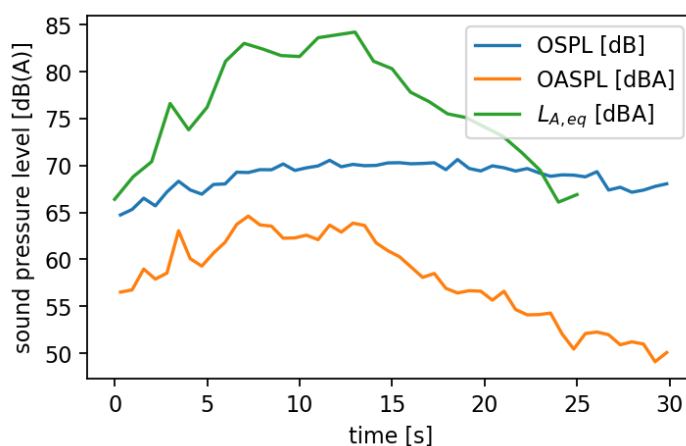


Figure 3.5: The overall sound pressure level over time, both with and without A-weighting (i.e. OASPL and OSPL respectively), with $\Delta t = .63\text{s}$. Additionally, the figure also includes the provided $L_{A,eq}$ data by ANOMS, with $\Delta t = 1\text{s}$. The event data provided an $L_{A,max}$ value of 84.2dBA and a SEL value of 93.3dBA for this event.

3.1.3. Measurement data used for this research

For this research the exact locations of the noise monitoring terminals as provided by Schiphol were used. However, since the altitudes were not provided, the microphone altitudes of all noise monitoring terminals were assumed to be at 5m altitude with respect to the altitude of the runways (which was assumed to be zero).

This research focuses on the noise of individual flights and its contribution to the long-term average noise production of aircraft operated around the airport. It is possible to obtain long-term average noise production of multiple noise events using various methods and thus from different types of data, however not all data listed in Table 3.1 could be used to obtain long-term average noise levels. Spectral data could not be used for long-term average noise level research, since it did not entail absolute noise levels. Additionally, it is also impossible to determine absolute noise levels from the audio files, thus audio files could not be used solely for this research.

So both event samples (time series) and event data could be used to obtain the absolute noise levels for comparison with the modelled results. However, obtaining event samples was cumbersome using ANOMS and did not provide additional value except the evolution of the noise production over time within the event. Using only event samples even has a disadvantage, because the $L_{A,max}$ values from the event data could not be derived from the $L_{A,eq}$ values of the event samples. Furthermore, aligning the event samples (and audio

files as well) with the calculations proved to be difficult, because the timestamps of NOMOS and the ADS-B data did not align. It is known that the timestamps of the ADS-B data are assigned by To70's remote server. This method might introduce a time shift related to the processing and transferring time of the ADS-B data. Additionally, the time of a server might drift over time unless it is regularly updated using an absolute time reference such as an atomic clock or GPS¹ signal.

Therefore, the event data was used in this research, because it allowed to determine long-term average noise levels based on the sound exposure level of each noise event. Additionally, using the event data also allowed to compare measured $L_{A,max}$ values with calculated $L_{A,max}$ values.

3.2. ADS-B flight path data

For this research, automatic dependent surveillance broadcast (ADS-B) data has been used. ADS-B is defined by Eurocontrol as 'A means by which aircraft, aerodrome vehicles and other objects can automatically transmit and/or receive data such as identification, position and additional data, as appropriate, in a broadcast mode via a data link.'² From the available data, the identification, position and velocity data was used for this research. The data used in this research was collected by To70. The current version of their ADS-B system is operational since the end of March 2018. To70 has airborne coverage around Amsterdam Airport Schiphol. An alternative source for the ADS-B data could be The OpenSky Network³ (free for research) or commercial services from Flightradar24⁴ or FlightAware⁵.

3.2.1. Ground track

The ground track is the projection of the flight path on the Earth's surface. The ground track is obtained from the ADS-B position data. To illustrate the data used in this research, a selection of the ground tracks are illustrated in Figure 3.6. Because ADS-B position data contains uncertainty, the data cannot be used directly in the noise calculations. The position error (i.e. difference between actual and communicated position of the aircraft) can be deconstructed in two parts, the systematic error (bias) and the random error. It has been assumed that the bias was small compared to the distance to the NMT locations, therefore the bias was not taken into account in the data processing. In terms of ground track data processing, the following steps have been performed:

- Remove duplicate data points (time and/or position)
- Align the ground track with the runway
- Smooth using a weighted B-spline

Because the timestamps of the ADS-B data were stored for each whole second, flights sometimes contained more than one position within a single second. Additionally, the dataset sometimes contained a duplicate position which could also be removed. Alignment with the runway was required in order to combine the ground tracks with standard flight performance profiles. The weights of the B-spline are determined using the provided position uncertainty of the ADS-B data. The inverse of the position's standard deviation was used as weight, except for the positions that are already aligned with the runway. The positions aligned with the runway were assumed to have no uncertainty.

Because the ECAC Doc. 29 noise calculations should be performed in a local Cartesian reference frame, all position data in this research (including the NOMOS data) was converted to the Dutch *Rijksdriehoek* coordinate reference frame (EPSG:28992) using the approximation by Schreutelkamp & Van Hees [38]. This reference frame is also used in the studies by Schiphol [8, 18].

3.2.2. Altitude and ground speed

The flight path data used for the flight performance derivation not only contains the ground track, but also the altitude and velocity. Although the ADS-B data contains the required data, some processing is required to make it usable within this research.

¹GPS: Global Positioning System

²Automatic Dependent Surveillance-Broadcast - EUROCONTROL ATM Lexicon https://ext.eurocontrol.int/lexicon/index.php/Automatic_Dependent_Surveillance-Broadcast [accessed 22 December 2019]

³The OpenSky Network - Free ADS-B and Mode S data for Research. <https://opensky-network.org/> [accessed 12 November 2019]

⁴Data services - data tailored to your business requirements | Flightradar24. <https://www.flightradar24.com/commercial-services/data-services> [accessed 12 November 2019]

⁵APIs FlightAware. <https://uk.flightaware.com/commercial/data> [accessed 12 November 2019]

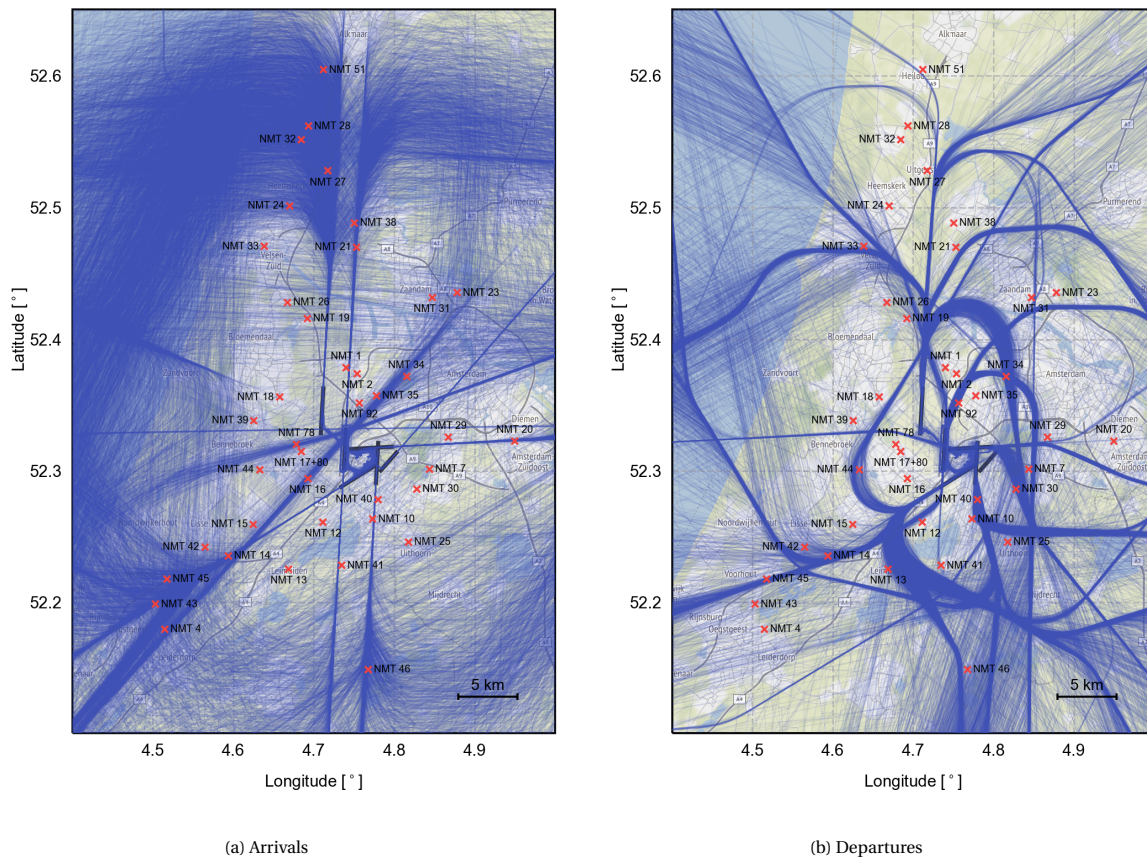


Figure 3.6: The ADS-B ground tracks of all A320 aircraft used in this research.

The altitude relative to the observers must be known to perform a noise calculation. From ADS-B data this can be obtained using the barometric altitude and the difference between the barometric altitude and the GNSS⁶ altitude. This information is not communicated within a single ADS-B message. The barometric altitude is part of the ADS-B position message, whereas the difference between the barometric altitude and the GNSS altitude is part of the ADS-B velocity message. Since ADS-B position messages are sent with different time intervals than the velocity messages, the data must be interpolated. Furthermore, the data must also be smoothed, because ADS-B messages can only contain discrete values for most parameters including the altitude and ground speed [20]. A weighted one-dimensional 3rd-order polynomial B-spline was used in order to do this. Similar to the ground track smoothing, weights are used to take into account the altitude uncertainty. Since the standard deviation was not available for the altitude, it was assumed that the step size was equal to 4 standard deviations. For the altitude the step size was 25 feet, leading to a standard deviation of 6.25 feet.

For a noise calculation, the ground speed V is required as is shown in subsection 2.1.2. Related is the acceleration a which is required to estimate the corrected net thrust as explained in subsection 2.4.3. Unlike the acceleration, the ground speed is contained in the ADS-B velocity data. Similar to the method described above, the ground speed is interpolated and smoothed. The acceleration could be determined by using the derivative of the ground speed. Unlike the altitude, smoothing of the velocity required a more delicate approach, since the derivative of the smoothed function was used for the thrust estimation. Too much smoothing would cause the thrust setting to be smoothed as well, making it hard to encapsulate abrupt changes in thrust setting, while changes in the thrust setting are generally applied within a short time frame. Therefore a 5th-order polynomial B-spline was used to smooth the ground speed, such that the acceleration would be based on a 4th-order polynomial B-spline, which would allow for more rapid changes in the thrust setting compared to a lower order polynomial B-spline. Similar to the altitude and ground track smoothing, weights are used to take into account the ground speed uncertainty. Since the standard deviation was not available for the altitude and the speed, it was assumed that the step size was equal to 4 standard deviations. For the

⁶GNSS: Global Navigation Satellite System

ground speed the step size was 1 knot, leading to a standard deviation of 0.25 knot.

3.2.3. Missing & ignored data

During the period of interest, there have been system outages, leading to missing data for those periods of time. The number of observations can be found in Figure C.5b, showing that May is largely affected by the missing data. It is expected that these outages will not impact the results of the study, except for a decrease in the number of total observations.

ADS-B receiver outages are not the only reason that not all flights are detected using ADS-B. ADS-B signals have to be sent actively by the aircraft, using an ADS-B transponder. Not all aircraft are currently equipped with an ADS-B transponder. Based on numbers by Eurocontrol⁷, the number of ADS-B equipped aircraft has grown rapidly in the past years. At the moment of writing, more than 50% of all EU-registered aircraft are equipped with ADS-B transponders, while the coverage in July 2018 was only slightly above 20%. Furthermore, since the ADS-B receivers are privately operated, the ADS-B receivers might not receive messages on the airport terrain itself because it has no line-of-sight coverage. Since coverage on the ground is required to identify (and align with) the runway, some flights did not contain sufficient data to be used in this research, which also decreased the number of flights that could be analysed.

The limitations of the ADS-B system were not the only reason that noise calculations could not be performed on all flights for which measurements were available. Some flights could not be calculated due to one of the following reasons:

- unknown ICAO type code
- no substitute in ANP database
- no standard performance profiles available

In some cases, the standard performance profiles were not available, since the substitution methods provided by the NLR are used. B738 is an example of an aircraft type which does not have a standard performance profile constructed by NLR, therefore it only has the default departure fixed point profile available from the ANP database, which does not allow us to assess the B738 arrivals.

For the remaining flights, it was found that some flights would return unrealistic calculated noise levels. The values above 120dBA are considered unrealistic, because higher values have not been measured (largest values for SEL and $L_{a,max}$ are 104dBA and 103.7dBA). It was found that these unrealistic results were largely related to the flight path that was used as input. Without removing results based on noise levels, the following requirements were used to objectively remove flights from further analysis:

- $\epsilon > 35^\circ$
- $V < 0$ m/s

In some cases the bank angles grew large because of insufficient smoothing of the ground track. This could happen, because it was assumed that the ground track would include a random error only. However, some ground tracks also contained outliers which could not be removed properly. There were also exceptional cases where the ground speed was zero. To mitigate issues with the noise calculations, these flights were also removed.

3.3. Meteorological data

To analyse the effect of using actual meteorological conditions instead of standard meteorological conditions, the actual conditions must be collected. The Royal Netherlands Meteorological Institute (KNMI)⁸ collects the meteorological conditions for every hour at Schiphol and provides free access to the data using an API or their website. Although the meteorological conditions might change every minute, it is assumed that using the hourly averaged meteorological conditions at the time of touchdown or liftoff is representative for the whole flight. Because the model does not include a high-fidelity lateral attenuation model such as proposed in [4], it is expected that hourly average conditions will result in sufficiently accurate results. The time of touchdown (for arrivals) or liftoff (for departures) is provided by Schiphol in the CISS⁹ data.

⁷ADS-B Implementation Status <https://ads-b-europe.eu> [accessed 22 December 2019]

⁸KNMI - Uurgegevens van het weer in Nederland - Download. <http://projects.knmi.nl/klimatologie/uurgegevens/selectie.cgi> [accessed 28 August 2019]

⁹CISS: Centraal Informatie Systeem Schiphol

3.4. Data processing

How the data is processed can be found in Figure 3.7. In section 3.2 it is explained how the position and velocity data is obtained. In section 3.3 it is described how the meteorological data is obtained. How the stage length, standard performance profile, and travelled distance shift are determined is described in chapter 2, as well as how the noise levels are calculated. However, it has not yet been explained how the various flight data sources (i.e. CISS, ADS-B and ANOMS) are connected to each other. This will be explained in the following section. A more detailed description of the total calculation procedure can be found in Appendix B.

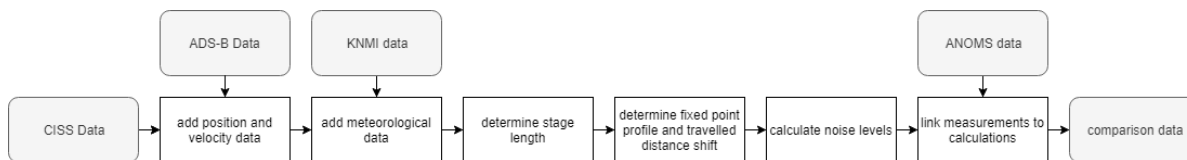


Figure 3.7: The flowchart visualising how the data is processed to obtain the desired data for comparison.

3.4.1. Correlation of flight data

As can be seen in Figure 3.7, position and velocity data is added to the CISS data. In order to do this, the CISS flights must be correlated to the ADS-B flights. Similarly, the measurements from ANOMS must be linked to the calculations. This is a problem, since the flight data of these three sources is not equal.

To tackle this problem, a method was developed which used the available properties in all datasets, namely the callsign and timestamp(s). While the CISS data only included a single timestamp, the ADS-B and ANOMS data included both a start- and end timestamp. The single timestamp included in the CISS data is the time of touch down for landings or time of lift-off for departures. ADS-B and ANOMS data include the timestamps of the observations (ANOMS data is based on radar data from LVNL).

To add the ADS-B data to the CISS data, all flights with the same callsign were grouped. Within these groups it was checked for each CISS flight if the timestamp is located within the start and end time of the ADS-B data. In case of double matches, both results were removed. Flights without any matches were not considered in the research, since the data was incomplete. After the CISS and ADS-B flight data are linked, a similar procedure was used to link the ANOMS data to the CISS and ADS-B flight data.

4

Results

Using the methods described in chapter 2 and the data as described in chapter 3, the noise levels of 151,108 flights could be calculated. Related to these flights were a total of 385,001 measurements that could be compared with calculations. A decomposition of the flight and measurement count for each type of operation can be found in Table 4.1. A more detailed decomposition of the data-set can be found in Appendix C.

Table 4.1: Result counts for each type of operation. The table lists the number of unique flights and unique measurements for which L_{AE} and $L_{A,max}$ have been calculated.

type of operation	flights	measurements
arrival	77,514	172,098
departure	73,594	212,903

As mentioned before, three calculation methods were used to calculate the noise levels for each flight. These three calculation methods are listed in Table 4.2. The following sections will address the results of each of these methods. Starting with the results of the baseline method (method A) in section 4.1. Addressing the results of using the actual meteorological conditions (method B) and comparing these with the baseline in section 4.2. After this, the effects of using derived flight performance (method C) instead of standard flight performance will be shown in section 4.3. Lastly, it was mentioned in section 2.3 that various noise level corrections could be applied afterwards to account for the effect of difference in certified noise levels between specific aircraft configurations. The effects of applying these various substitution corrections will be provided in section 4.4.

Table 4.2: The research matrix. Derived flight performance is not combined with standard meteorological conditions because the meteorological conditions are used to derive the flight performance.

	standard flight performance	derived flight performance
standard meteorological conditions	A (baseline)	-
actual meteorological conditions	B	C

4.1. The baseline method

The sound exposure level results of the baseline method are visualised in Figure 4.1. Similar to other research, a scatterplot is used in Figure 4.1a to show how the measurements are related to the calculations. If the calculations would match the measurements perfectly, the results would all be located on the diagonal dashed line. This diagonal dashed line indicates a perfect correlation between the measurements and calculations. To quantify the correlation between the measurement and the calculation, the Pearson correlation coefficient R is determined for the data. A perfect correlation as indicated with the dashed line would have a value of

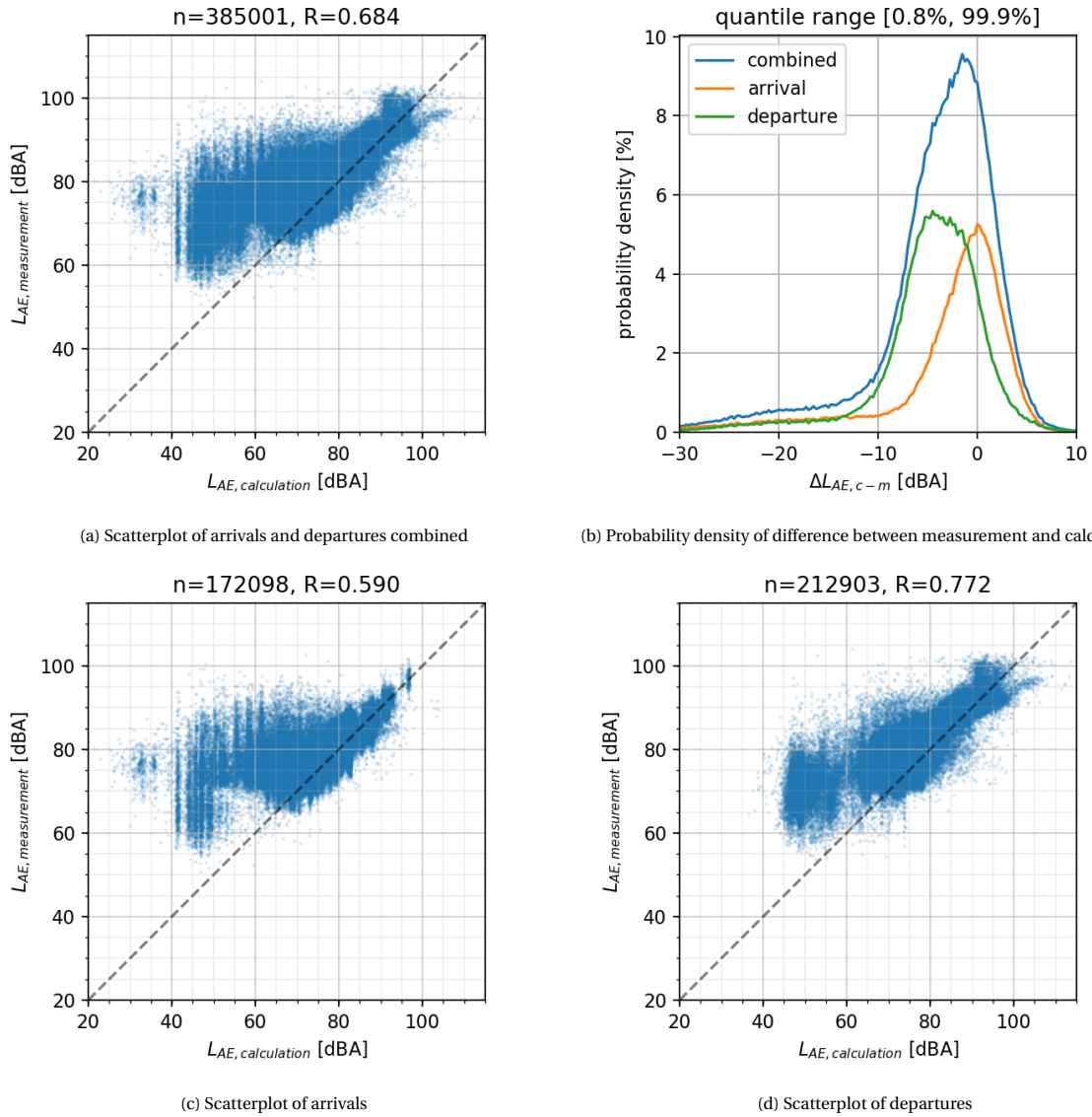


Figure 4.1: Collection of all sound exposure level results using the baseline calculation method.

$R = 1$. Together with the number of results n shown in the figure, the Pearson correlation coefficient R can be found above the figure. With a value of $R = 0.684$ shown in Figure 4.1a it is indicated that the measurements and calculations have a positive correlation, meaning that within this dataset a larger measured noise level will typically result in a larger calculated noise level. Furthermore, since $R \neq 1$, it can be concluded that the measurements are not perfectly correlated. However, R in itself does not tell us more about the absolute differences between the measured and calculated noise levels, it only indicates how they perform relative to each other. For absolute values, one should look at the noise levels themselves. From the figure it can be seen that measurements typically do not drop below 55dBA, whereas the calculated noise levels can get as low as 25dBA. For calculated noise levels up to 60dBA, almost all measurements are larger than the calculations. Furthermore, it can be observed in this figure that the measurements are often larger than the calculations. At least more often than they are smaller than the calculations.

To further examine the differences between the measurements and the calculations, the results are separated by type of operation. In Figure 4.1c the results of the arrivals are shown, while Figure 4.1d shows the results of the departures. In Figure 4.1c the results with calculated noise levels above 80dBA seem to be centered around the dashed line, indicating that around half of the time the measurements are higher than the calculations. The other half of the time the measurements are below the calculations. In contrast, the calculated noise levels below 65dBA typically have higher measured noise levels associated with them. This indi-

cates that the results below calculated noise levels of 65dBA might not be correlated with the measurements. These two observations could also be made in the scatter plot with all results, still the correlation coefficient of $R = 0.590$ is lower than the overall correlation coefficient. This is probably related to the group of results that can be identified with measured results below 70dBA and calculated results below 60 dBA. Additional analysis showed that this group was related to NMT80, which will be addressed later in this section. Lastly, vertical patterns could be observed in the arrival results. Similar results have been found in [41], where they were attributed to assumptions in the calculations which will be further discussed in chapter 5. Looking at the departure results in Figure 4.1d, it can be seen that calculated noise levels below 65dBA typically have measured noise levels that are larger than the calculated noise levels, which is again similar to the other results. Again, a group of results (below calculated values of 60dBA) can be seen in the departure results which can also be attributed to NMT80. Unlike arrivals, where the results with calculated noise levels above 80dBA seem to be centered around the dashed line, the results of the departures seem to be typically above the dashed line. Furthermore, where for the arrivals the differences between measurement and calculation seem to converge with increasing noise levels, the departures show divergence. An example of this is the group of results with calculated values above 100dBA. Additional analysis showed that this group of results is related to NMT40.

It is observed that both calculated and measured noise levels can be higher for departures compared to arrivals. Ultimately, the difference between the measurement and the calculation is of interest. Although the scatter plots provide us with an insight of how the measurements and calculations are related, this visualisation technique makes it hard to spot and quantify the typical differences between measurement and calculation. Therefore the probability density curve of the differences between the measurement and calculation is shown in Figure 4.1b. Additionally, the probability density is separated for each type of operation. Again, it can be seen in this figure that the measurements are often larger than the calculations. Furthermore, the difference in modelling performance between arrivals and departures becomes very clear. Whereas the maximum probability density is located at zero for arrivals, the maximum probability density for departures is located at -5dBA. Furthermore, the width of the arrival curve is smaller compared to the departure curve.

Although the L_{AE} results are shown in these figures, the same visualisations have been created for the $L_{A,max}$ values in Figure E.1. Although other calculation methods will be discussed later in the results, the other methods have also been visualised using these four visualisations. These visualisations can be found in Appendix E for both L_{AE} as well as $L_{A,max}$.

4.1.1. Definition of long-term average noise

Long-term average noise can have many metrics, of which L_{DEN} and L_{night} are commonly used in The Netherlands [18]. These are weighted averages, used to address the issue that the time of day affects how people experience the annoyance of an aircraft flying over. Night flights are more annoying to residents compared to flights during daytime. For this research, the equivalent noise level normalised with the number of observations but without a weight factor will be used in to assess the long-term average noise.

$$L_{eq} = 10 \cdot \log_{10} \left(\frac{1}{N} \sum_{i=1}^N 10^{L_{AE,i}/10} \right) \quad (4.1)$$

where L_{eq} is the equivalent noise level in dBA, N is the number of observations, i is the index of the observation, and $L_{AE,i}$ is the sound exposure level of the observation i in dBA.

This method is used because it is of primary interest for this research to get a better understanding of the long-term average differences between measurement and calculation. Time-based weighting will not contribute to this because the weighting factors will be the same for both the measurement and calculation. For the three methods listed in Table 4.2 the L_{DEN} values will also be provided as a reference to see if the time-based weighting influences the observed differences between the calculated and measured long-term average noise levels. Since both methods include the results of all noise monitoring terminals, it should be stressed that the values are not related to a single physical location. Therefore they should only be compared to the values of other methods.

Although the $\Delta L_{eq,c-m}$ results are already provided for aircraft types and noise monitoring terminals in Figure 4.2 and Figure 4.3, for the baseline method it was found that $L_{eq} = 82.59$ dBA and $L_{DEN} = 65.52$ dBA. For reference, the measured L_{eq} and L_{DEN} are 83.69dBA and 66.58dBA, which equals a difference of $\Delta L_{eq,c-m} = -1.10$ dBA and $\Delta L_{DEN,c-m} = -1.06$ dBA. Separated by type of operation, the calculated L_{eq} values are 81.82dBA for arrivals and 83.41dBA for departures. Comparing these with measured values of 82.49dBA and 84.71dBA for arrivals and departures, differences of -0.67dBA and -1.30dBA could be observed.

L_{DEN} and L_{eq} use different weighting, still the values are close to each other and both show that measured long-term average noise levels are higher compared to calculated long-term average noise levels. Furthermore, it is found that long-term average noise level of departures is around 3dBA higher compared to the noise level of arrivals. In Figure 4.1b it could be seen that the differences between measurement and calculation of single events are typically larger for departures when compared to arrivals. The same can be seen for the long-term average noise level, however, the performance of departures and arrivals is closer to each other. Where $\Delta L_{eq,c-m} = -0.67$ dBA for arrivals is below the maximum probability density at 0dBA from Figure 4.1b, $\Delta L_{eq,c-m} = -1.30$ is above the maximum probability density at -5dBA for departures. This indicates that the probability density visualisation is useful for comparison of the noise levels of individual events, but is not necessarily useful for the estimation of the long-term average noise level.

4.1.2. Uncertainty of long-term average noise

The difference between measurement and calculation of individual noise levels can be very large. The probability density values in Figure 4.1b provide an estimation of the uncertainty of the observed difference between measurements and calculations of individual events. However, the probability density is not necessarily related to the differences that are observed between the calculated and measured long-term average noise levels. This is required to indicate how much confidence there is that the difference that is observed is actually occurring. A different approach is required to estimate the uncertainty of the long-term average noise levels. The long-term average noise level is based on all single-event noise levels. Therefore, only one long-term average noise level can be calculated. The long-term average noise level is not linearly related to single-event noise levels and neither are their probability density functions. Therefore, a different approach is required to assess the uncertainty of the long-term average noise level. A statistical bootstrapping method is used to quantify the uncertainty of the long-term average noise levels (Appendix H). The results of the statistical bootstrapping method are used to construct a confidence bound for the long-term average noise level.

It was found that $\Delta L_{eq,c-m} = -0.67 \pm 0.07$ dBA for arrivals and $\Delta L_{eq,c-m} = -1.30 \pm 0.24$ dBA for departures. Although the absolute values of these uncertainties cannot be related to the uncertainty of $\Delta L_{AE,c-m}$ directly, it is clear that the larger uncertainty of $\Delta L_{AE,c-m}$ for departures (when compared to arrivals) can also be observed in the results of the long-term average noise level uncertainties.

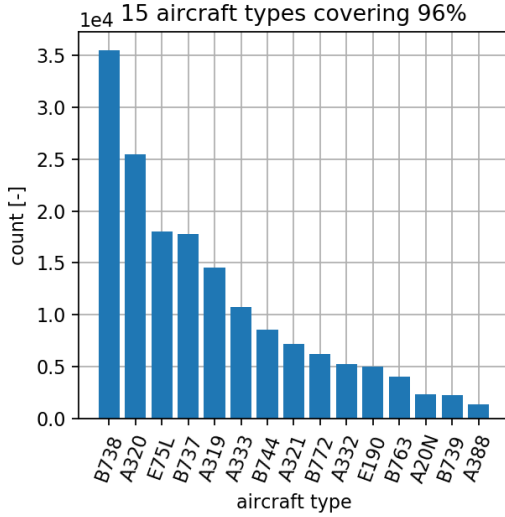
4.1.3. Separated by aircraft type

To show the influence of the aircraft type on the difference between measurement and calculation, $\Delta L_{eq,c-m}$ and $\Delta L_{AE,c-m}$ for each aircraft type are visualised in Figure 4.2. The figure only shows the most common aircraft types, together they cover at least 95% of all observations. The number of measurements for all aircraft types can be found in Appendix C. The subfigures in Figure 4.2 list the number of unique observations (sorted by number of observations) and the typical differences between calculation and measurement. The boxplots indicate the difference of individual noise levels $\Delta L_{AE,c-m}$, the red arrow indicates the difference of the long-term average noise level $\Delta L_{eq,c-m}$. Similar to the figure with all results in a scatter plot, the data is split by type of operation. From Figure 4.2 a difference in behavior can be observed in terms of the relation with the aircraft type.

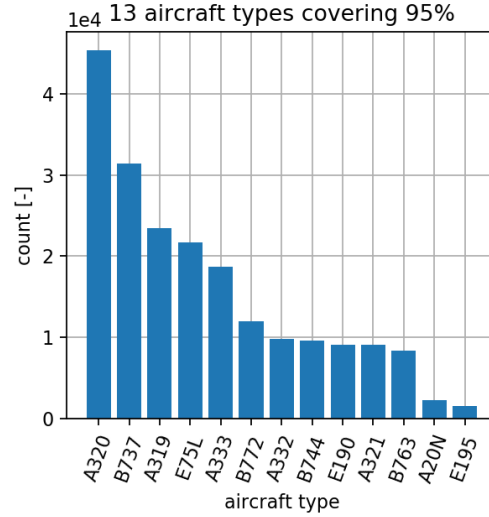
For arrivals it can be seen that typical differences between measurements and calculations vary between aircraft types. For instance, the aircraft types B738 and B744 both have a median and $\Delta L_{eq,c-m}$ close to zero. However the whiskers of the B744 boxplot span less than 20 dBA, whereas the B738 whiskers span more than 20 dBA. For departures it can also be observed that the aircraft type influences the differences between measurement and calculation. Compared to the arrivals, the differences between aircraft types are larger. Furthermore, for the same aircraft type, $\Delta L_{AE,c-m}$ for arrivals might be different from $\Delta L_{AE,c-m}$ for departures. An example is aircraft type A320 which shows more underestimations for arrivals compared to the departures e.g. $(\Delta L_{eq,c-m})_{arrivals} > (\Delta L_{eq,c-m})_{departures}$. The figure with departures also includes some clear examples where it is shown that $\Delta L_{eq,c-m}$ is not necessarily related to the distribution of $\Delta L_{AE,c-m}$. For instance, for aircraft type B772 it is shown that event noise levels $\Delta L_{AE,c-m}$ are typically underestimated ($\Delta L_{AE,c-m} < 0$ dBA), while the long-term average noise level is overestimated ($\Delta L_{eq,c-m} > 0$ dBA).

It can also be observed from these results that not all aircraft types are present for both arrivals and departures. For instance, aircraft type B738 is not present in departures. This is a result of the fact that there were no standard flight performance profiles available for departures and only one standard flight performance profile for arrivals.

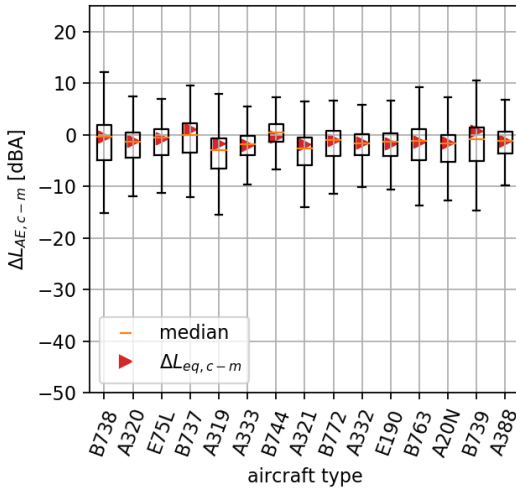
To further quantify the effect of the aircraft type on the difference between measurement and calculation



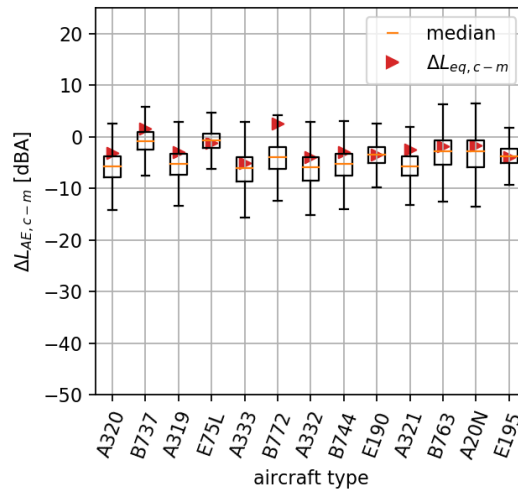
(a) Number of measurements from arrivals, separated by aircraft type



(b) Number of measurements from departures, separated by aircraft type



(c) Difference between measurement and calculations for arrivals, separated by aircraft type



(d) Boxplot of departures

Figure 4.2: Result for each aircraft type and type of operation combination.

$\Delta L_{AE,c-m}$, a number of statistical methods are used. From the probability density visualisations it is clear that the data is not normal distributed, therefore non-parametric statistics must be used. The Kruskal-Wallis test is a non-parametric statistic that uses ranks to determine if there are differences between various groups [14]. As explained in [14], the results of the Kruskal-Wallis test are commonly reported as $H(k-1) = \nu$, where ν is the value of the test-statistic and k is the number of groups tested. Additionally, the p -value is provided. The p -value indicates the probability of seeing significant effect, while in reality there isn't. Using Fisher's criterion, a result is significant if the p -value is below 0.05.

In this analysis each aircraft type represents a single group. Although the difference between measurement and calculation is defined as the calculation minus the measurement ($\Delta L_{AE,c-m}$), testing this will only tell if the results of aircraft type A are more often over-estimated compared to aircraft type B. Therefore, the absolute difference between measurement and calculation $|\Delta L_{AE,c-m}|$ is also tested, because this value will tell directly if the calculations are closer to the measurements for aircraft type A compared to aircraft type B. The statistical tests conducted for this section, as well as the tests in the remainder of the report, are conducted using IBM SPSS¹.

Using the Kruskal-Wallis test it was found that $\Delta L_{AE,c-m}$ was significantly affected by the aircraft type

¹<https://www.ibm.com/analytics/spss-statistics-software>

of the arrival measurement ($H(68) = 11071.6$, $p < 0.001$). $|\Delta L_{AE,c-m}|$ was also significantly affected by the aircraft type of the arrival measurement ($H(68) = 5607.2$, $p < 0.001$). From these results it is clear that some aircraft types are overestimated (or underestimated) more compared to others. However, the effect on the absolute difference between measurement and calculation is smaller than the effect on the signed values of the difference between measurement and calculation. Although this confirms the differences that were found in the visual findings, further analysis is required to determine how much effect the aircraft type has on the difference between measurement and calculation.

To follow-up these findings, Mann-Whitney tests were used. Whereas the Kruskal-Wallis test can be used to test multiple groups, a Mann-Whitney can only be used to test two groups with each other. However, using a Mann-Whitney the effect size can be determined. The Mann-Whitney test is commonly reported with the value of the Mann-Whitney test U and the effect size r . The effect size r provides an indication of the importance of the difference, with values being close to 0 not that important, while values beyond 0.5 are considered large effects and thus very important [14]. Since comparisons can only be performed per pair of groups, only the largest groups will be compared. To get an idea of the effect size within the arrival results, aircraft type B738 (representing the largest group) is compared to two aircraft types: A320 and E75L (i.e. the second and third largest group). The results can be found in Table 4.3.

Table 4.3: The effect of aircraft type on the difference between measurement and calculation of arrivals compared to aircraft type B738.

aircraft type	metric	compared to B738	Mann-Whitney test statistic U	effect size r
A320	$\Delta L_{AE,c-m}$	smaller	388620193	-0.12
A320	$ \Delta L_{AE,c-m} $	smaller	396532180	-0.10
E75L	$\Delta L_{AE,c-m}$	smaller	303057894	-0.04
E75L	$ \Delta L_{AE,c-m} $	smaller	272643320	-0.12

For departures it was found that $\Delta L_{AE,c-m}$ was also significantly affected by the aircraft type ($H(51) = 69574.7$, $p < 0.001$). Furthermore, $|\Delta L_{AE,c-m}|$ was also significantly affected by the aircraft type ($H(51) = 58472.7$, $p < 0.001$). To follow-up this findings, Mann-Whitney tests were used to determine the effects of A320 (the largest group) compared to B737 and A319 (the second and third largest group). These results can be found in Table 4.4.

Table 4.4: The effect of aircraft type on the difference between measurement and calculation of departures compared to aircraft type A320.

aircraft type	metric	compared to A320	Mann-Whitney test statistic U	effect size r
B737	$\Delta L_{AE,c-m}$	larger	193588475	-0.62
B737	$ \Delta L_{AE,c-m} $	smaller	247153425	-0.56
A319	$\Delta L_{AE,c-m}$	larger	484951436	-0.07
A319	$ \Delta L_{AE,c-m} $	smaller	484354610	-0.07

Based on the results for both the arrivals and the departures, it is clear that there are differences between aircraft types in terms of the difference between measurement and calculation. However, how the difference between measurement and calculation is affected depends on the aircraft type as well as the type of operation.

4.1.4. Separated by NMT

Similar to the separation by aircraft type, the results can also be separated by the noise monitoring terminal (NMT) at which the measurement took place. The results for the NMTs covering at least 95% of the results are visualised in Figure 4.3. The number of measurements for each NMT can be found in Appendix C. The subfigures in Figure 4.3 list the number of unique observations, sorted by number of observations and the typical difference between calculation and measurement. The boxplots indicate the difference of individual noise levels $\Delta L_{AE,c-m}$, the red arrow indicates the difference of the long-term average noise level $\Delta L_{eq,c-m}$. Additionally, the roof locations are marked with a star * in the bottom figures. Similar to the figures with results separated by aircraft type, the data is split by type of operation and a difference in performance can be observed between the two groups.

From Figure 4.3 it can be observed that the differences between measurement and calculation are affected by the NMT. Moreover, compared to the separation by aircraft type, the differences between measurement

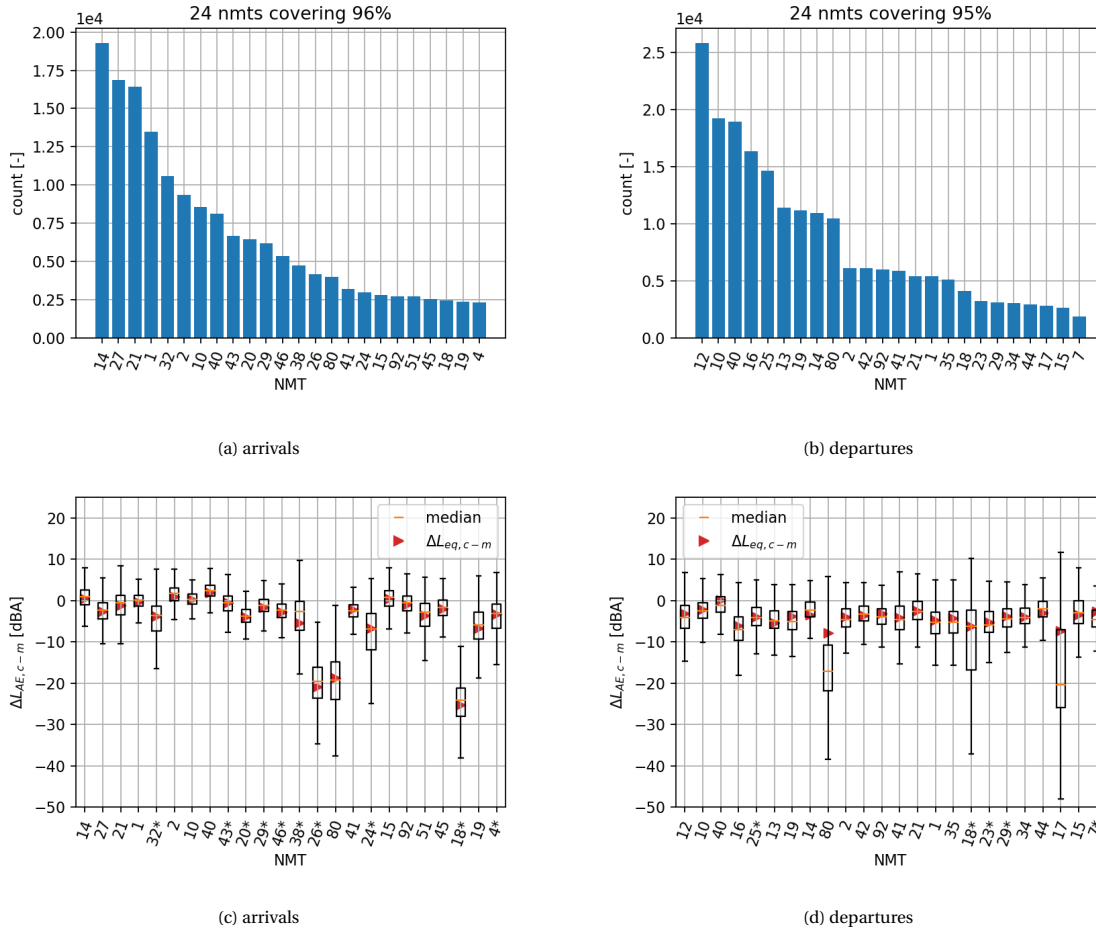


Figure 4.3: Result for each NMT and type of operation combination.

and calculation seem to be more affected by the NMT than the aircraft type, because the observed differences between NMTs are larger. For some NMTs, the differences are so large that they could even be considered as outliers. Examples of such NMTs are 18, 26 and 80 for arrivals and 18, 18 and 80 for departures.

Using the Kruskal-Wallis test as explained in the previous section, it was found that for arrivals $\Delta L_{AE,c-m}$ was significantly affected by the NMT of the measurement ($H(40) = 74054.6, p < 0.001$). $|\Delta L_{AE,c-m}|$ was also significantly affected by the NMT of the measurement ($H(40) = 48440.1, p < 0.001$). To follow-up this finding, Mann-Whitney tests were used to determine the effects of NMT 14 (the largest group) compared to NMT 27 and NMT 21 (the second and third largest group). The results of these tests can be found in Table 4.5.

Table 4.5: The effect of NMT on the difference between measurement and calculation of arrivals compared to NMT 14.

NMT	metric	compared to NMT 14	Mann-Whitney test statistic U	effect size r
27	$\Delta L_{AE,c-m}$	smaller	65467766	-0.52
27	$ \Delta L_{AE,c-m} $	larger	132851768	-0.16
21	$\Delta L_{AE,c-m}$	smaller	109429590	-0.27
21	$ \Delta L_{AE,c-m} $	larger	143458022	-0.08

For departures, it was found that $\Delta L_{AE,c-m}$ was significantly affected by the NMT of the measurement ($H(40) = 51676.6, p < 0.001$). Furthermore, it was found that $|\Delta L_{AE,c-m}|$ was also significantly affected by the NMT of the measurement ($H(40) = 48720.9, p < 0.001$). To follow-up this findings, Mann-Whitney tests were used to determine the effects of NMT 12 (the largest group) compared to NMT 10 and NMT 40 (the second and third largest group). The results of these tests can be found in Table 4.6.

Based on the results for both the arrivals and the departures, it is clear that there are differences between NMTs in terms of the difference between measurement and calculation. However, how the difference be-

Table 4.6: The effect of NMT on the difference between measurement and calculation of departures compared to NMT 12.

NMT	metric	compared to NMT 12	Mann-Whitney test statistic U	effect size r
10	$\Delta L_{AE,c-m}$	smaller	184241472	-0.22
10	$ \Delta L_{AE,c-m} $	larger	174919937	-0.25
40	$\Delta L_{AE,c-m}$	smaller	134485471	-0.39
40	$ \Delta L_{AE,c-m} $	larger	152054463	-0.33

tween measurement and calculation is affected depends on the NMT as well as the type of operation. Although the results for all NMTs are analysed with the Kruskal-Wallis statistic, it should be noted that NMT80 and NMT78 are low-frequency NMTs. As mentioned before, it could be observed that typical values from NMT80 are different from other stations based on the visualisations in Figure 4.3. Therefore the data from low-frequency NMTs is removed from the comparison in the following sections.

4.2. Effect of meteorological adjustment

To get an idea of the effect of the meteorological adjustment, the results of method A and method B from Table 4.2 are compared with each other. Both calculation methods use standard aircraft performance, but where method A uses standard meteorological conditions, method B uses actual meteorological conditions. The comparison is performed by analysing the difference between measurement and calculation. Although the noise level differences are of primary interest, it is good to have a better understanding of the differences between the standard meteorological conditions and the actual meteorological conditions as well. Therefore, histograms of the actual meteorological conditions (wind direction, wind speed, pressure, temperature, and relative humidity) can be found in Figure C.3.

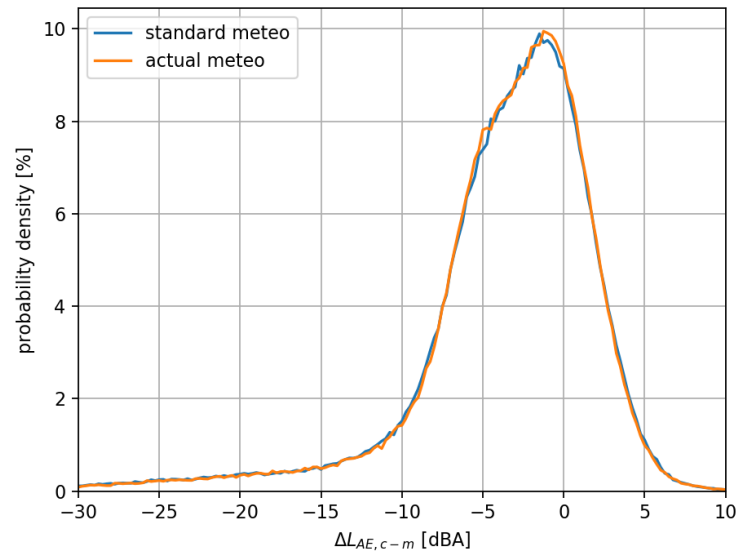


Figure 4.4: The probability densities of the standard flight performance method using both standard and actual meteorological conditions. Metric used in this comparison is the sound exposure level.

Similar to the baseline method, multiple scatter plots and a probability density visualisation have been created and can be found in Figure E.2. It can be observed that the correlation coefficient of the arrivals increases slightly (from $R = 0.590$ to $R = 0.593$), leading to a small (+0.002) increase in the correlation coefficient of both arrivals and departures combined. The probability density of $\Delta L_{AE,c-m}$ for actual conditions is compared with the probability density of the baseline method in Figure 4.4. From this figure alone, it is difficult to pinpoint the difference between the two methods, therefore additional analysis is required to identify the effect of using actual meteorological conditions.

The differences between measurement and calculation of the long-term average noise level can be found

Table 4.7: The long-term average noise levels for method B: the calculation method using standard flight performance profiles and actual meteorological conditions.

Noise level	Difference with measurement
$L_{eq} = 82.52\text{dBA}$	$\Delta L_{eq,c-m} = -1.17\text{dBA}$
$L_{DEN} = 65.52\text{dBA}$	$\Delta L_{DEN,c-m} = -1.06\text{dBA}$

Table 4.8: The long-term average noise levels uncertainties for method B: the calculation method using standard flight performance profiles and actual meteorological conditions separated by type of operation.

Type of operation	$\Delta L_{eq,c-m}$ [dBA]
arrival	-0.80 ± 0.07
departure	-1.33 ± 0.24

in Table 4.7 and in Table 4.8. Comparing these results with the results of the baseline method, it can be seen that L_{DEN} is equal and the uncertainties of $\Delta L_{eq,c-m}$ for both arrival and departures are equal. L_{eq} values are slightly different, with a difference of 0.07dBA for both operations combined, 0.13dBA for arrivals, and 0.03dBA for departures. For departures, this difference is smaller than the quantified uncertainty (0.03dBA < 0.24dBA), indicating that the difference between method A and method B on the departure calculations might also be attributed to the stochastic properties of this dataset. For arrivals, the difference is bigger than the quantified uncertainty (0.13dBA > 0.07dBA), indicating that the differences can be attributed to the different calculation methods. Using the actual meteorological conditions has a negative effect on the difference between the measured and calculated long-term average noise level of arrivals.

Although some differences are observed due to the use of actual meteorological conditions, these differences are rather small, therefore further analysis is required to get a better understanding of the effects on the calculated noise levels. The first step is to show that the behavior of the meteorological adjustment is physically correct, by assessing the differences between method A and B with a number of back-of-the-envelope calculations of the pure-tone absorption in various meteorological conditions.

4.2.1. Pure-tone absorption calculation

As explained in section 2.2, the meteorological adjustment consists of two components: the acoustic impedance correction and the NPD correction for non-reference atmospheric absorption. Although both are used in the noise calculations, the acoustic impedance correction is typically small (< 1dBA, see also Table 2.1), therefore the non-reference atmospheric absorption will cause the largest differences between the calculated noise levels using standard and actual meteorological conditions. To see if the atmospheric attenuation model is working properly, the modelled results are compared with back-of-the-envelope calculations of the pure-tone absorptions.

In this research, the NPD data is corrected using the atmospheric attenuation model described in standard SAE ARP5534. SAE ARP5534 uses the temperature, relative humidity and pressure to determine the absorption coefficient. In Figure 4.5 the atmospheric absorption using SAE ARP5534 is shown. As can be seen in the figure, the meteorological conditions of the flights are distributed over a wide range of temperatures and relative humidities. The standard meteorological condition ($T = 15^\circ\text{C}$, $h_{rel} = 70\%$, $p = 101325\text{Pa}$) is located roughly in the centre of all observations. It can be observed that the temperature has a strong negative correlation with relative humidity ($R = -0.655$), indicating that an increase in temperature is often related to a decrease in relative humidity. From this figure, it can also be observed that the frequency influences the way that the atmospheric absorption depends on temperature and humidity. This is the reason why it cannot be concluded that a change in temperature only, will always lead to higher (or lower) atmospheric absorptions. For the indicated frequencies, the atmospheric absorption will only increase with temperature for $f = 1000\text{Hz}$ and even for this frequency it is only true for increasing temperatures starting from the standard meteorological conditions. However, in combination with the negative correlation of temperature and relative humidity, it is expected that for this dataset, a temperature increase will lead to an increasing absorption coefficient. Consequently, this will result in lower calculated noise levels compared to standard meteorological conditions.

To get a better understanding of the relation between change in atmospheric absorption and change in event noise levels (L_{AE}), a number of flights are analysed in more detail.

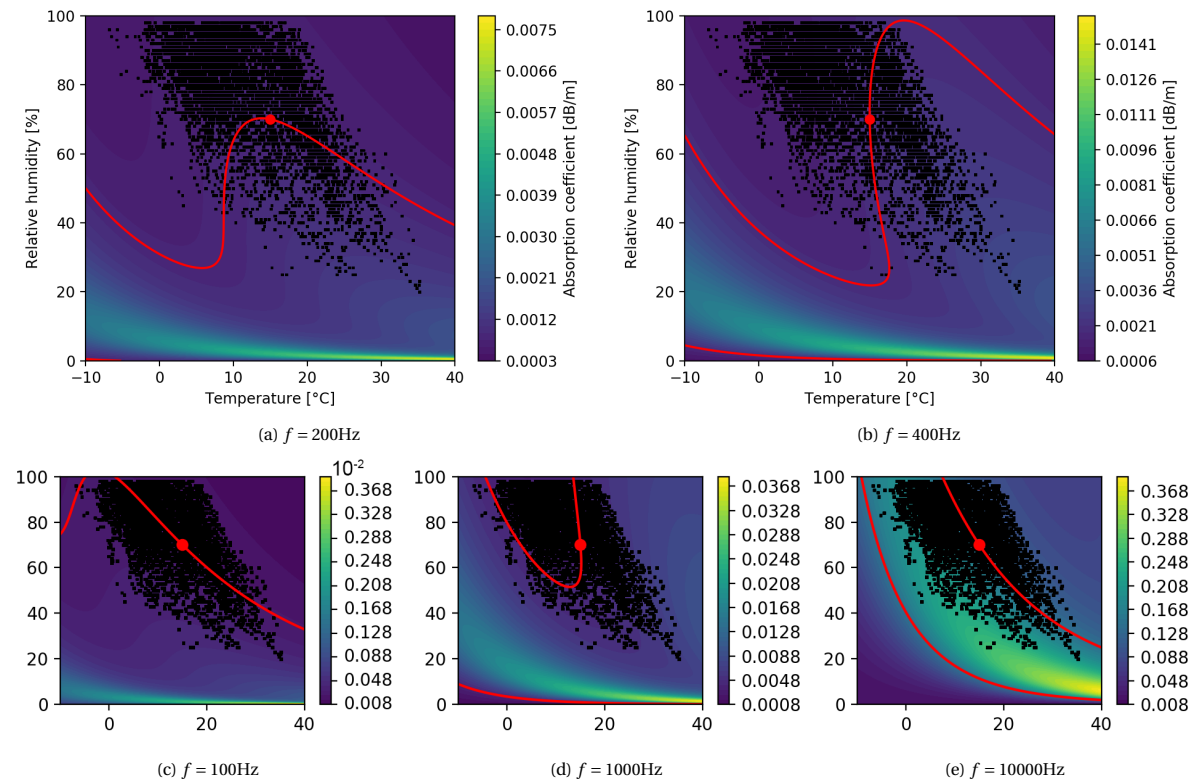


Figure 4.5: The SAE ARP5534 absorption coefficients α_{5534} at various frequencies, using $p = 101325\text{Pa}$. The black dots indicate the meteorological conditions at which the flights from this study took place, the red dot indicates the relative humidity and temperature of the standard meteorological condition, and the red line indicates the conditions at which the absorption coefficient is equal to the absorption coefficient at the standard meteorological condition. The axis for the smaller figures (c, d, and e) are equal to the axis of the larger figures (a and b).

Method

The flights used are listed in Table 4.9 with their corresponding meteorological conditions. All flights are with aircraft type A320, because it has the most arrivals and departures as can be seen in Figure 4.2. Furthermore, two arrivals and two departures are used, because departures and arrivals make use of a different noise spectra. For each type of operation, a flight with meteorological conditions close to average temperature ($10^\circ\text{C} < T < 15^\circ\text{C}$) was selected, as well as a flight at an extreme temperature ($T > 30^\circ\text{C}$). The flights are selected based on the number of measurements available. Wind speed for all flights equal or below 5 m/s.

Table 4.9: The flights used for the back-of-the-envelope calculation.

Flight ID	Type of operation	Temperature	Pressure	Relative humidity
873320	arrival	35.2 °C	101000 Pa	20 %
865993	departure	34.3 °C	101230 Pa	35 %
724261	arrival	13.4 °C	101920 Pa	87 %
725469	departure	11.6 °C	101870 Pa	97 %

The following steps are performed for each flight:

1. Determine the absorption coefficient at the two meteorological conditions for two atmospheric attenuation models: ARP 5534 and ARP866B.
2. Determine the additional absorption due to the applied hourly average meteorological condition at the distance of 1000m
3. Determine the dominant frequency band at 1000ft after A-weighting

4. Perform back-of-the-envelope calculation using the minimum distance of the noise monitoring terminal (NMT) to the track.

Determine the absorption coefficient and the additional absorption

The absorption coefficient is calculated with two atmospheric attenuation models for the two meteorological conditions. ARP866B is the older atmospheric attenuation model and uses temperature and relative humidity to determine the absorption coefficient for a given frequency. ARP866B is provided as reference. ARP5534 is the newer atmospheric attenuation model and uses temperature, relative humidity and pressure to determine the absorption coefficient. ARP5534 is used for the final event noise calculations. The additional absorption due to the application of the actual meteorological conditions instead of the standard meteorological conditions is also visualised for a distance of 1000m to provide insight in the order of magnitude of the atmospheric absorption for various frequencies.

Determine the dominant frequency band

By visualising the spectral class of the aircraft in Figure 4.6, for which the data can be obtained from the ANP database, the dominant frequency can be determined. Since the spectral classes are provided at a reference distance of 1000ft (or 304.8m), this distance is also used to determine the dominant frequency. The dominant frequency is based on the A-weighted noise spectra. The dominant frequencies that can be obtained from the figures are 800Hz for arrivals and 1600Hz for departures.

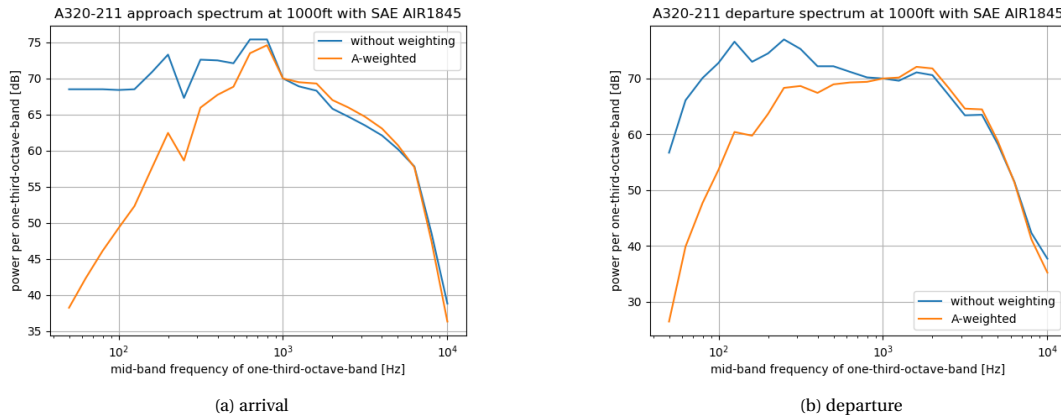


Figure 4.6: Noise level spectra for the A320-211.

The back-of-the-envelope calculation

The additional absorption at the dominant frequency band is calculated using the following equations to determine if the final results are consistent.

$$\Delta_{f_d} = (\alpha_{actual, f_d} - \alpha_{standard, f_d}) d_{min} \quad (4.2)$$

where f_d is the dominant frequency in Hz, Δ_{f_d} is the noise level difference at the dominant frequency in dB, α_{actual, f_d} is the absorption coefficient at the dominant frequency at the actual meteorological conditions in dB/m, $\alpha_{standard, f_d}$ is the absorption coefficient at the dominant frequency at the standard meteorological conditions in dB/m, and d_{min} is the minimum observed difference between the NMT and the track of the aircraft in m. Δ_{f_d} is calculated for both ARP866B and ARP5534.

Flight 873320: Arrival on runway 18C

The figure below (Figure 4.7) shows the absorption coefficient for the pure-tone frequencies. It can be seen that the absorption coefficient of the actual meteorological conditions is higher than the standard meteorological conditions for all frequencies for both models.

The event was observed at 3 NMTs. Since the absorption coefficient is larger for the actual meteorological conditions, the difference between the results of the baseline method and the method with actual meteorological conditions $\Delta L_{AE, a-s} = L_{AE, actual} - L_{AE, standard}$ increases with the distance to the track.

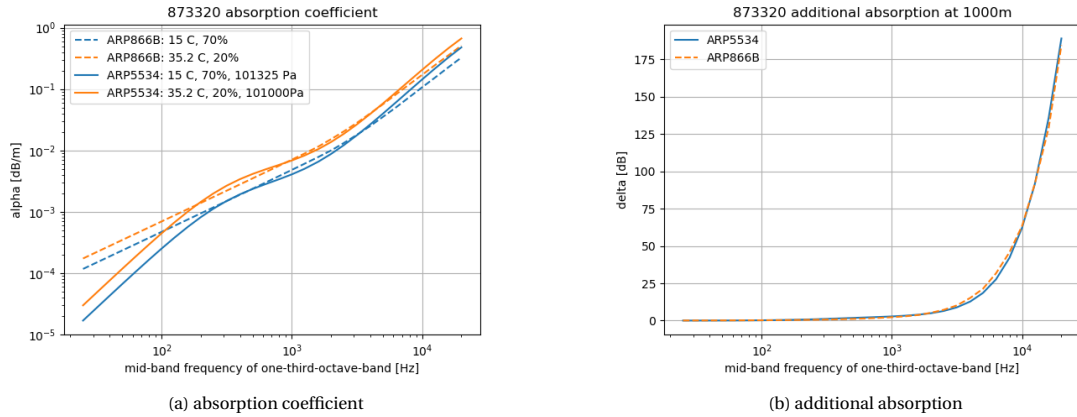


Figure 4.7: Noise level absorption coefficient for flight 873320 for various mid-band frequencies as well as the change in absorption compared to the baseline absorption.

Table 4.10: The flights used for the back-of-the-envelope calculation.

NMT	$L_{AE,actual}$	$L_{AE,standard}$	d_{min}	$\Delta L_{AE,a-s}$	$\Delta f_{d,5534}$	$\Delta f_{d,866B}$
1	82.5 dBA	83.9 dBA	409 m	-1.4 dBA	-1.0 dBA	-0.7 dBA
2	75.9 dBA	77.9 dBA	725 m	-2.0 dBA	-1.8 dBA	-1.3 dBA
21	74.4 dBA	76.6 dBA	822 m	-2.2 dBA	-2.0 dBA	-1.5 dBA

$\Delta f_{d,5534} > \Delta L_{AE,a-s}$ for all NMTs. An explanation could be that there is more absorption at higher frequencies. High frequencies have higher atmospheric absorption than lower frequencies, resulting in more dominance at small distances compared to large distances. This also explains that the difference at NMT 1 is also larger compared to NMT 2 and NMT 21.

$\Delta f_{d,866B} > \Delta f_{d,5534}$ for all NMTs. This difference is increasing with distance, indicating that this can be attributed to the dominant frequencies at larger distances, which are the lower frequencies.

Flight 865993: A320 Departure from runway 36C

In Figure 4.8 it can be seen that the absorption coefficient of the actual meteorological conditions calculated using ARP5534 is comparable to the standard meteorological conditions, except for the middle one-third-octave-bands. For ARP866B, the frequencies below 5kHz have larger absorption coefficients for the actual meteorological conditions when compared to the standard meteorological conditions.

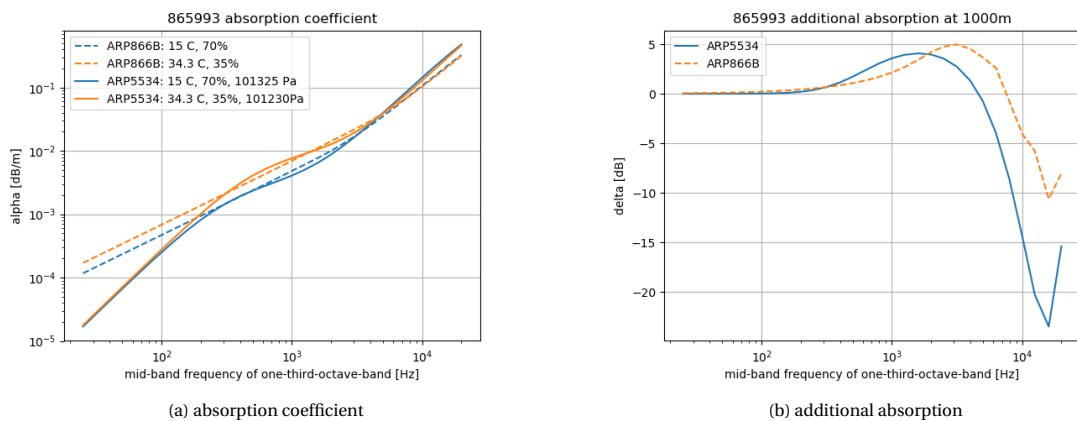


Figure 4.8: Noise level absorption coefficient for flight 865993 for various mid-band frequencies as well as the change in absorption compared to the baseline absorption.

The event was observed at 5 NMTs. Since the absorption coefficient is larger for the actual meteorological conditions at the dominant one-third-octave-bands, the difference between the results of the baseline

method and the method with meteorological correction increases with the distance to the track.

Table 4.11: The flights used for the back-of-the-envelope calculation.

NMT	$L_{AE,actual}$	$L_{AE,standard}$	d_{min}	$\Delta L_{AE,a-s}$	$\Delta_{f_d,5534}$	$\Delta_{f_d,866B}$
92	79.0 dBA	80.9 dBA	680	-1.9 dBA	-2.8 dBA	-2.3 dBA
34	74.3 dBA	76.6 dBA	1015	-2.3 dBA	-4.1 dBA	-3.5 dBA
2	72.4 dBA	74.8 dBA	1234	-2.4 dBA	-5.0 dBA	-4.2 dBA
29	66.9 dBA	69.7 dBA	1799	-2.8 dBA	-7.3 dBA	-6.2 dBA
7	66.4 dBA	69.2 dBA	1857	-2.8 dBA	-7.6 dBA	-6.4 dBA

$\Delta L_{AE,a-s} < \Delta_{f_d,5534}$ for all NMTs, indicating that this frequency has an above average atmospheric absorption, compared to the other frequencies. The difference between $\Delta L_{AE,a-s}$ and $\Delta_{f_d,5534}$ is increasing with the distance d_{min} , indicating that that average atmospheric absorption coefficient for all frequencies is lower than the absorption coefficient at 1600Hz.

$\Delta_{f_d,866B} > \Delta_{f_d,5534}$ for all NMTs. Similar to flight 873320 this difference is increasing with distance, indicating that this can be attributed to the dominant frequencies at larger distances: the lower frequencies. Around 1kHz, the additional absorption from ARP5534 is larger than ARP866B.

Flight 724261: A320 Arrival on runway 36R

In Figure 4.9 it can be seen that the absorption coefficient of the actual meteorological conditions is comparable for ARP5534, but overall lower than the standard meteorological conditions for all frequencies. The absorption coefficient for ARP866B is almost equal for frequencies up to 3kHz. After 3kHz, the absorption coefficient of the actual meteorological conditions is (similar to ARP5534) lower than the standard meteorological conditions.

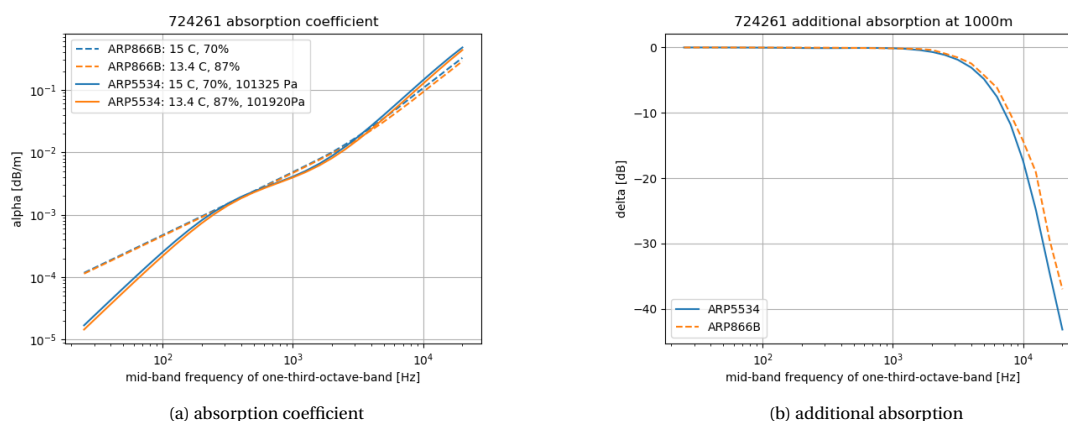


Figure 4.9: Noise level absorption coefficient for flight 724261 for various mid-band frequencies as well as the change in absorption compared to the baseline absorption.

The event was observed at 3 NMTs. Since the absorption coefficient is lower for the actual meteorological conditions, the difference between the results of the baseline method and method with meteorological correction increases with the distance to the track.

Table 4.12: The flights used for the back-of-the-envelope calculation.

NMT	$L_{AE,actual}$	$L_{AE,standard}$	d_{min}	$\Delta L_{AE,a-s}$	$\Delta_{f_d,5534}$	$\Delta_{f_d,866B}$
10	89.7 dBA	89.6 dBA	180	+0.1 dBA	+0.0 dBA	+0.0 dBA
40	85.1 dBA	84.8 dBA	282	+0.3 dBA	+0.0 dBA	+0.0 dBA
46	76.4 dBA	76.2 dBA	889	+0.2 dBA	+0.1 dBA	+0.1 dBA

Δ_{f_d} is close to zero for both methods, indicating that the absorption for both atmospheric attenuation models are comparable for the dominant frequency f_d of 800 Hz. Since the $\Delta L_{AE,a-s}$ shows larger differences,

there still is a change in absorption, which can be attributed to the decreased absorption at higher frequencies, since the values are increasing with distance d_{min} . Compared to the other cases, $\Delta L_{AE,a-s}$ shows the smallest numbers here due to the fact that the atmospheric conditions are closest to the standard meteorological conditions.

Flight 725469: A320 Departure from runway 06

In Figure 4.10 it can be seen that the absorption coefficient of the actual meteorological conditions is comparable for both atmospheric attenuation models, but overall lower than the standard meteorological conditions for all frequencies. Similar to the case study of flight 724261, the effect is larger for higher frequencies ($f > 3\text{kHz}$).

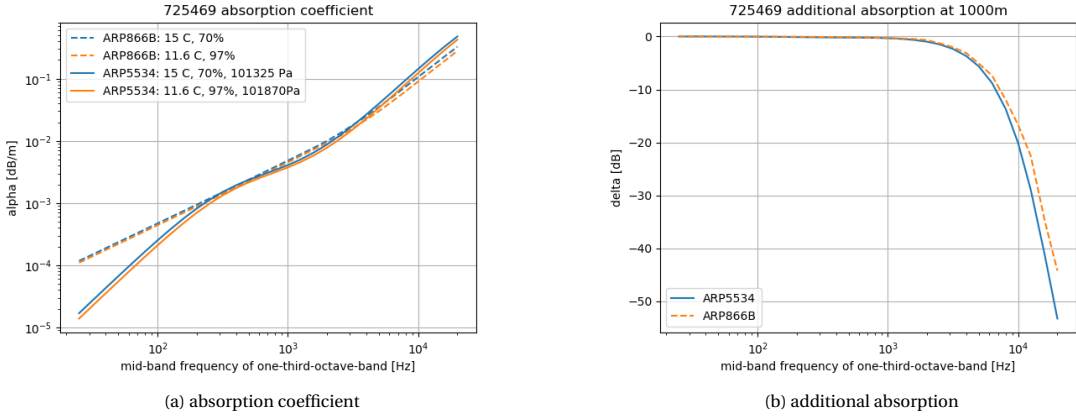


Figure 4.10: Noise level absorption coefficient for flight 725469 for various mid-band frequencies as well as the change in absorption compared to the baseline absorption.

The event was observed at 2 NMTs. Since the absorption coefficient is lower for the actual meteorological conditions at the dominant one-third-octave-bands, the difference between the baseline method results and the results using meteorological correction increases with the distance to the track.

Table 4.13: The flights used for the back-of-the-envelope calculation.

NMT	$L_{AE,actual}$	$L_{AE,standard}$	d_{min}	$\Delta L_{AE,a-s}$	$\Delta f_{d,5534}$	$\Delta f_{d,866B}$
30	79.7 dBA	79.3 dBA	842	+0.4 dBA	+0.6 dBA	+0.4 dBA
7	73.6 dBA	73.1 dBA	1393	+0.5 dBA	+0.9 dBA	+0.7 dBA

$\Delta f_{d,5534} > \Delta L_{AE,a-s}$ for all NMTs, indicating that there is a larger decrease in atmospheric absorption at the dominant frequency f_d of 1600Hz compared to other frequencies. Similar to the other departure case (flight 865993) where the absolute value of $\Delta f_{d,5534}$ was also larger than the absolute value of $\Delta L_{AE,a-s}$.

$\Delta f_{d,5534} > \Delta f_{d,866B}$ for all NMTs. For the distances used, the difference is not increasing. This might indicate that the differences over the various frequencies lead to a consistent change in noise level.

Discussion

Although there can be differences between the back-of-the-envelope calculation and the full modelled results, the sign and order of magnitude are comparable for all cases in the case study. The differences can be explained by the fact that the back-of-the-envelope calculation is performed on a single (i.e. pure-tone) frequency and does not include all frequency bands. In addition, the frequency was selected at the reference distance of 1000ft, whereas the dominant frequencies is depending on d_{min} as well. Furthermore the absorption of the pure-tone frequency is used and not the absorption of the frequency band as explained in subsection 2.2.2. This correction might result in lower absorption compared to the pure-tone frequency absorption. Based on the single frequency results, estimations could be made about the effect of the neighbouring frequencies, resulting in the conclusion that the atmospheric absorption correction is implemented correctly.

4.2.2. Statistics and pattern

As mentioned before, the overall differences between the two methods are rather small. Still differences could be found in the absorption coefficients over various meteorological conditions. To show that there are actually differences due to the use of actual meteorological conditions, a number of statistical methods are used in combination with the visualisation of the confidence bounds over various meteorological conditions.

As explained before, non-parametric statistics must be used because the data is not normal distributed. To investigate whether there are differences between the calculations using standard and actual meteorological conditions, a Wilcoxon's T-test is performed. As explained in [14], the results of the Wilcoxon's T-test are commonly reported as the lowest sum of either the positive or negative ranks. Additionally, the p -value is provided, which is similar to the Kruskal-Wallis test. When a result is significant, the effect size r can be calculated. Again, these effect sizes can be interpreted in the same way as explained in section 4.1.

Using Wilcoxon's T-test, it was observed that the meteorological adjustment had a significant effect on the difference between measurement and calculation. The calculated values $L_{AE,calculation}$ increased with meteorological adjustment, $T = 2.96 \cdot 10^{10}$, $p < 0.001$, $r = -.08$. The absolute difference between the measurement and the calculation $|\Delta L_{AE,c-m}|$ decreased with applying meteorological adjustment, $T = 2.84 \cdot 10^{10}$, $p < 0.001$, $r = -.10$. Although the effect sizes are small, this test shows that applying the meteorological correction based on actual meteorological conditions will decrease the absolute difference between measurement and calculation of event noise levels. This is in contrast with the effect on the long-term average noise levels, however, it is known that the long-term average noise levels are not linearly related to the event noise levels. This makes it possible that small positive effects on $\Delta L_{AE,c-m}$ lead to a small negative effect on $\Delta L_{eq,c-m}$.

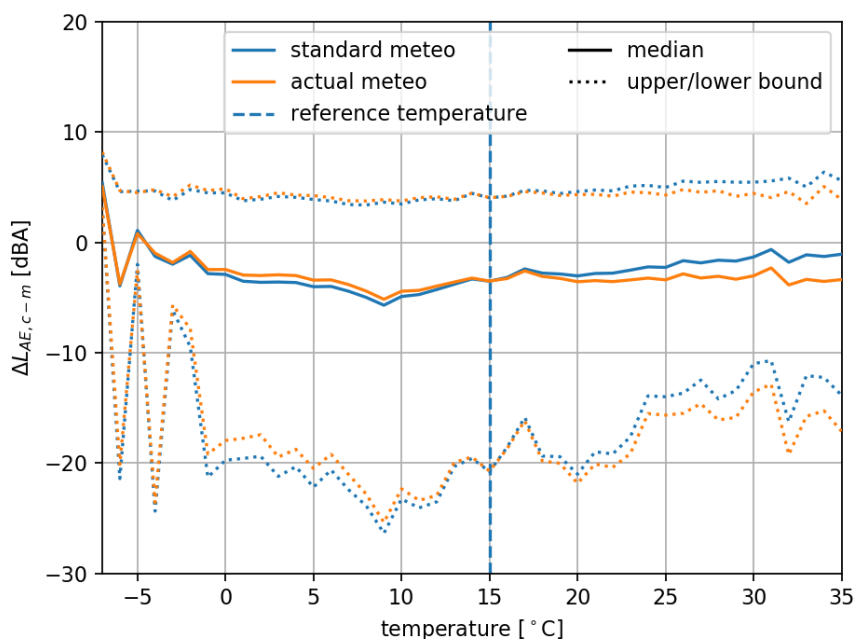


Figure 4.11: The 95% confidence bounds of the difference between the sound exposure level calculation and measurement $\Delta L_{AE,c-m}$ versus the temperature. Calculations using standard aircraft performance with both standard and actual meteorological conditions.

To further illustrate the effect of applying the meteorological correction, the differences between measurement and calculated versus the temperature are visualised in Figure 4.11 for the calculation with standard meteorological conditions and actual meteorological conditions. The results of the calculations using standard meteorological conditions are typically higher for higher temperatures ($T > 15^\circ\text{C}$) compared to the results of the calculations with actual meteorological conditions. This agrees with the idea that due to the correlation of temperature and relative humidity, the absorption tends to increase for higher noise levels causing $\Delta L_{AE,c-m}$ to go down for actual meteorological conditions compared to standard meteorological conditions. As can be seen in the figure, the meteorological correction tends to lead to a more consistent difference between measurement and calculation i.e. the median and 95% confidence bounds tend to stay on the same value (does not change with temperature). To quantify this, a constant value is fitted on three percentiles: the

median (50%), and the lower and upper bound of the 95% confidence interval (i.e. the 2.5% and 97.5% percentiles). To determine the percentiles, the results must be collected in bins. The bins are similar to the bins of a histogram, though a histogram uses only the counts, while in this analysis, the percentiles are used. The bins used for this analysis have a width of 1°C and are centered around each integer value. Using a weighted least squares method, where the weight is determined by the number of observations (e.g. the results of the histogram), the constant value is fitted to the percentiles over various temperatures. Both the constant values and the residuals are listed in Table 4.14. The residual indicates what the adherence is to this constant value along the various temperature bins.

Table 4.14: The effect of applying the actual meteorological conditions on the difference between calculation and measurement $\Delta L_{AE,c-m}$ analysing the consistency of multiple percentiles over a range of temperatures.

meteorological condition	percentile	constant [dBA]	residual [dBA ²]	residual decrease [%]
standard	2.5%	-21.57	$4.07 \cdot 10^{10}$	-
standard	50.0%	-3.99	$5.42 \cdot 10^9$	-
standard	97.5%	3.99	$1.53 \cdot 10^9$	-
actual	2.5%	-21.11	$2.74 \cdot 10^{10}$	32.7
actual	50.0%	-3.81	$2.29 \cdot 10^9$	57.9
actual	97.5%	4.08	$4.27 \cdot 10^8$	72.0

The results in Table 4.14 show that the variability due to temperature is removed when using actual meteorological conditions, since the residual of the results with actual meteorological conditions are lower than the residuals with standard meteorological conditions. Furthermore, it can be seen that the residual is related to the percentile, with residuals being larger for lower percentiles. Moreover the residual decrease due to the use of actual meteorological conditions is also related to the percentile, with higher percentiles showing higher residual decrease, further increasing the differences between the residuals of different percentiles.

This indicates that overestimations ($\Delta L_{AE,c-m} > 0$) are affected more by the use of actual meteorological conditions compared to underestimations ($\Delta L_{AE,c-m} < 0$). This is consistent with the analysis in Appendix A where it is argued that overestimations can only come from modelling and measurement error, whereas for underestimations, there is also a chance that factors other than modelling or measurement error influence the results. The meteorological adjustment thus successfully removes the variability over temperature. Similar results can be found for pressure and relative humidity which are also present as input parameter for the meteorological adjustment. These results can be found in Appendix F. All indicate that the remaining variability found in the results is due to other factors than the meteorological conditions used for the meteorological adjustment.

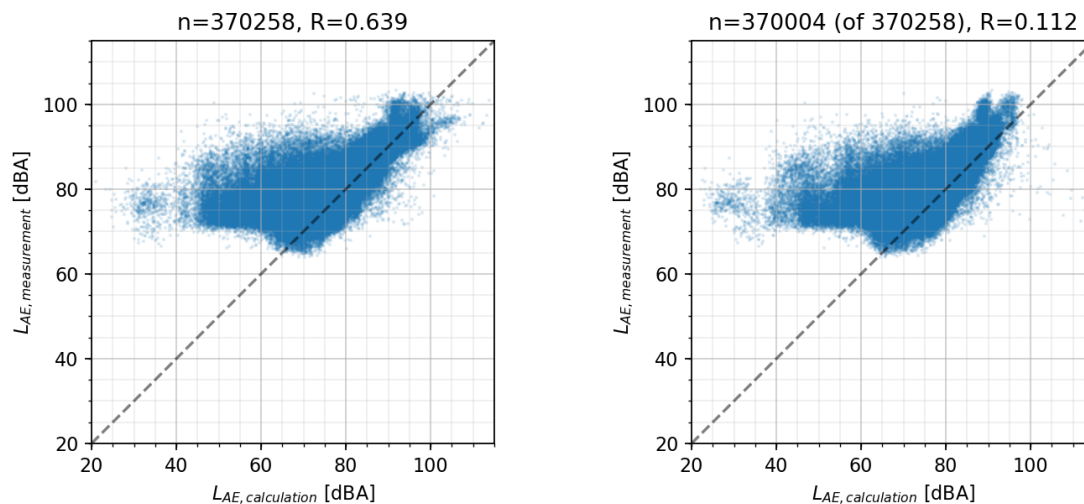
To summarise, although there is a significant difference in how the $\Delta L_{AE,c-m}$ values are distributed, the effect size is small and there is only a marginal effect on the long-term average noise level L_{eq} and no effect on L_{DEN} at all.

4.3. Effect of speed and thrust adjustment

Using the results of the standard flight performance and derived flight performance method both in combination with the actual meteorological conditions, the impact of speed and thrust adjustment can be determined. Referring to the names from Table 4.2, method C is compared with method B in this section. Because they both use the actual meteorological conditions, the differences in the results belong to the differences in altitude, speed and thrust. However, the altitude will be comparable, since the fixed point profiles are matched based on the altitude. The results are visualised in Figure 4.12.

From Figure 4.12 it can be seen that some results of the derived flight performance calculations - 254 to be precise - can not be visualised in the indicated window. This is because some of these results go beyond $L_{AE,calculation} > 115\text{dBA}$. Subsequently, this also affects the correlation coefficient R , which is much lower for the derived flight performance ($R = 0.112$) compared to standard flight performance ($R = 0.639$). When assessing the scatter of the individual results, it is found that the group of over-estimations ($L_{AE,calculation} > 100\text{dBA}$ and $L_{AE,measurement} \approx 95\text{dBA}$) in Figure 4.12a cannot be identified anymore in Figure 4.12b. Based on the visual assessment, it is likely that there will be less over-estimations by the calculations for the method using derived flight performance.

Wilcoxon's T-test was used to test the differences between the standard and derived flight performance calculations. It was observed that $\Delta L_{AE,c-m}$ decreased with the use of derived flight performance (compared



(a) Results using standard aircraft performance and actual meteorological conditions. (b) Results using derived aircraft performance and actual meteorological conditions.

Figure 4.12: Result for each calculation method. The figures shows the calculated sound exposure levels compared with the measured sound exposure levels.

to standard flight performance), $T = 2.31 \cdot 10^{10}$, $p < 0.001$, $r = -.20$. The absolute difference between the measurement and the calculation $|\Delta L_{AE,c-m}|$ increased with derived flight performance compared to standard flight performance, $T = 2.72 \cdot 10^{10}$, $p < 0.001$, $r = -.13$. The results are further separated by type of operation, leading to the following results in Table 4.15.

Table 4.15: The effect of the derived flight performance method on the absolute difference between the calculation and measurement for each type of operation, $p < 0.001$

operation	effect on $ \Delta L_{AE,c-m} $	Wilcoxon's test statistic T	effect size r
arrival	decrease	$6.54 \cdot 10^9$	-.04
departure	increase	$4.60 \cdot 10^9$	-.26

To compare the various methods, long-term average noise levels should also be determined for the results using derived flight performance. However, using all $L_{AE,calculation}$ led to unrealistic L_{eq} values, because the long-term average noise level is sensitive to large values and the calculations using derived flight performance include many of these large results. To illustrate the problem, 2694dBA is the largest $L_{AE,calculation}$ value in the results of method C. Including such high values would result in $L_{eq} = 2639$ dBA. So in order to make a fair comparison between the long-term average noise level, observations with $(L_{AE,calculation})_{method C} > 120$ dBA were removed from the long-term average noise level analysis.

Although the outlier results could be removed based on the noise level, additional investigation was performed on some cases to better understand where these values came from. Therefore, a number of cases were checked manually, for all these cases it was found that the uncertainty of the ADS-B data caused the smoothing of the velocity to work poorly, resulting in unrealistically high noise levels. More specifically, since the standard flight performance calculation methods did produce realistic results, it can be concluded that it is the use of the velocity that is causing the problem, because the other data was also used for the standard flight performance calculations (either for the calculation itself or the profile selection).

Table 4.16: The long-term average noise levels for method C: the calculation method using derived flight performance profiles and actual meteorological conditions.

Noise level	Difference with measurement
$L_{eq} = 81.12$ dBA	$\Delta L_{eq,c-m} = -2.57$ dBA
$L_{DEN} = 64.32$ dBA	$\Delta L_{DEN,c-m} = -2.26$ dBA

Table 4.17: The long-term average noise levels uncertainties for method C: the calculation method using derived flight performance profiles and actual meteorological conditions separated by type of operation.

Type of operation	$\Delta L_{eq,c-m}$ [dBA]
arrival	-1.33 ± 0.75
departure	-3.51 ± 1.16

The long-term average noise levels for the derived flight performance are listed in Table 4.16 and in Table 4.17. These long-term average noise levels using derived flight performance could be compared with the results from Table 4.7 and Table 4.8. From the contents of these tables it can be seen that both L_{DEN} and L_{eq} decreased for the derived flight performance, leading to increased differences between measured and calculated long-term average noise level $\Delta L_{eq,c-m}$ (-1.4dBA) and $\Delta L_{DEN,c-m}$ (-1.2dBA). The same could also be found for the long-term average noise level separated by type of operation. $\Delta L_{eq,c-m}$ dropped from -0.80dBA to -1.33dBA for arrivals and from -1.33dBA to -3.51dBA for departures. Furthermore, the quantified uncertainties of the derived flight performance results are larger compared to the uncertainties of the standard flight performance (and thus the baseline method, because they have equal uncertainties). The uncertainty of the long-term average noise level for arrivals is about ten times larger compared to the baseline method. For departures, the uncertainty is about five times larger compared to the baseline method.

Except for the decrease in $|\Delta L_{AE,c-m}|$ for arrivals it is shown with the comparison of both the event as well as the long-term average noise levels that using derived flight performance has a negative effect on the difference between the measured and calculated average noise levels. Furthermore, the derived flight performance has a negative effect on the uncertainty of the calculated long-term average noise levels. Although a larger performance decrease was found for arrivals, the departures still perform worse compared to arrivals. To get a better understanding of how the derived flight performance changes $\Delta L_{AE,c-m}$, the probability density for each type of operation is visualised in Figure 4.13.

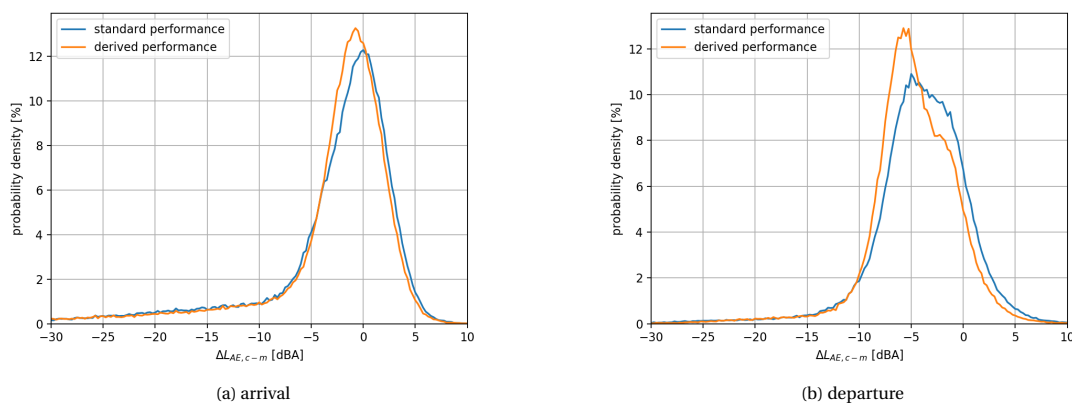


Figure 4.13: Probability densities for type of operation, separated by calculation method. The figures shows the calculated sound exposure levels compared with the measured sound exposure levels.

In Figure 4.13 it can be observed that the derived flight performance method decreased the number of over-estimations for both arrivals and departures, increasing the number of underestimations. Furthermore, the results seem to be more concentrated, e.g. the maximum probability is higher for the derived flight performance method.

For arrivals, the method seems to improve the results in terms of consistency, since the peak of the probability density function is higher. Although the peak moves slightly away from zero, indicating that there still is a bias present in the calculated values. Still, since $|\Delta L_{AE,c-m}|$ decreased, it can be concluded that the derived flight performance method has a better performance than the standard flight performance method for arrivals.

For departures, the effect is more complex. Where the arrival data shows a smooth single distribution, it seems that the departures show a combination of two (or more) distributions. To investigate this further, the probability density function is deconstructed by aircraft type. The deconstructed probability densities for both arrivals and departures are visualised in Figure 4.14.

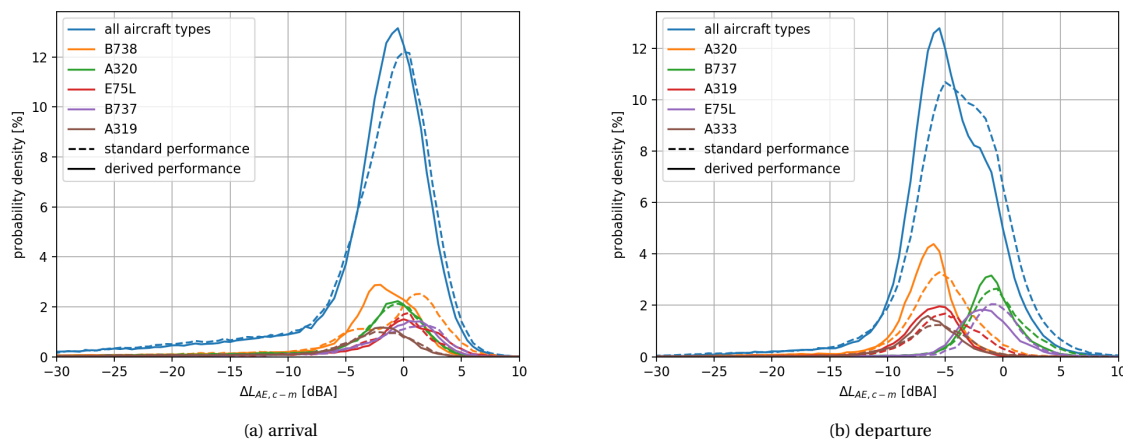


Figure 4.14: Probability densities for type of operation, separated by calculation method and aircraft type. The figures shows the difference between the calculated sound exposure levels and the measured sound exposure levels. The 5 most dominant aircraft types are visualised.

In Figure 4.14 it can be seen that the derived flight performance method shows a different results for each aircraft type. For arrivals, the largest differences can be observed for aircraft type B738. For this aircraft type, the mode² shifts from +2dBA for the standard flight performance results to -2.5dBA when using derived flight performance. As explained in section 4.1, only one standard flight performance profile was available for arrivals, therefore the groundspeed, thrust setting and altitude can all be very different for the derived flight performance compared to the standard flight performance. This is in contrast with the aircraft types for which more standard flight performance profiles were available. The other aircraft types show very similar results for both the standard and derived flight performance methods. For departures, it can be seen that there are two groups of aircraft types: a group with a mode of $\Delta L_{AE,c-m} \approx -5$ dBA for the standard performance results and a group with a mode of $\Delta L_{AE,c-m} \approx -1$ dBA. For all aircraft types, it can be observed that the mode becomes more negative when using the derived flight performance. Furthermore, an increase in the maximum probability can be observed, with the exception of aircraft type E75L which shows a minor decrease.

Since the derived flight performance uses the acceleration, a term that might be influenced by the headwind, the differences between measurement and calculation are also shown in relation to the wind speed for all calculation methods in Figure 4.15. The figure shows the same median and 95% confidence as used in Figure 4.11. In Figure 4.15 it can be seen that for all methods, $\Delta L_{AE,c-m}$ tends to decrease with increasing wind speed. For the upper bound, the difference between $\Delta L_{AE,c-m}$ for low and high wind speeds is smaller for the derived flight performance compared to standard flight performance. The same is true for the median, however, for the median it can also be observed that there is more variability over the various wind speeds i.e. the line is less smooth. For the lower bound the opposite effect can be observed. The difference between $\Delta L_{AE,c-m}$ for low and high wind speeds increases when comparing derived with standard flight performance results. To quantify these results, constant values have been fitted in the same way as has been performed for the temperature in section 4.2. The results of this method can be found in Table 4.18. The residuals confirm the findings that variability due to wind speed decreases for the median and the upper bound, while the variability of the lower bound increases.

4.4. Effect of aircraft substitution correction

It is mentioned before in section 2.3 that it is possible to assess the influence of the aircraft substitution correction after the noise levels have been calculated using one of the three methods as listed in Table 4.2. Without using additional data, only the effect of the ICAO type correction can be assessed. The long-term averages with and without ICAO type code correction are listed in Table 4.19.

From Table 4.19 it can be seen that the ICAO type code correction causes $\Delta L_{eq,c-m}$ to move closer to

²The mode of a probability density function is the value which is the most common in the data set i.e. the value with the largest probability.

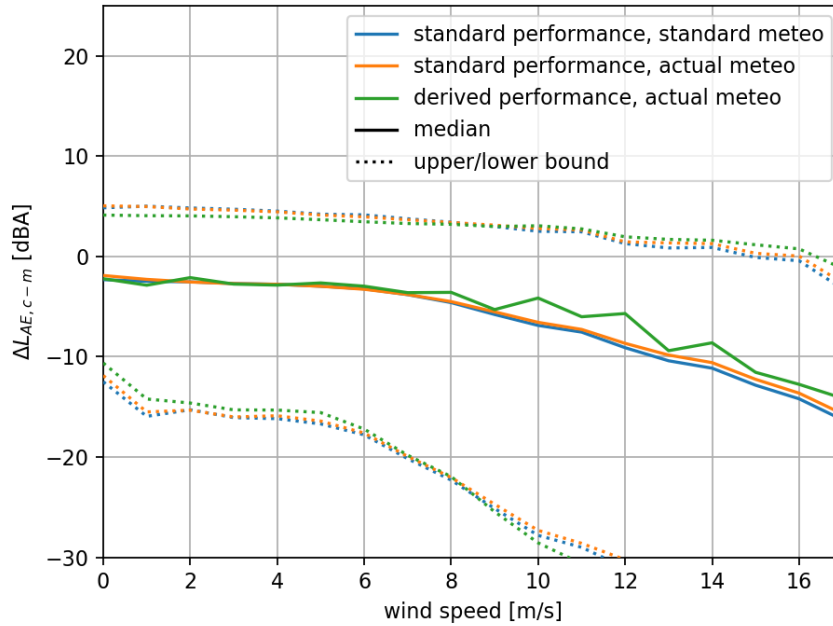


Figure 4.15: The 95% confidence bounds of the difference between the sound exposure level calculation and measurement $\Delta L_{AE,c-m}$ versus the wind speed. Calculations using standard aircraft performance with both standard and actual meteorological conditions and the derived aircraft performance with actual meteorological conditions.

Table 4.18: The consistency of the difference between calculation and measurement $\Delta L_{AE,c-m}$ over a range of wind speeds.

aircraft performance	percentile	constant [dBA]	residual [dBA ²]	residual decrease [%]
standard	2.5%	-17.10	$8.57 \cdot 10^{10}$	-
standard	50.0%	-3.11	$9.69 \cdot 10^9$	-
standard	97.5%	4.23	$3.24 \cdot 10^9$	-
derived	2.5%	-16.56	$1.14 \cdot 10^{11}$	-33.5
derived	50.0%	-2.92	$5.54 \cdot 10^9$	42.8
derived	97.5%	3.71	$1.37 \cdot 10^9$	57.7

zero for all calculation methods. When assessing the results of both arrivals and departures combined, it can be observed that the results of the standard flight performance are almost equal to zero. This can be attributed primarily to the large improvements observed for the departures which go from $\Delta L_{eq,c-m} \approx 1.3$ dBA to $\Delta L_{eq,c-m} = 0.04$ dBA and $\Delta L_{eq,c-m} = 0.08$ dBA. The correction even causes the departures to perform better than the arrivals, while the contrary is true for the standard flight performance results without correction. Besides the rounding errors, it seems that the ICAO type code correction does not influence the uncertainty of the long-term average noise levels.

Looking at the derived flight performance results, improvements of the same order of magnitude can be found, with an overall $\Delta L_{eq,c-m}$ decrease of around 0.9 dBA and a decrease of 0.4 dBA for arrivals and 1.3 dBA for departures. In contrast with the standard flight performance results, the substitution correction influences the uncertainty of the long-term average noise level. The uncertainty of the long-term average noise level for departures increased with 0.3 dBA, which subsequently led to an increase of the uncertainty of the long-term average noise level for both arrivals and departures combined.

As explained in section 2.3, the substitution can also be based on the aircraft configuration, though the required data is not available for all aircraft based on ADS-B data only. However, using the Dutch aircraft register, the EASA record numbers (which can be used directly for substitution by aircraft configuration) are provided for all aircraft registered in The Netherlands.

The aircraft registration numbers could be found in the Schiphol flight data. An EASA record number could be found for 68000 (of 151108) flights in the Dutch aircraft register. For 4745 flights, the substitution

Table 4.19: The difference between measured and calculated long-term average noise levels $\Delta L_{eq,c-m}$ of the various calculation methods for each type of operation, both with and without ICAO type code correction.

operation	flight performance	meteo condition	no correction [dBA]	ICAO correction [dBA]
all	standard	standard	-1.08 ± 0.16	-0.11 ± 0.17
all	standard	actual	-1.15 ± 0.16	-0.17 ± 0.17
all	derived	actual	-2.65 ± 0.69	-1.72 ± 0.90
arrival	standard	standard	-0.67 ± 0.07	-0.24 ± 0.07
arrival	standard	actual	-0.80 ± 0.07	-0.37 ± 0.07
arrival	derived	actual	-1.33 ± 0.75	-0.91 ± 0.72
departure	standard	standard	-1.30 ± 0.24	-0.04 ± 0.23
departure	standard	actual	-1.33 ± 0.24	-0.08 ± 0.24
departure	derived	actual	-3.51 ± 1.16	-2.19 ± 1.47

using EASA record number resulted in a different aircraft type compared to the aircraft type obtained using ICAO type code substitution. The effects of using a different aircraft type for substitution could not be assessed without performing additional calculations, therefore only the 63255 flights for which the EASA record number substitution resulted in the same aircraft type as the ICAO type code substitution were taken into account. Although the suggested aircraft types are the same for both methods, the suggested correction factor might be different for each substitution method as was shown before in Figure 2.8. The effect of applying 1) no correction, 2) the ICAO type code correction, 3) the aircraft configuration correction, is visualised in Figure 4.16.

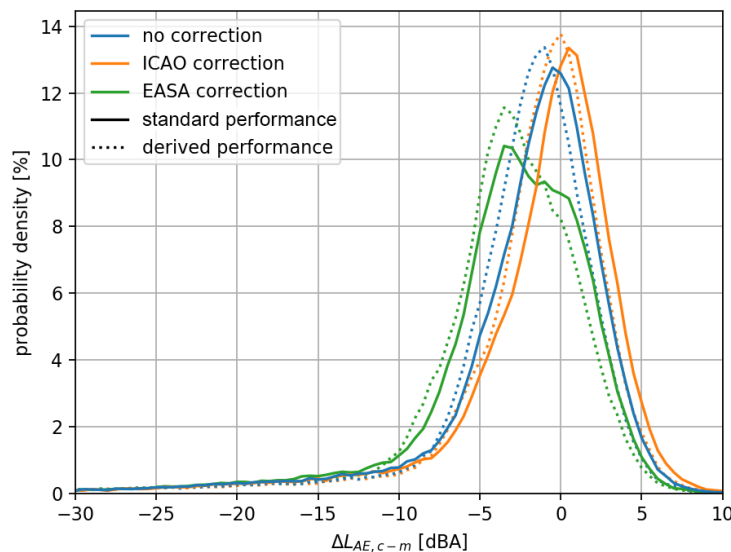


Figure 4.16: The probability densities for each substitution method for both the standard flight performance and derived flight performance method, both using actual meteorological conditions. The line colors indicate the substitution method and the line style (solid/dotted) indicates the calculation method. Metric used in this comparison is the sound exposure level.

In Figure 4.16 it can be seen that the correction from the ICAO type code substitution typically increases the calculated noise levels, whereas the correction from aircraft configuration (i.e. EASA record number) typically decreases the calculated noise levels. Compared with the results without correction, the ICAO type code correction causes the results to be more concentrated, i.e. the maximum probability is higher. In contrast, the results using EASA record number corrections are less concentrated. What can also be observed is the difference in shape of the probability density curve of the results with EASA record number corrections in combination with the standard flight performance calculation. Compared with the other corrections applied to the standard flight performance results, the EASA record number correction has a complex effect on the probability density of $\Delta L_{AE,c-m}$. This probability density function seems to be constructed of multiple prob-

ability density functions with different modes. When compared with the results of the EASA record number corrections using derived flight performance, the effect of these probability density functions with different modes seem to be less pronounced. It is clear that the effect of the substitution correction depends on calculation method. Therefore additional analysis is required to quantify these effects.

To analyse the effect of three corrections in combination with the calculation method, a Friedman's ANOVA was used. Similar to Wilcoxon's T-test, the Friedman's ANOVA is used for non-parametric data and is reported with a p -value to indicate the significance. However, instead of the test statistic T , the χ^2 value is provided. $\chi^2(k-1)$ is a function of the ranks and sample size, the number k indicates the number of conditions tested[14]. Large values for χ^2 indicate that the variables are dependent. When assessing the results of all calculation methods together, $|\Delta L_{AE,c-m}|$ was significantly affected by the correction, $\chi^2(2) = 79114.164$, $p < 0.001$. Wilcoxon T-tests were used to follow-up this finding. $|\Delta L_{AE,c-m}|$ increased significantly after applying the EASA corrections, $T = 3.42 \cdot 10^{10}$, $r = -0.31$. Applying the ICAO type code correction significantly decreased $|\Delta L_{AE,c-m}|$, $T = 2.32 \cdot 10^{10}$, $r = -0.09$. Within each calculation method, $|\Delta L_{AE,c-m}|$ was significantly affected by the correction as can be seen in Table 4.20. Similar to the aforementioned assessment for all calculation methods combined, Wilcoxon T-tests were used to assess the effect of the correction within each calculation method. The results of these tests can be found in Table 4.21.

Table 4.20: The effect of the correction on $|\Delta L_{AE,c-m}|$ for each calculation method.

meteorological condition	flight performance	Chi-Squared test statistic $\chi^2(2)$	Probability p
standard	standard	18158.861	< 0.001
actual	standard	17377.588	< 0.001
actual	derived	49381.508	< 0.001

Table 4.21: The effect of the correction on $|\Delta L_{AE,c-m}|$ within each calculation method, $p < 0.001$

meteorological condition	flight performance	correction	effect on $ \Delta L_{AE,c-m} $	Wilcoxon's test statistic T	effect size r
standard	standard	EASA	increase	$2.77 \cdot 10^9$	-.29
standard	standard	ICAO	decrease	$4.10 \cdot 10^9$	-.05
actual	standard	EASA	increase	$2.83 \cdot 10^9$	-.28
actual	standard	ICAO	decrease	$4.15 \cdot 10^9$	-.05
actual	derived	EASA	increase	$2.14 \cdot 10^9$	-.36
actual	derived	ICAO	decrease	$3.16 \cdot 10^9$	-.17

From these results, it is clear that compared to the results without correction, applying the ICAO correction decreases $|\Delta L_{AE,c-m}|$ while the EASA correction increases $|\Delta L_{AE,c-m}|$. Furthermore, it can be concluded that the effect is larger when applied to the derived flight performance calculations.

5

Discussion

This research addressed the following research question: *What is the effect of ECAC Doc. 29 model improvements on the differences between measured and calculated aircraft noise levels?* In order to answer the research question, the work is interpreted in this chapter using the results from the previous chapter.

5.1. Comparisons within baseline method results

Using standard flight performance and standard meteorological conditions, an initial comparison between measurements and calculations could be made. To structure the discussion, the comparison of the baseline method results is discussed within the following subsections, each addressing the results of a specific subject variable.

Difference between types of operation

Comparing the individual results of arrivals to departures using Figure 4.1b, the differences between measurement and calculation for arrivals are often closer to zero than departures. Furthermore, the width of the probability density function is larger for departures, indicating that the results of departures contain more variability compared to the results of arrivals. The same pattern is found for the long-term average noise levels, with confidence bounds of ± 0.07 dBA for arrivals compared to ± 0.24 dBA for departures. This shows that the uncertainty for departures is larger than the uncertainty of the arrivals, which is consistent with the probability density. In contrast, the correlation coefficient of departures is higher than the correlation coefficient of arrivals, indicating that the measurements and calculations of departures have a stronger relation to each other compared to the arrivals.

The primary reason for the large width of the probability density function is caused by variation in aircraft types as will be explained in the next subsection. Still, this does not explain why $\Delta L_{AE,c-m}$ values are more negative for departures compared to arrivals and why the correlation coefficient is different for each type of operation. The following reasons that might explain these differences are identified:

1. effect of ground roll segments
2. number of available standard performance profiles
3. estimation of aircraft weight (stage length)
4. ground track coherence

The first reason is the (lack of) effect of the ground roll segments. Because the ground roll is not included in the calculations, the noise levels in this research are always smaller or equal to the calculations including the ground roll. For arrivals, the ground roll segments might not contribute significantly to the noise levels. However, based on these results, the departure calculations might be affected more by the absence of the ground roll phase.

The second reason is the availability of standard performance profiles. Typically, there are 38 profiles available for arrivals per aircraft type, while there are only 4 profiles for departures. This should allow the arrivals to better match the actual altitude, where there might be larger differences between the actual altitude and the altitude from the performance profile for departures. However, for the departure calculations to

perform worse, the measurement should be larger than the calculation, which is expected if the altitudes in the standard performance profiles are too low or if the thrust settings are too low. Both are not the case, as will be further explained in section 5.3. Therefore this is not a likely explanation for the worse performance of departures compared to arrivals.

The third reason is also linked to the standard performance, namely the stage length. Arrivals use only one stage length, because it is assumed that within an aircraft type, all aircraft land with the same weight. For departures, the stage length is based on the destination of the aircraft, because this determines the amount of fuel and therefore the actual weight. The largest stage length observed in this dataset is stage length 8, whereas the theoretical maximum is stage length 9. It might be that aircraft are heavier than what is estimated based on the destination of the aircraft, because of additional payload or tinkering procedures. Because the stage length allows for more variation for departures, this might cause the correlation coefficient to be larger for departures than for arrivals.

The fourth reason is in the ground track coherence. From Figure 3.6 it can be seen that departures follow the standard instrument departure (SID) for a very long distance. Dispersion of the ground track might vary along the various phases of the SID, including near the runway because of early turns. Arrivals show more dispersion further away from the airport, but close to the airport (≈ 5 nautical miles), the navigation accuracy is very high due to the instrument landing system (ILS). Because for departures the variability of the ground track is larger close to the airport, it is expected that there is more variability in the measured noise levels close to the airport for the departures. However, since the actual ground tracks are taken into account for each flight, these calculated noise levels should be different as well. Still, it should be noted that it was assumed that the ground track does not contain bias and error. Based on the assessed cases for the outliers, it was found that position data also included a bias. Therefore it is likely that ground track coherence causes differences between measurement and calculation. However, it does not solely explain the difference between the two types of operation.

Ultimately, it is likely that a combination of these factors causes the vertical patterns to emerge in the scatter plots, because these vertical patterns typically arise within NMT (noise-monitoring-terminal) results with the same aircraft type-route-profile-stage length combination. An example of this vertical pattern for high calculated noise levels can be found in Figure 4.1c. The height of these vertical patterns are in the order of 5 dBA nearby $L_{AE,calculation} = 97$ dBA whereas the vertical pattern around $L_{AE,calculation} = 42$ dBA spans roughly 20 dBA, indicating the possibility of a large amount of false positives for the observations at $L_{AE,calculation} = 42$ dBA. Since arrivals use only one stage length, these patterns appear more clear in the arrival scatter plot. These patterns are also the main reason for the decreased correlation coefficient for arrivals compared to the departures.

The long-term average noise level uncertainty observed in this research is smaller than the uncertainty derived by Schäffer, et al. for FLULA2 [39]. The values are different because two different methods have been used to determine the uncertainty. The method in this research estimates the uncertainty based on a comparison with measurements. Schäffer, et al. estimated the various uncertainty components of an aircraft noise calculation to be able to estimate the long-term average uncertainty. Their method requires knowledge of the partial uncertainties.

Differences between aircraft types

The typical differences between measurements and calculations vary between aircraft types as is shown in Figure 4.2. The differences between aircraft types are smaller for arrivals compared to the values for departures, not only in terms of the size of the boxplot, but also in terms of the long-term average noise level $\Delta L_{eq,c-m}$.

These results might indicate that the fixed point profiles were better constructed for arrivals than for departures. However, it should be noted that ICAO type code B738 is only present in the arrivals, since there are no standard departure profiles for this aircraft type. Moreover, aircraft type B738 only has one profile available: the default arrival profile from the ANP database. The B738 standard flight performance was not available in the set of NLR performance profiles for Amsterdam Airport Schiphol, because they concluded that there was not enough flight performance data available to determine the actual thrust setting [18]. So the B738 results found in this research are the results of the default flight performance profile from the ANP database. Interestingly, this caused the median of the single-event comparisons and the long-term average difference to be near zero.

The explanation for the differences between aircraft types is primarily in the availability and quality of ANP data. Although addressed in section 5.4, the lack of a proper NPD correction might cause the calculations

of certain aircraft types to be biased. Furthermore, differences might also come forth from how the aircraft is operated. This is often related to the aircraft operators, which typically fly a fleet of the same aircraft types.

Differences between NMTs

In Figure 4.3 it can be seen that the performance of NMTs are different. Not only do they show different values for $\Delta L_{AE,c-m}$, some NMTs also show different values for $\Delta L_{eq,c-m}$. For some NMTs, these differences are so large that they could be considered as outliers. Examples of such NMTs are NMT 18, 24, and 26 for arrivals and NMT 17 and 18 for departures. The performance of NMTs is also dependent on the type of operation. Both in terms of boxplot size, which is typically larger for departures, and in terms of the median and long-term average. Since the measurement uncertainty is the same for all NMTs, the differences between NMTs are primarily related to their location.

Some NMTs do not detect both arrivals and departures, because they are only close to either departure or arrival routes. Furthermore, the performance of an NMT is different for arrivals and departures, which might be due to the fact that arrivals typically produce less noise. This is stressed with the long-term average noise levels $\Delta L_{eq,c-m}$ that are below -10dBA , which are only observed for arrivals, while some boxplots show large negative values for departures as well. Since the long-term average noise level is sensitive to large noise levels, a small number of noisy departures might already cause the calculated long-term average noise level to become high compared to (or close to) the measurements. For arrivals, the noise levels are typically lower. Therefore it is less likely that noisy flights are present, which causes the calculated long-term average noise level to get close to the measured long-term average noise level.

Several reasons are identified for the presence of outliers. A number of these divergent NMTs will be addressed. For NMT 18, a large boxplot can be observed for both arrivals and departures. The long-term average performance of departures is close to the performance of other NMTs. However, the individual results show large differences. For arrivals, both the individual results and the long-term average noise levels show large differences, indicating that NMT 18 detects many false positives for arrivals. This can be solved by increasing the threshold used for the detection of arrivals. Results for NMT 17 are only shown for departures, since almost no arrivals are detected by the NMT. The long-term average difference is one of the worst shown in the figure. This can be explained by the presence of a large number of other noise sources, coming from the sports/playing fields nearby. Also showing poor results is NMT 26, which primarily detected arrivals. The primary reason for the poor results is that NMT 26 is not located directly below any of the flight paths. Looking at the A320 ground tracks, NMT 19 is considered to be superior over NMT 26, because it is closer to both the arrival and departure tracks. However, it is interesting to observe that the number of arrival observations for NMT 19 is smaller than the number of observations for NMT 26. This indicates that the threshold for detection is better tuned for NMT 19 or there are typically more non-aircraft noise sources around NMT 26. Additionally, NMT 19 has departure observations where NMT 26 does not. Thus, the location of NMT 26 is considered to be poor.

For the other NMTs, the variation in noise level differences is caused by surroundings, due to ground- and building reflections or noise introduced by non-aircraft sources that are nearby, such as roads and schools. Additionally, variation of NMT performance is caused by the initial assumption that all microphones are located 5 meter altitude relative to the runway. This is not the case for many roof locations, such as NMT 7 Figure 3.2b. Still, the latter is not expected to solely cause the observed differences between NMTs from Figure 4.3.

Not all measurements are higher than the calculations. For example, $\Delta L_{AE,c-m}$ and $\Delta L_{eq,c-m}$ of NMT 40 are typically high compared to those of other NMTs. This is because of its close proximity to the runways 18L-36R and 04-22. The fact that calculations are larger than measurements, can be a result of either the modelling error or the measurement error as explained in Appendix A. Since the measurement and NPD data uncertainty are known, the large differences can be attributed primarily to the errors in position (including altitude), velocity and thrust setting. In the case of NMT 40, it was observed that the altitude contained in the ADS-B data would sometimes drop below zero, also after applying the correction for GNSS-Barometer difference. Because the altitude is not used directly for the noise calculation, this should not directly influence the results of the calculations using standard performance profiles. However, it does influence these results because the actual altitude is used to determine the touchdown point, which is used to combine the profile and the ground track.

To conclude, the typical differences between measurements and calculations depend on the location of the NMT and its surroundings. To decrease the variation between NMTs, the actual height of the microphones should be used in the calculations and the surroundings should be analysed for possible reflection effects and

presence of other sound sources.

5.2. Effect of meteorological adjustment

Using the results of the calculations based on standard flight performance with both the standard and actual meteorological conditions, the impact of the meteorological adjustment can be determined. The results show almost identical probability densities of the difference between measurement and calculation $\Delta L_{AE,c-m}$. Additionally, the long-term averages $\Delta L_{eq,c-m}$ of the two meteorological conditions differ only 0.13 dBA and 0.03 dBA for arrivals and departures respectively. This is below the estimated uncertainty of 0.24 dBA for departures and close to the estimated uncertainty of 0.07 dBA for arrivals. Moreover, the L_{DEN} values for both meteorological conditions are the same.

However, Figure 4.11 shows that both the median and the 95% confidence bounds of $\Delta L_{AE,c-m}$ change over various temperatures. These changes are expected due to the changing atmospheric absorptions over various meteorological conditions. To quantify the change of $\Delta L_{AE,c-m}$ over a range of temperatures, a constant value was fitted to the various percentiles using a weighted least-squares method, where the weights are based on the number of observations for each temperature. The residuals can be used to indicate the variability that remains over the various temperatures, because it quantifies the remaining difference between the best-matching constant value and the actual values at the various temperatures. It is shown that the residual decreases with increasing percentile locations. Furthermore, it is shown that the residuals decrease by applying the actual meteorological conditions. Additionally, it is shown that residual decrease is larger for higher percentile locations. This indicates that in the case where calculations are larger than the measurements, the effect of applying actual meteorological conditions has an increasing effect.

The tipping point of the curve is 15°C, which makes sense, because 15°C is the temperature used within the standard meteorological conditions. Furthermore, it seems that the effect is larger for higher temperatures. However, majority of observations are within 2°C and 25°C, with most observations at 8°C. Thus, although the effect seems smaller for lower temperatures (<15°C), the number of observations in this temperature range compensates for the larger effects at high (>15°C) temperatures.

The irregular differences between measurements and calculations at temperatures below -2°C and above 30°C can be explained by the fact that there are few observations there. This can be seen in Figure C.3a.

Although 8°C is the most dominant temperature, it shows a minimum for both the median and 2.5th percentile, indicating a larger difference between measurement and calculation compared to its neighbouring values. This could indicate that there are more false positives, because the 97.5th percentile at 8°C is consistent with the other temperatures. Similarly, there is a local maximum of the median and 2.5th percentile at 17°C, with roughly the same value for the 97.5th percentile. It is likely that the remaining variations can be attributed to other factors, such as wind. This could mean that wind occurred more often at 8°C than at 17°C.

Applying actual meteorological conditions thus removes the effect of temperature on the difference between measurement and calculation, making the difference between measurement and calculation independent of temperature. Since similar effects have been found for pressure and relative humidity, it can be concluded that using actual meteorological conditions makes the difference between measurement and calculation also independent of pressure and relative humidity. It should be noted that this does not include the wind direction and wind speed, since these factors are not included in the meteorological adjustment. Despite the fact that the use of actual meteorological conditions removed the effect of these meteorological conditions, it can also be concluded that the impact on the long-term average noise levels is very small. Similar effects have been found by Arntzen et al. [4]. However, as opposed to the research by Arntzen et al., the current study validated the findings using measurements. The use of standard meteorological conditions for long-term average noise calculations around Amsterdam Airport Schiphol as suggested in [18] is therefore justified. Still, this conclusion is related to the meteorological conditions of Amsterdam Airport Schiphol, therefore it cannot be generalized to other airports without additional research.

5.3. Effect of speed and thrust adjustment

Using the results of the calculations using standard flight performance and derived flight performance, both with actual meteorological conditions, the impact of the speed and thrust adjustment can be determined. In theory, the derived flight performance should make the calculation more realistic in terms of altitude, groundspeed and thrust setting.

Overall, the results of the derived flight performance decreased the calculated noise levels, leading to a further increase of the difference between measurement and calculation. This could be observed with

$\Delta L_{eq,c-m}$ which decreased from -1.15dBA to -2.65dBA, a drop of 1.5dBA, and the decrease in $\Delta L_{DEN,c-m}$ of 1.20dBA. Additionally, the correlation coefficient of the derived flight performance ($R=0.112$) was also much lower compared to the standard flight performance results ($R=0.639$). Lastly, the differences were found for both arrivals and departures, with $\Delta L_{eq,c-m} = -1.33 \pm 0.75$ dBA for arrivals and -3.51 ± 1.16 dBA for departures, whereas the standard flight performance calculations resulted in $\Delta L_{eq,c-m} = -0.67 \pm 0.07$ dBA and $\Delta L_{eq,c-m} = -1.30 \pm 0.24$ dBA for arrivals and departures respectively.

As mentioned in the results, the derived flight performance results contained outliers, which are indicated by the number of results (254) that could not be visualised in Figure 4.12b and the low correlation coefficient $R=0.112$. In order to obtain the long-term average noise levels for the derived flight performance results, the outliers have to be removed. To remove these outliers, a fixed noise level of 120dBA is used to mark the outliers, because the long-term average is sensitive to the higher noise levels. The result is a long-term average noise level that can be compared with the values of the standard flight performance results. Using this method for outlier removal, the calculated values slightly below this fixed value were still taken into account in the long-term average calculations, while the measured noise levels belonging to these observations could be much lower. Using the subsampling method described in Appendix H, taking such an observation into account (or not) might lead to large differences in calculated long-term average noise levels while the long-term average noise level based on measurements is hardly affected. Therefore, it can be concluded that the primary reason for the increase in uncertainty of $\Delta L_{eq,c-m}$ is the presence of outliers in the results.

What is also mentioned in the results is the fact that some cases were checked manually, to get a better understanding of these outliers. From this check it was concluded that the uncertainty of the ADS-B velocity data caused the noise levels to become unrealistically high. Ultimately, it is not the data itself that is the problem, but it is the smoothing that is performed on this data, because this method should be able to cope with the uncertainty. Furthermore the smoothing is important, because the acceleration is taken as the derivative of this velocity. Thus poor smoothing led to unlikely accelerations and thus unlikely thrust settings (going beyond 110% of the maximum sea level static thrust). Such flights should therefore be classified as outliers. Since the smoothing algorithm should have been able to cope with the uncertainty in the data, it is concluded that the implementation contains an error. Thus, the outliers that were found are a result of an implementation error of the derived flight performance method.

Although the implementation error explains the outliers and thus the uncertainty, it should still be discussed why different effects were found for arrivals and departures. Therefore the results for each type of operation will be discussed separately in the following subsections.

Interaction effect for arrivals

Although the noise levels typically decreased for arrivals, $\Delta L_{AE,c-m}$ decreased significantly as well. This is because the number of over-estimations is decreased. The mode of the baseline method was located at $\Delta L_{AE,c-m} = 0$ dBA, whereas the mode of the derived flight performance calculations was located below zero ($\Delta L_{AE,c-m} \approx -1$ dBA). Furthermore, the probability of the mode also increased, indicating that the variability of the differences between measurements and calculations is reduced. This is in contrast with the increased uncertainty of the long-term average noise level differences, again proving that the relation between $\Delta L_{AE,c-m}$ and $\Delta L_{eq,c-m}$ is not linear. Furthermore, this makes it more likely that the increased uncertainty of $\Delta L_{eq,c-m}$ is primarily related to the presence of outliers.

Separating the arrival results by aircraft type, it can be observed that most aircraft types have similar performance for both calculation methods. However, the performance for aircraft type B738 is different. As mentioned before in section 5.1, aircraft type B738 only had one standard performance profile available, where the others had 38 or more. Using the derived flight performance calculation method, the probability density function of the B738 shifts further to the left into the negative numbers. This agrees with the results from Op de Woert [28], which also found that the derived flight performance method resulted in less over-estimations. However, the results are now underestimating the measured noise levels. This can be attributed to noise from other sources, though it is more likely that it is related to the flight performance coefficients used for this aircraft type.

The results of other aircraft types are consistent with the results of the standard flight performance calculations. This is primarily due to the availability of many (38+) standard performance profiles, making it possible to include the required details when assigning a standard performance profile. Since it was expected that the derived flight performance is more realistic in terms of altitude, velocity, and thrust setting, it can be concluded that the standard performance profiles used in this research contain a sufficient level of detail to obtain the desired modelling fidelity. However, since the profiles used in this research are created for Amster-

dam Airport Schiphol specifically [18], it can also be concluded that the derived flight performance method is better suited to be generalized because it does not depend on pre-defined flight performance profiles.

To conclude, the differences between the derived flight performance calculations and standard flight performance calculations of arrivals are small when the standard flight performance profiles are well-constructed.

Interaction effect for departures

As discussed before, the typical differences between measurements and calculations of departures depend on the aircraft type. The same has also been found for the derived flight performance. Overall, it is observed in Figure 4.14a that there is less variability in the difference between measurement and calculation for derived flight performance calculations compared to the standard flight performance calculations. However, the probability density function moves further away from $\Delta L_{AE,c-m} = 0$ dBA, indicating that the derived flight performance performs worse in terms of absolute difference between measurement and calculation. This is also stressed with the decrease in long-term average noise level.

In Figure 4.14b it is shown that the differences between aircraft types are also present for the results using derived flight performance calculations. All aircraft types show a decreasing mode as well as an increasing maximum probability, except for aircraft type E75L, for which the maximum value of the probability density function decreases. Although the differences between aircraft types seem to be increasing, because the results of the derived flight performance are close to the baseline results, it can be concluded that the derived flight performance enhances the differences between aircraft types that are already present. Although some aircraft types perform worse compared to others, this effect will be reduced by the use of the substitution correction as will be discussed later.

From the list of factors causing the differences between arrivals and departures at beginning of the discussion in section 5.1, factors could be identified that could cause the derived flight performance to be different from the standard flight performance. From this list, the impact of ground roll, stage length and the ground track coherence should all be equal, since these are the same for the calculations using standard flight performance and derived flight performance. Leaving only one possibility, namely the lack of detail in the standard flight performance data.

A maximum of 5 profiles are available for an aircraft type with a given stage length. The lack of detail in altitudes of standard flight performance should be fully removed by using derived flight performance. This might be the reason why the width of the departure probability density function using derived flight performance is smaller than the departure probability density function using standard flight performance.

Still, the performance gets worse because $\Delta L_{AE,c-m}$ becomes more negative. This might be because the force-balance equation is behaving poorly because the thrust is mostly constant. Furthermore, the aerodynamic coefficients (drag-over-lift ratio) can change over various flight phases, where the analysis in this research assumes an average value over all flight phases. A different reason could be that the groundspeed is used to estimate the acceleration, while the true airspeed should be used for this, as will be further explained in the next subsection.

Thus, derived flight performance does not eliminate the differences that have been identified earlier in the type of operation comparison within the baseline method results. It tends to enhance the differences that are already present between the different aircraft types. The derived flight performance thus underestimates the noise from departing aircraft.

Relation with wind

Using Figure 4.15, the following observations can be made. The difference between measurement and calculation increases with increasing wind speed for all calculation methods. The medians of all calculation methods have roughly the same shape up to a wind speed of 7 meters per second. The 95% confidence bounds of derived flight performance are smaller than the standard flight performance up to 8 meters per second. The upper bound and median show higher values of $\Delta L_{AE,c-m}$ for derived flight performance compared to standard flight performance. The lower bound shows lower values starting from 8 meters per second, thus increasing the confidence bounds for derived flight performance from 8 meters per second and higher. Additionally, the median of the derived flight performance shows more variation compared to neighbouring wind speeds.

The standard flight performance profiles are constructed using a constant headwind of 8 knots. Even when the wind speed is exactly 8 knots, depending on the direction, the aircraft might experience a headwind or a tailwind. Although this affects the performance of the aircraft, the flight performance derivation method used in this research is not affected by the headwind (or tailwind). Additionally, by definition, the

groundspeed should be used in the flight path as input for the duration correction.

As can be seen in Equation 2.27, the only variable related to the wind is the acceleration. However, as explained in ECAC Doc. 29 [13], the acceleration is the change of speed along flight path, which is the groundspeed divided by the cosine of the flight path angle. In this research, a direct derivative of the smoothed ground speed was used, without correction for the flight path angle. This causes an underestimation of the thrust, leading to noise levels that might be lower than they should be.

A different hypothesis is that the wind is not included because the groundspeed is used and not the true airspeed. However, using Equation 5.1 from [13], it can be seen that the groundspeed includes both the true airspeed and the headwind. Thus, although the flight performance depends on the amount of headwind, the values that are observed in the ADS-B data can be used directly for the derived flight performance.

$$V = V_T \cdot \cos\gamma - w \quad (5.1)$$

where V is the groundspeed in m/s, V_T is the true airspeed in m/s, γ is the flight path angle, and w is the headwind in m/s.

In terms of improvements, using derived flight performance successfully removes variability within results up to 7 meters per second of wind. After these 7 meters per second, minor improvements of the derived flight performance can be observed, but both confidence bounds and the median tend to go down still.

This effect is caused by other phenomena related to wind that affect the difference between calculations and measurements. For example wind gradients causes microphones upwind of the aircraft to observe lower noise levels, while microphones downwind should observe higher noise levels. Refraction effects due to wind gradients as researched by Arntzen et al. [4] were not included in this research. As mentioned by Arntzen et al., adding this ray-tracing model will reduce variability of single-event noise levels due to wind effects. Although this method has not been validated using measurements, it is expected that applying such a method would successfully reduce part of the variations can still be found in the results of this research.

However, such a method will not remove all variability due to wind effect, because the wind itself also causes the noise levels of the measurements to increase. Not only because the turbulence of the air and the wind itself are detected, but also because of rustling vegetation/trees/leaves. Knowing this, the calculations are expected to underestimate, and the measurement will over-estimate the noise of aircraft, since it will include other noise effects ϵ_{other} .

Practicality of the method

In terms of usability, the flight performance derivation has a number of benefits over using standard flight performance profiles. For historic evaluations of flights, standard flight performance profiles do not need to be constructed in advance. Profiles used in this research have been constructed specifically for Schiphol by analysing flight data. However, this empirical method requires large amounts of data and like any other empirical model, this only allows for modelling of flights that are similar to the ones from the past. Furthermore, selection of a standard flight performance profile is required. Selecting the best-matching profile can be subjective due to the fact there are only a limited number of options. Goodness of fit might vary along the flight path. Furthermore, there are multiple parameters that can be used to determine goodness of fit. Currently only the altitude is being used in the standard profiles. This leaves aircraft speed, which is also observable and also influencing the amount of noise produced by the aircraft, unaddressed.

It could be argued that standard flight performance profiles are more user-friendly, because a profile is related to a procedure. So if the procedure is known, flight performance and noise levels can be estimated. Furthermore, the noise levels of flights using the same procedures can be grouped, which makes it easier to perform noise assessments for future traffic scenarios. Still, it should be kept in mind that in these cases the combined noise levels of the derived flight performance methods could also be used, as long as the groups are well-defined.

Relation to other fields of research

Additionally, using derived flight performance, the research can be linked directly to air traffic management research. In subsection 2.4.1, an effort was made to use recent developments in air traffic management research as input for aircraft noise calculations. The initial solution proposed in this section was to use the method from Sun et al. [40] to estimate the actual mass of the aircraft only. However, since this method is based on the total-energy model from BADA, it could also be possible to determine the thrust directly (without having to estimate the mass first). Additionally, it also uses ADS-B data as input, which is similar to this

research. So applying the model developed by Sun et al. in the field of aircraft noise modelling, a full noise calculation can be performed using only ADS-B and ANP data. One of the limitations of the method by Sun et al. is the limited amount of aircraft included in the validation. At the moment of writing, the method was only validated using flights of a Cessna Citation II.

Although the derived flight performance method currently has lower performance in terms of long-term average uncertainty, it is expected that such zero-configuration noise calculations are the future of historic aircraft noise assessments.

5.4. Effect of aircraft substitution

Aircraft substitution correction has a pronounced effect on the differences between measurements and calculations. In theory, the EASA substitution correction should give the best results, since it is the most detailed correction. Furthermore, the ICAO type code correction should provide higher calculated noise levels compared to the EASA correction, since it is always equal to the highest EASA correction related to this ICAO type code.

Comparing the ICAO type code correction results to the results without correction, it can be seen that the correction causes the long-term average noise levels to get closer to zero for all calculation methods. There is also an interaction effects with the type of operation. The long-term average noise level improvement for departures is larger compared to the arrivals. The improvements of the long-term averages indicate that the variability due to aircraft type specific effects are further removed using the ICAO type code correction. It is clear that the suggested corrections based on ICAO type are successful in minimising the gap between measurement and calculation. Based on the research by Asensio et al. [5], it can be concluded that it is very likely that the remaining differences are related to aircraft noise identification errors (e.g. falsely identifying aircraft noise events, while it is a result from other noise sources).

Comparing the ICAO correction with the EASA correction, the EASA correction shows lower calculated noise levels. This makes sense, since the ICAO substitution correction uses the maximum correction found within all EASA corrections related to this ICAO type code. The ICAO correction is thus overestimating when compared to the EASA correction. It was found before that the measurement is typically higher than the calculation. This is why the ICAO performs better in terms of difference between measurement and calculation. Still, the decreased differences between measurement and calculation are not indisputably linked to the calculation error $\epsilon_{calculation}$, since there is also an unknown contribution of other noise sources ϵ_{other} .

Assuming that the EASA corrections has the highest fidelity and is therefore the most realistic, three reasons have been identified for the fact that the EASA correction performs worse than the other two corrections:

1. the noise levels of the NPD data are too low,
2. the applicable correction has changed over time, and
3. the measurements are systematically too high due to noise from other sources.

Firstly, similar to noise certification campaigns, the NPD data is obtained using measurements. Therefore it might be influenced by uncertainty as well, causing the overall noise levels in the NPD data to be too low. However, since the measurement uncertainty is not biased it is unlikely that this explains the larger differences that are observed for the results with EASA correction.

Secondly, because the EASA correction is based on certification noise levels, it can be that during its time in operation, the typical noise levels of the aircraft might have changed over the years due to maintenance and other wearing effects. However, to get a better understanding how the typical noise production of an aircraft changes over time, further investigation is required.

Lastly, as addressed before, the measurements of the NMTs can be systematically too high. However, if this would be the only reason that the results of the EASA record number are worse compared to the ICAO type code correction, the results using ICAO corrections would not necessarily show a smaller difference between the measurement and calculation. Therefore it is not likely that this is the sole reason for the increased differences between measurement and calculation, but more research in the area of substitution correction is required.

To conclude, the ICAO type code should be used for the long-term average noise level calculations when a minimum difference with the long-term average measurements is desired. To get the best representation of the noise level of a single flight, more research needs to be performed on why the EASA record number is underperforming the other methods.

6

Conclusions & Recommendations

The objective of this thesis was to make recommendations on how to improve calculations based on the difference between measurements and calculations of long-term aircraft noise, by analysing noise measurements and ECAC Doc. 29 calculations of individual flights.

6.1. Conclusions

In this research it has been shown that differences and uncertainties between measurement and ECAC Doc. 29 calculation depend on type of operation, aircraft type and position of the microphone. Additionally, it has also been shown that validation can be performed using an existing network of noise monitoring terminals. However, the ability to perform a fair comparison depends on the location and the configuration of the noise monitoring terminal.

Uncertainty of the cumulative noise level estimations using ADS-B track data depends on how the noise levels are calculated. Three methods have been assessed, of which the baseline method showed the smallest differences between measured and calculated noise levels. Within the bounds of this research, it was shown that using actual meteorological conditions did not lead to a better estimation of the measured long-term average noise level, because the standard meteorological conditions were representative for the full set of observations. However, the use of actual meteorological conditions showed the ability to reduce variability due to temperature, relative humidity, and pressure. Using derived flight performance instead of the standard flight performance, the difference between the calculated and measured long-term average noise level increased. Although it showed the ability to reduce the effect of wind up to 8 meters per second, more careful selection of aerodynamic coefficients should be applied.

In addition to the calculation methods, the aircraft substitution corrections provided in the ANP database were assessed. Applying the substitution correction based on ICAO type code resulted in a decreased difference between measurement and calculation. While the substitution based on aircraft configuration (i.e. EASA record number) should be the most accurate, this method showed an increase in the difference between measurement and calculation.

In the end, this research showed that the proposed model improvements did not reduce the difference between the measured and calculated long-term average noise levels. However, this is only true when an appropriate standard meteorological condition is used.

6.2. Recommendations

This research has several strengths, such as the use of a large number of individual flight events, actual meteorological conditions, and all available microphones and aircraft types. This led to relevant insights on the modelling of aircraft noise. However, this research also has some limitations. These limitations, and how they can be overcome in future research, are listed in this section.

From this research it can be concluded that wind speed has a significant effect on the difference between measurements and calculations. In the derived flight performance model used in this research, the derived thrust setting was used, leading to less variability between measurement and calculation up to 8 meters per second compared to the baseline method. However, to account fully for the effect of wind, more research

should be performed on the difference between calculations and measurements at wind speeds above 8 meters per second.

Counterintuitively, the corrections suggested in the ANP substitution table by aircraft configuration i.e. EASA recordnumber, perform worse compared to applying the corrections from the substitution by ICAO type code. These corrections are even worse compared to the situation where no correction is applied at all. To get a better understanding of why the correction for aircraft configuration performs worse compared to the other corrections, more research should be performed assessing the noise for a number of specific aircraft in detail.

From this research it can be concluded that derived flight performance is more susceptible to implementation errors. Smoothing using B-splines proved to be insufficient in terms of stability, leading to a number of outliers in the calculated results. To tackle this problem in the future, it is suggested to use more advanced smoothing and/or filtering methods such as a Kalman filter.

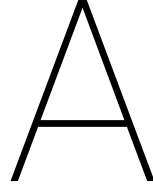
Furthermore, large differences ($> 3\text{dBA}$) between measurements and calculations of single flight events have been found for all calculation methods. For all methods, it is recommended to include the phase of the aircraft on the ground. Furthermore, it is recommended to further research the derived flight performance model, because the smaller probability density functions of this method indicate that model performance might improve when the observable bias is eliminated. Bias might be removed by using a correction of the noise-power-distance data, similar to the method used by the CAA [1]. Additionally, the variability of performance due to different aircraft configurations in different flight phases might be interesting to investigate further. This research assumed average aerodynamic coefficients for the whole flight. However, this might impact the performance of specific flight phases. Using the instantaneous A-weighted noise levels from the measurements and the noise levels for individual flight segments, the application of flight phase specific coefficients might be further investigated.

Future research in derived flight performance for aircraft noise calculations should be related to research in the area of air traffic operations. In terms of both thrust and weight estimation, the BADA-based actual take-off weight estimation method developed by Sun et al. [40] can be adapted to be suited for noise calculations.

Ideally, this research would suggest improvements to ECAC Doc. 29. However, it was found that the uncertainty of the input data remains the main point of attention. It is therefore suggested to validate all flight performance data using spectrum analysis and FDR data.

In an effort to make suggestions for model improvements, an estimation of the modelling error must be made. In order to do this, more information needs to be present about the noise due to other sources. This can either be done by performing measurements with more advanced measurement equipment, such as an acoustic array, or by using more properties of the existing microphone network. Using an existing microphone network, measurements at different microphones belonging to the same flight could be used to eliminate uncertainties due to aircraft configuration. Other properties of the measurements could be used as well, such as the shape of the sound pressure level over time, other numerical values such as the 10dB-down time, and the more detailed noise spectra. For example, filters could be developed to separate aircraft noise from other noise sources within a single measurement, based on the analysis of these noise spectra.

Finally, this research focused on the differences between measurements and calculations. However, estimations of long-term noise and annoyance are often visualised and quantified as contours within noise assessments of airports. Assessing the effects of model improvements on noise contours and annoyance is suggested for future research.



The challenge of comparing measurements and aircraft noise calculations

In this research, the difference between measurements and calculations is considered to be the dependent variable. Equation A.1 and Equation A.2 describe the relationship between the measurement and the calculation as addressed in this research. Equation A.1 assumes that the sound waves of the aircraft and other sources do not interact with each other. The equation shows the energetic summation of two noise events.

$$L_{total} = 10 \cdot \log_{10} (10^{L_{aircraft}/10} + 10^{L_{other}/10}) \quad (A.1)$$

$$L_{aircraft} = L_{calculation} \pm \epsilon_{calculation}, \quad L_{total} = L_{measurement} \pm \epsilon_{measurement} \quad (A.2)$$

where L_{total} is the noise level of all sources in dBA, $L_{aircraft}$ is the actual aircraft noise level in dBA, L_{other} is the noise level due to other than aircraft sources in dBA, $L_{measurement}$ is the measured noise level in dBA, $L_{calculation}$ is the calculated aircraft noise level in dBA, $\epsilon_{measurement}$ is the error of the noise level measurement in dBA, and $\epsilon_{calculation}$ is the error of the calculated aircraft noise level in dBA.

From this relation it can be concluded that noise from other sources can have a significant impact on the total noise and the skewness of the shape of the error distributions. This makes the comparison of aircraft noise calculations and measurements a complicated exercise. Only if $L_{aircraft}$ is significantly larger than L_{other} , a fair comparison between the two can be made. To provide a calculation example, if the aircraft noise is $60dB$ and other sources are $50dB$, the total noise will be $60.4dB$. When combining the aircraft noise with noise from other sources both equal to $60dB$, the total noise will be $63.0dB$.

L_{other} is written as an additional error ($+\epsilon_{other}$) on the aircraft noise in Equation A.3. The limits of this error are shown in Equation A.4, to illustrate that the error ϵ_{other} can only be positive.

$$10^{L_{aircraft}/10} + 10^{L_{other}/10} = 10^{(L_{aircraft} + \epsilon_{other})/10} \rightarrow \epsilon_{other} = 10 \log_{10} (10^{(L_{other} - L_{aircraft})/10} + 1) \quad (A.3)$$

$$\lim_{\Delta L_{o-a} \rightarrow -\infty} 10 \log_{10} (10^{\Delta L_{o-a}/10} + 1) = 0 \quad \text{and} \quad \lim_{\Delta L_{o-a} \rightarrow +\infty} 10 \log_{10} (10^{\Delta L_{o-a}/10} + 1) = +\infty \quad (A.4)$$

where ϵ_{other} is the noise level due to other than aircraft sources written as additional error on top of the actual aircraft noise level in dBA and $\Delta L_{o-a} = L_{other} - L_{aircraft}$ is the difference between the actual aircraft noise and the noise from other sources in dBA. Combining Equation A.1, Equation A.2, and Equation A.3 leads to the following equation:

$$L_{calculation} - L_{measurement} = \pm \epsilon_{calculation} \pm \epsilon_{measurement} - \epsilon_{other} = \Delta L_{c-m} \quad (A.5)$$

where ΔL_{c-m} is the difference between the aircraft noise calculation and the observed measurement in dBA. Although the measurements have a known measurement uncertainty (see section 3.1), within this research there is no accurate information about the noise from other sources or the actual measurement error for a single measurement. The definition of a more accurate estimation is therefore not simply a ΔL_{c-m} value closer to zero, but an $\epsilon_{calculation}$ closer to zero, while having an unknown $\epsilon_{measurement}$ and ϵ_{other} .

B

Calculation procedure

The procedures used for calculating aircraft noise using the various calculation methods are described here. For each noise calculation the following steps were undertaken:

1. Get airborne flight track segments
2. Get observer locations
3. Get aircraft data from ANP database
4. Get NPD data from ANP database
5. Correct NPD data for provided meteorological conditions
6. Calculate noise levels
7. Store noise levels

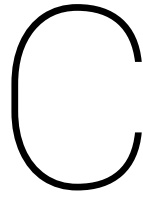
For standard aircraft performance methods, the following steps were undertaken to obtain the desired flight track segments.

1. Get ground track from position data
2. Align ground track with runway
3. Get fixed point profile
4. Combine ground track with fixed point profile into a flight track
5. Estimate bank angle based on ground track positions and fixed point profile velocity

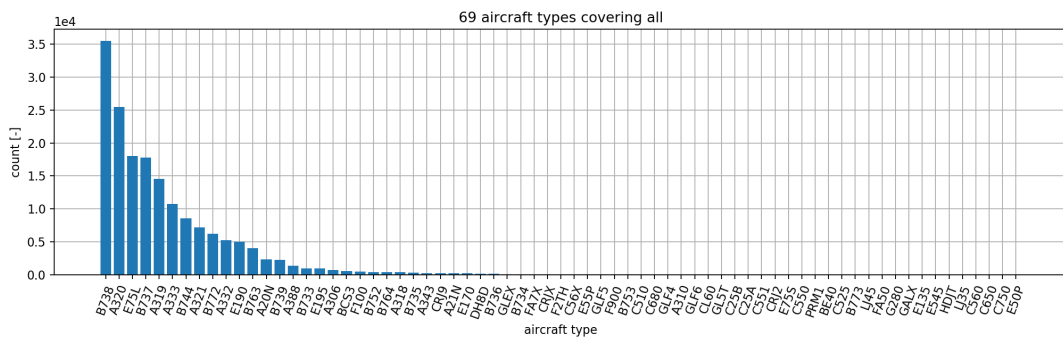
For derived aircraft performance, the steps undertaken are slightly different:

1. Get ground track from position data
2. Remove duplicates
3. Remove groundspeed outliers based on comparison with rolling average.
4. Remove unsorted messages based on timestamps.
5. Get the corrected altitude, i.e. barometric altitude combined with provided difference between GNSS and barometer (ADS-B message).
6. Smooth corrected altitude with a spline
7. Add the ground speed (and acceleration) to the positions data
8. Check if $V > 0$
9. Calculate climb angle (deg)
10. Estimate bank angle
11. Remove outliers based on rolling average

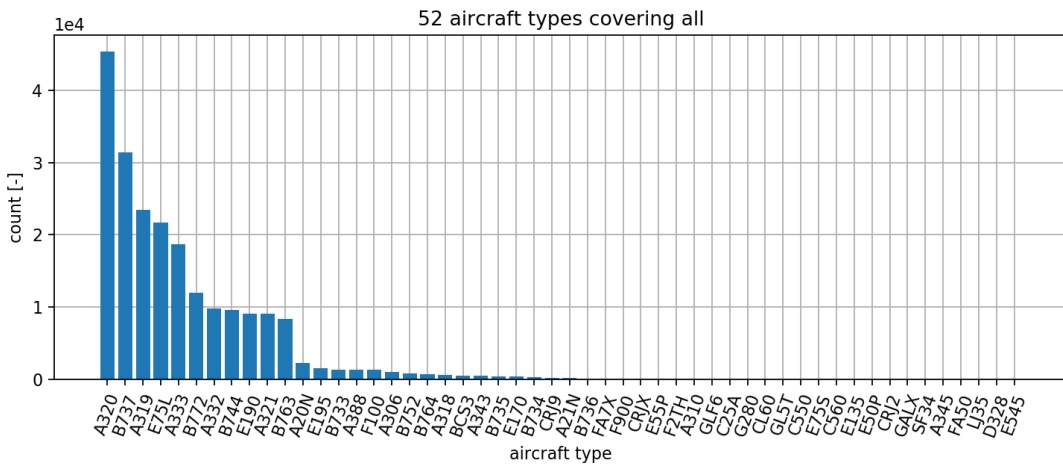
12. Check if $\epsilon \leq 35$
13. Get the local pressure (using lapse rate model and actual meteorological conditions)
14. Estimate thrust setting
15. Remove points to speed up calculations
16. Align ground track with runway
17. Get fixed point profile
18. Combine ground track with fixed point profile into a flight track
19. Estimate bank angle based on ground track positions and fixed point profile velocity



Statistic description of the dataset

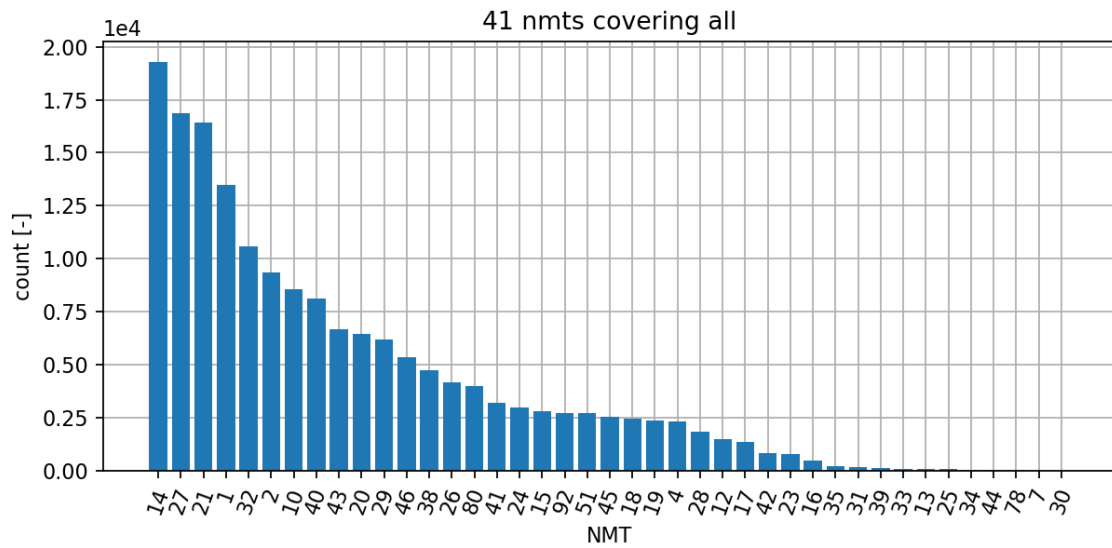


(a) arrival

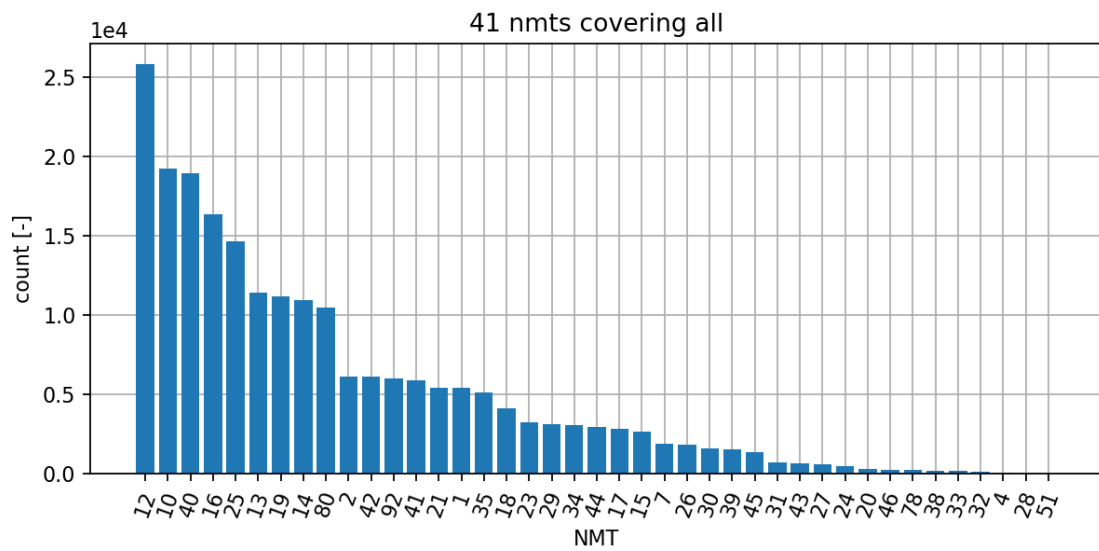


(b) departure

Figure C.1: Distribution of the number of observations for various aircraft types

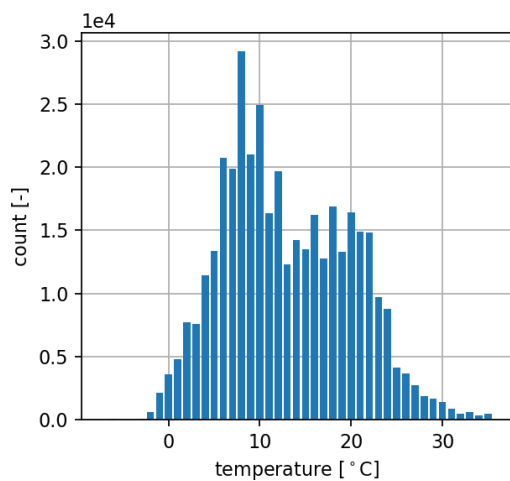


(a) arrival

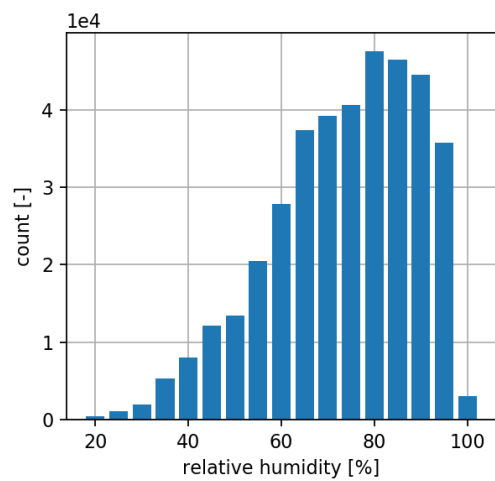


(b) departure

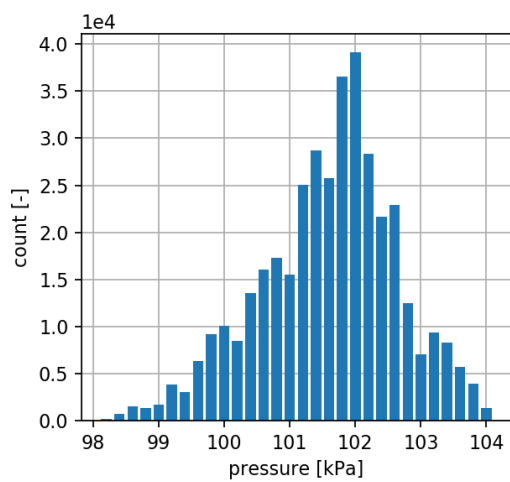
Figure C.2: Distribution of the number of observations for various nmts



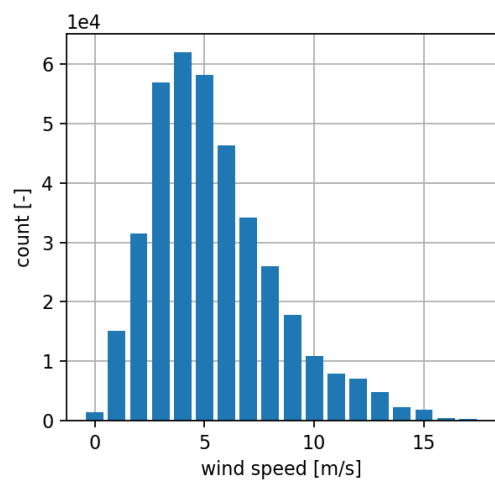
(a)



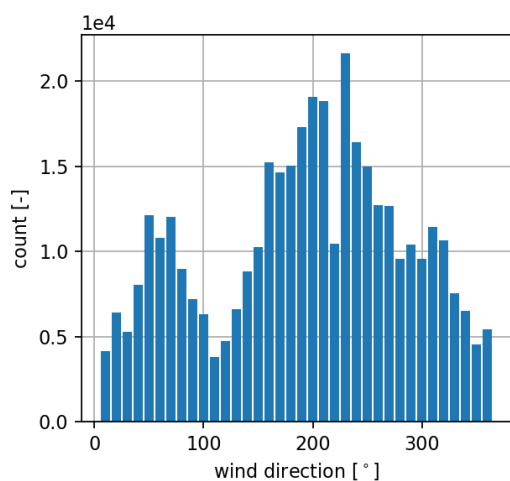
(b)



(c)



(d)



(e)

Figure C.3: Distribution of the number of observations for various meteorological conditions

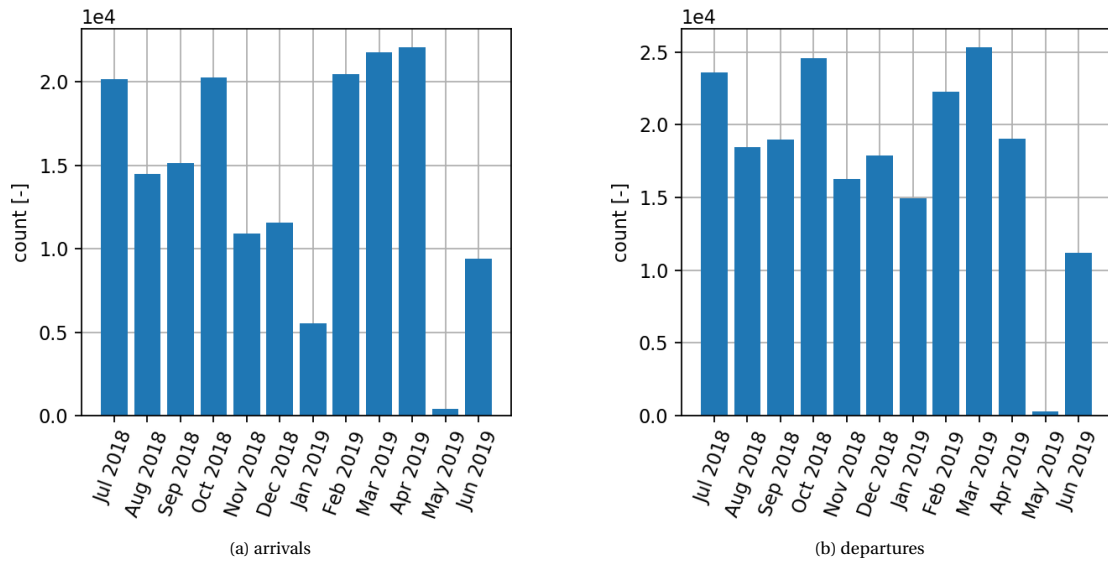


Figure C.4: Distribution of the number of observations for various months

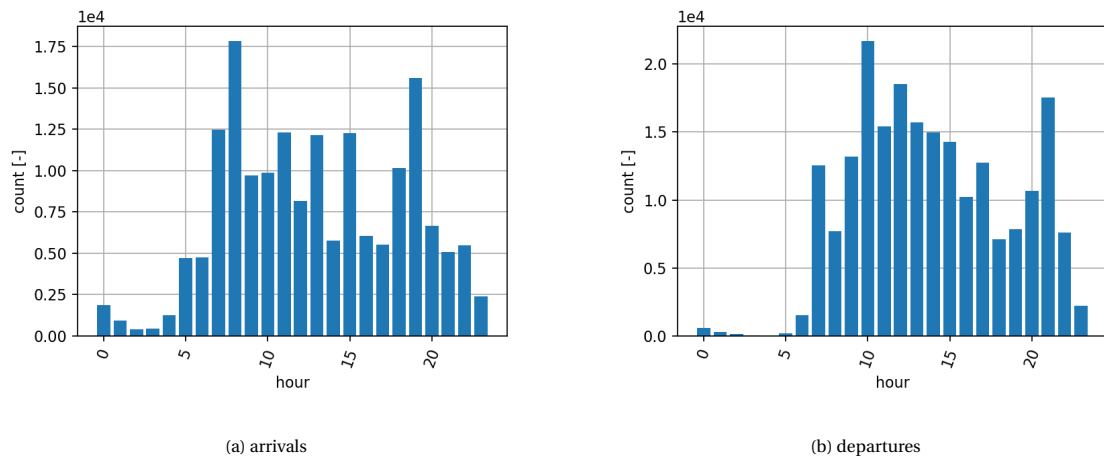


Figure C.5: Distribution of the number of observations for various hours

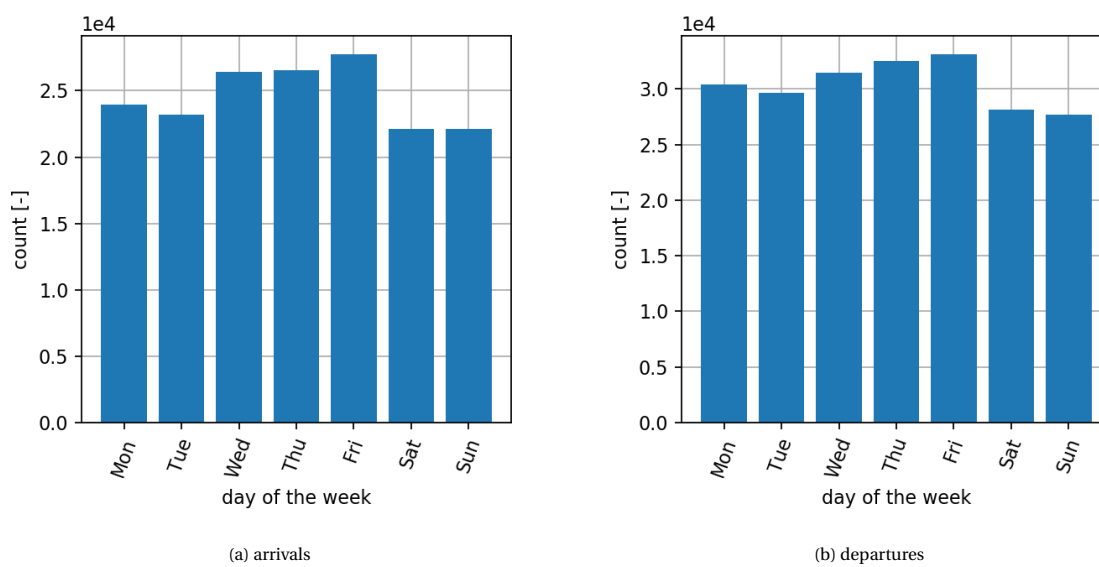


Figure C.6: Distribution of the number of observations for various days



AerLabs Echo verification

Using the described methods in the 4th version of ECAC Doc 29, a model called Echo was developed by AerLabs for the purpose of doing ECAC Doc 29 compliant calculations. This document describes the correctness of Echo by comparing the results of the new implementation with the verification results as provided in ECAC Doc 29 Volume 3, Part 1. To generate the results, Echo version 1.1.2 was used in this document.

D.1. Receptor results

For twelve reference cases, the SEL results at 18 receptor locations are provided in ECAC Doc 29. SEL results have been determined using Echo. The difference between the reference results and the results from Echo can be found in the two tables below. The tables show the Echo calculations minus the reference results as provided in ECAC Doc 29. All SEL values are provided in dBA.

Table D.1: The difference between Echo's receptor results and the reference results from ECAC Doc. 29 4th Edition: Volume 3, Part 1[13] for the cases JETFAC, JETFAS, JETFDC, JETFDS, JETWAC and JETWAS.

Receptor Identifier	JETFAC	JETFAS	JETFDC	JETFDS	JETWAC	JETWAS
R01			0.0	0.01		
R02	0.0	0.0	0.0	0.0	0.0	0.0
R03	0.0	0.0	0.0	0.0	0.0	0.0
R04	0.0	0.0	0.0	0.0	0.0	0.0
R05	0.0	0.0	0.0	0.0	0.0	0.0
R06			0.0			
R07			0.0			
R08			0.0			
R09			0.0			
R10			0.0			
R11			0.0			
R12	0.0				0.0	
R13	0.0	0.0			0.0	0.0
R14	0.0				0.0	
R15	0.0				0.0	
R16	0.01				0.0	
R17	0.0				0.0	
R18	0.0	0.0			0.0	0.0

D.2. Grid results

For twelve reference cases, the SEL results of a grid were provided. Only SEL values of 80 dBA and up were included. For the same points, the results have also been determined using Echo. For all grid points defined

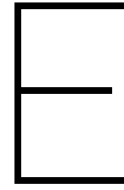
Table D.2: The difference between Echo's receptor results and the reference results from ECAC Doc. 29 4th Edition: Volume 3, Part 1[13] for the cases JETWDC, JETWDS, PROPAC, PROPAS, PROPDC and PROPDS.

Receptor Identifier	JETWDC	JETWDS	PROPAC	PROPAS	PROPCD	PROPDS
R01	0.0	0.01			0.0	0.0
R02	0.0	0.0	0.0	0.0	0.0	0.0
R03	0.0	0.0	0.0	0.0	0.0	0.0
R04	0.0	0.0	0.0	0.0	0.0	0.0
R05	0.0	0.0	0.0	0.0	0.0	0.0
R06	0.0				0.0	
R07	0.0				0.0	
R08	0.0				0.0	
R09	0.0				0.0	
R10	0.0				0.0	
R11	0.0				0.0	
R12			0.0			
R13			0.0	0.0		
R14			0.0			
R15			0.0			
R16			0.0			
R17			0.0			
R18			0.0	0.0		

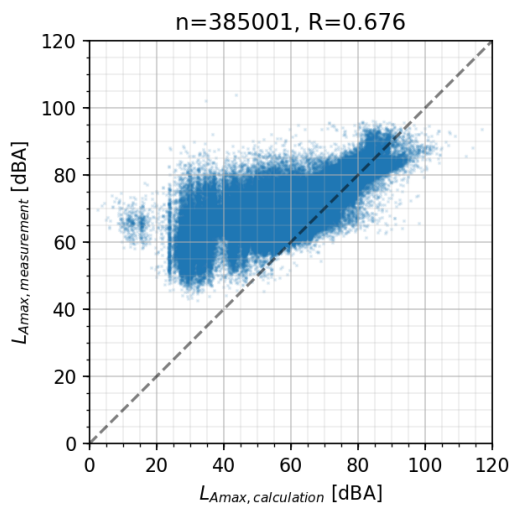
in the reference cases in ECAC Doc 29, the error δ is calculated. The error is calculated using the SEL results of Echo minus the reference results as provided in ECAC Doc 29 in dBA. The table below lists the maximum errors δ_{max} and root mean square error δ_{RMS} for each case.

Table D.3: The difference between Echo's grid results and the reference results from ECAC Doc. 29 4th Edition: Volume 3, Part 1[13].

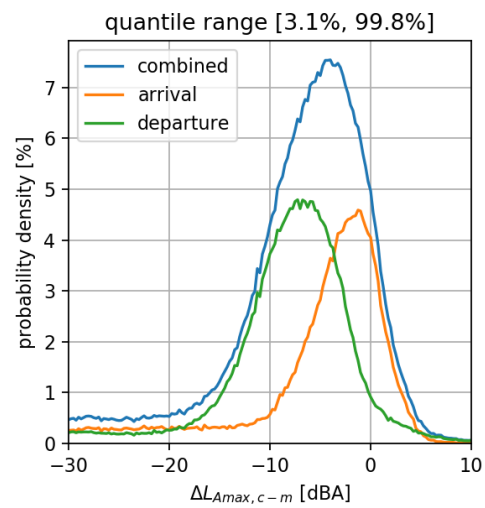
	δ_{max} [dBA]	δ_{RMS} [dBA]
JETFAC	0.01	0.003
JETFAS	0.01	0.003
JETFDC	0.01	0.003
JETFDS	0.01	0.003
JETWAC	0.01	0.003
JETWAS	0.01	0.003
JETWDC	0.01	0.003
JETWDS	0.01	0.003
PROPAC	0.01	0.003
PROPAS	0.01	0.003
PROPCD	0.01	0.003
PROPDS	0.01	0.003



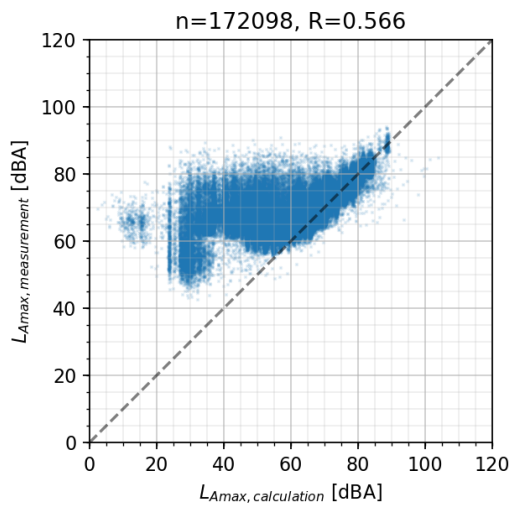
Distribution of the noise levels



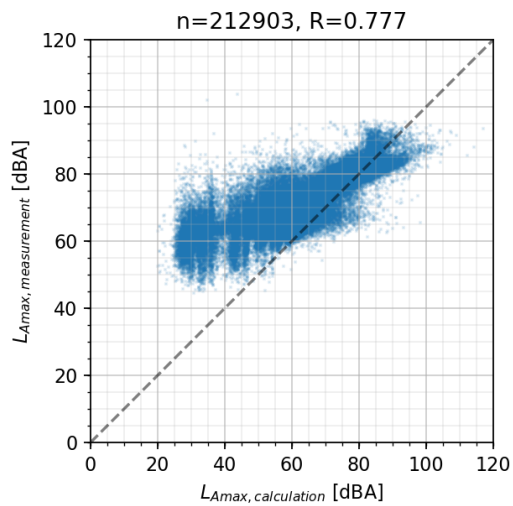
(a) Scatterplot of arrivals and departures combined



(b) Probability density of difference between measurement and calculation

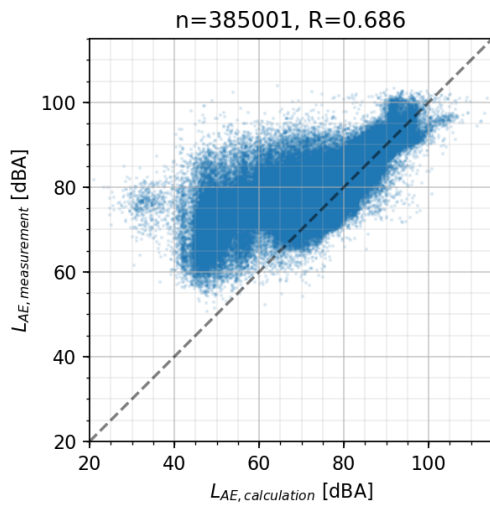


(c) Scatterplot of arrivals

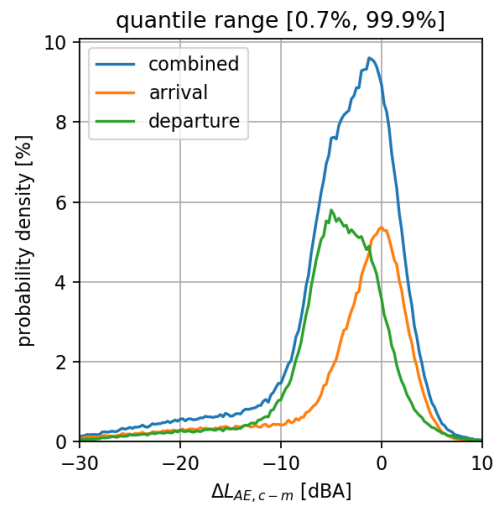


(d) Scatterplot of departures

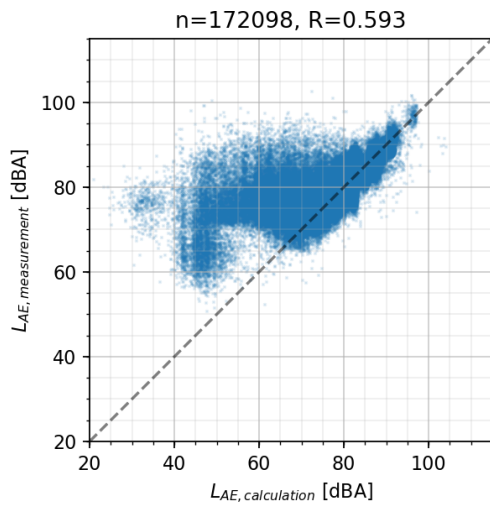
Figure E.1: Collection of all L_{Amax} results using the calculation method with standard flight performance and standard meteorological conditions.



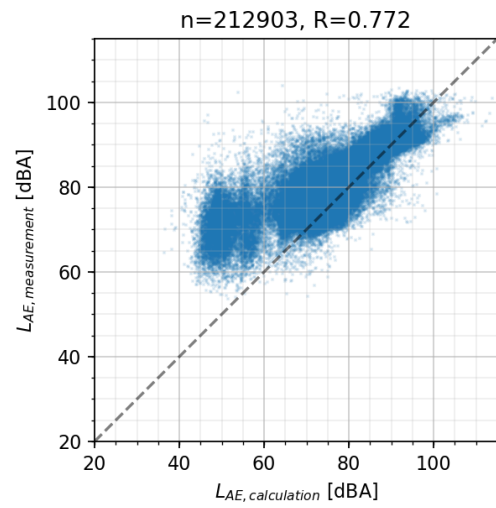
(a) Scatterplot of arrivals and departures combined



(b) Probability density of difference between measurement and calculation

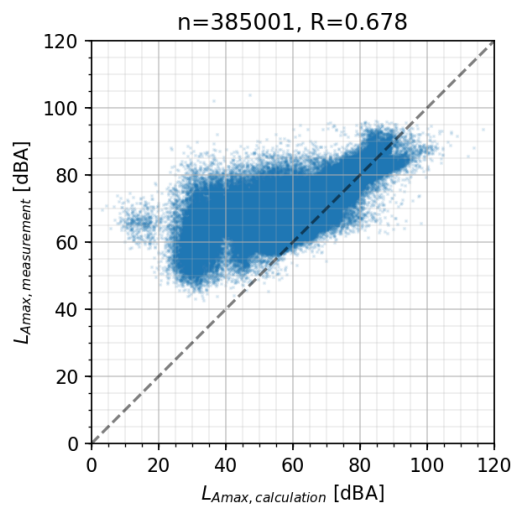


(c) Scatterplot of arrivals

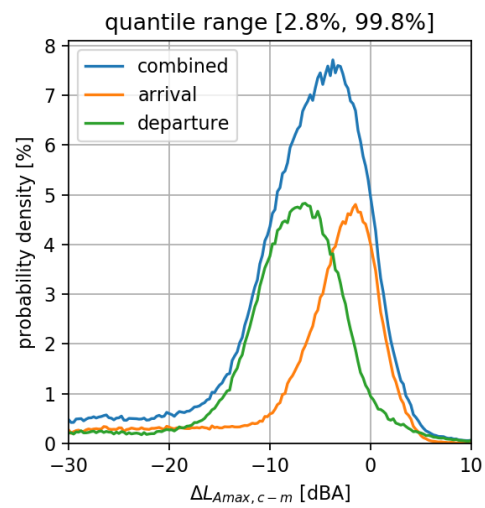


(d) Scatterplot of departures

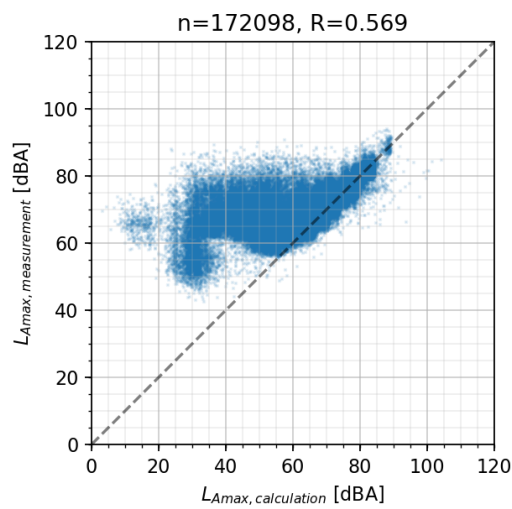
Figure E.2: Collection of all SEL results using the calculation method with standard flight performance and actual meteorological conditions (method B).



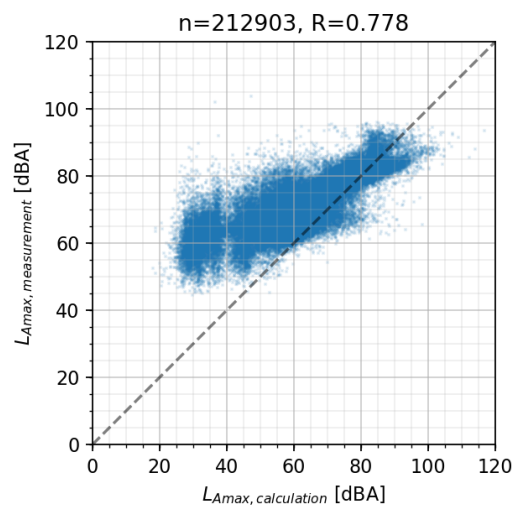
(a) Scatterplot of arrivals and departures combined



(b) Probability density of difference between measurement and calculation

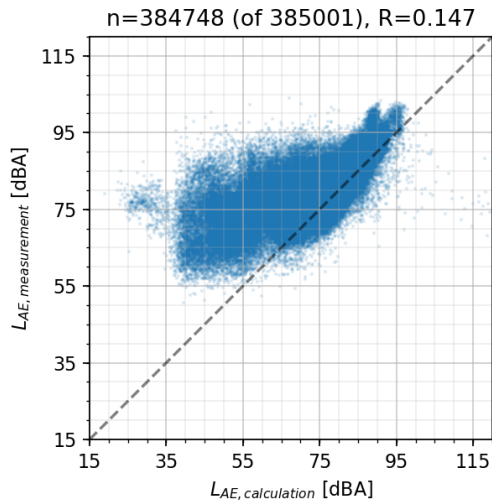


(c) Scatterplot of arrivals

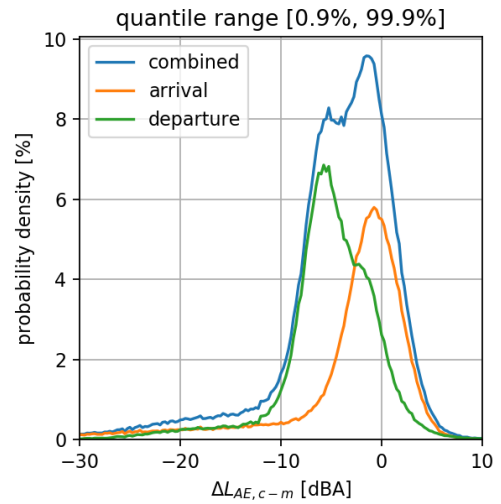


(d) Scatterplot of departures

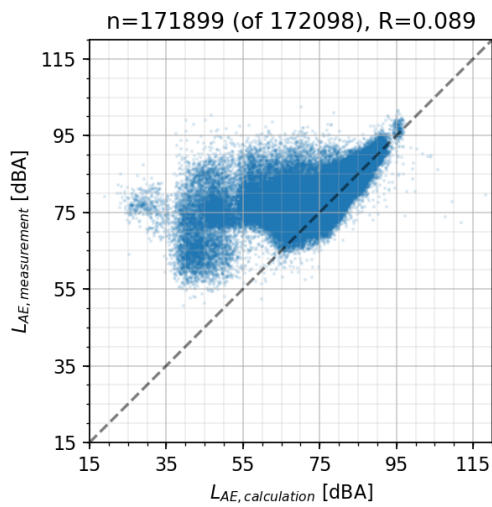
Figure E.3: Collection of all L_{Amax} results using the calculation method with standard flight performance and actual meteorological conditions (method B).



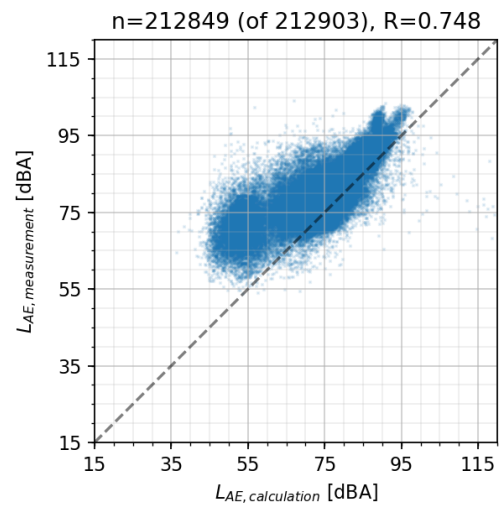
(a) Scatterplot of arrivals and departures combined



(b) Probability density of difference between measurement and calculation



(c) Scatterplot of arrivals



(d) Scatterplot of departures

Figure E.4: Collection of all SEL results using the calculation method with derived flight performance and actual meteorological conditions (method C).

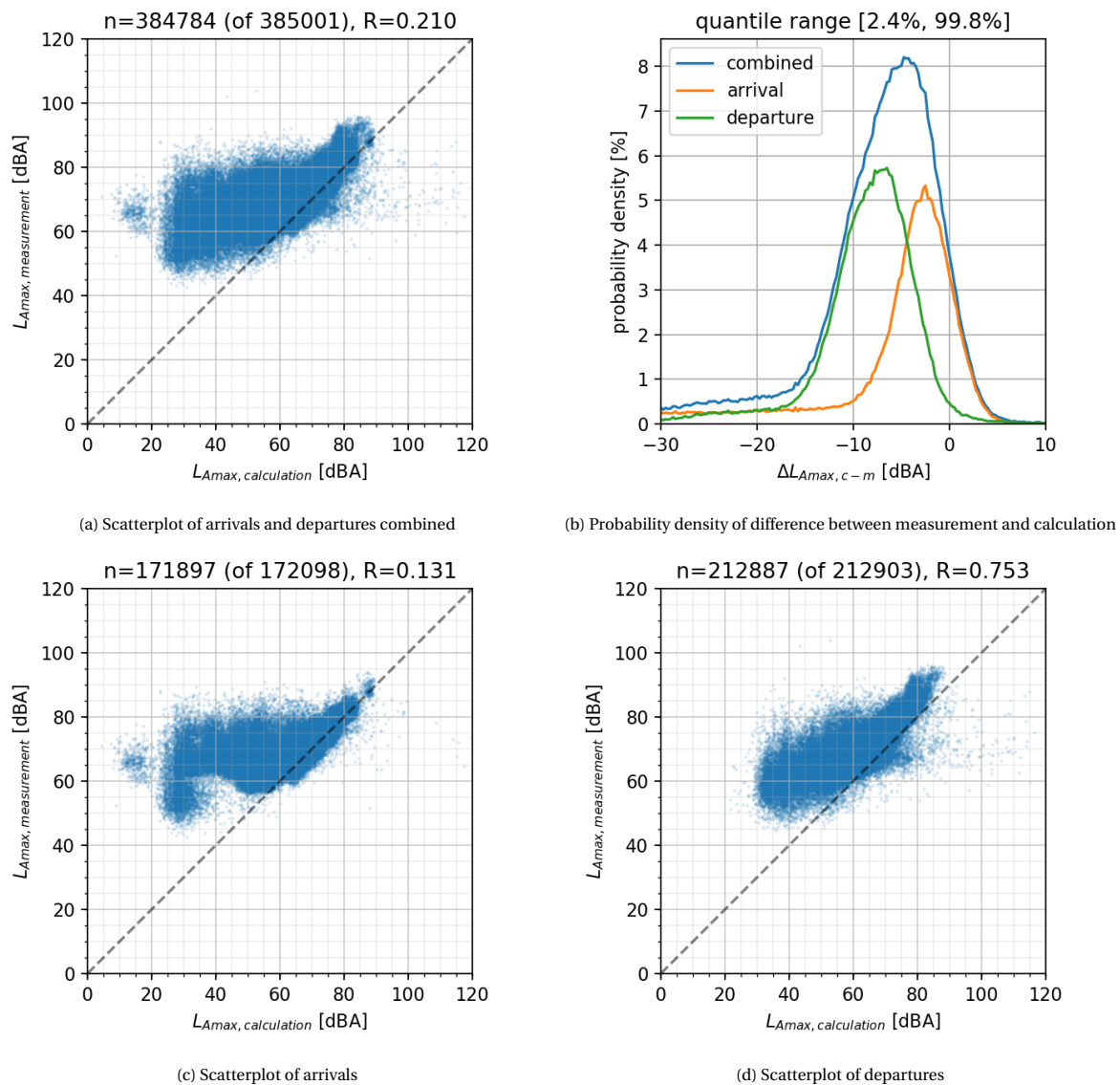
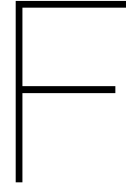


Figure E.5: Collection of all L_{Amax} results using the calculation method with derived flight performance and actual meteorological conditions (method C).



Meteorological adjustment

The collection of all results comparing the results of standard meteorological conditions with actual meteorological conditions, both using the standard aircraft performance calculation method. In this chapter, the results without NMT 78 and NMT 80 were used.

F.1. Actual meteorological conditions

Table F1: The consistency of the difference between calculation and measurement $\Delta L_{AE,c-m}$ over a range of pressures.

meteorological condition	quantile	constant [dBA]	residual [dBA ²]	residual decrease [%]
standard	2.5%	-19.53	$4.11 \cdot 10^{10}$	-
standard	50.0%	-3.35	$4.29 \cdot 10^9$	-
standard	97.5%	4.32	$1.15 \cdot 10^9$	-
actual	2.5%	-19.26	$3.87 \cdot 10^{10}$	5.9
actual	50.0%	-3.40	$3.18 \cdot 10^9$	25.9
actual	97.5%	4.21	$7.64 \cdot 10^8$	33.4

Table F2: The consistency of the difference between calculation and measurement $\Delta L_{AE,c-m}$ over a range of relative humidities.

meteorological condition	quantile	constant [dBA]	residual [dBA ²]	residual decrease [%]
standard	2.5%	-21.72	$2.72 \cdot 10^{10}$	-
standard	50.0%	-3.87	$2.08 \cdot 10^9$	-
standard	97.5%	4.05	$1.22 \cdot 10^9$	-
actual	2.5%	-21.13	$2.03 \cdot 10^{10}$	25.4
actual	50.0%	-3.69	$1.66 \cdot 10^9$	20.0
actual	97.5%	4.14	$4.77 \cdot 10^8$	61.1

Table F3: The consistency of the difference between calculation and measurement $\Delta L_{AE,c-m}$ over a range of temperatures.

meteorological condition	quantile	constant [dBA]	residual [dBA ²]	residual decrease [%]
standard	2.5%	-21.57	$4.07 \cdot 10^{10}$	-
standard	50.0%	-3.99	$5.42 \cdot 10^9$	-
standard	97.5%	3.99	$1.53 \cdot 10^9$	-
actual	2.5%	-21.11	$2.74 \cdot 10^{10}$	32.7
actual	50.0%	-3.81	$2.29 \cdot 10^9$	57.9
actual	97.5%	4.08	$4.27 \cdot 10^8$	72.0

F.2. Wind

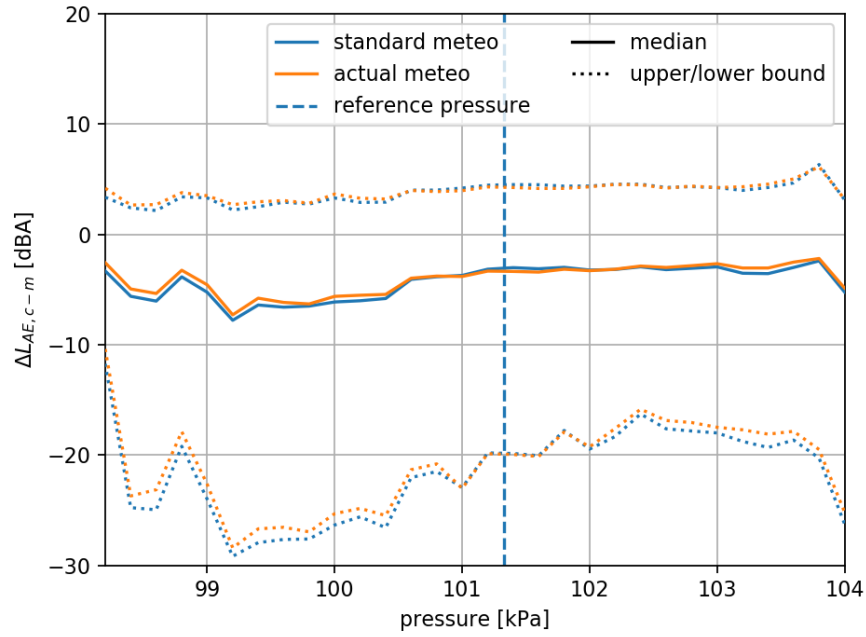


Figure F1: The 95% confidence bounds of the difference between the sound exposure level calculation and measurement $\Delta L_{AE,c-m}$ versus the pressure. Calculations using standard aircraft performance with both standard and actual meteorological conditions.

Table F4: The consistency of the difference between calculation and measurement $\Delta L_{AE,c-m}$ over a range of wind directions.

meteorological condition	quantile	constant [dBA]	residual [$dB A^2$]	residual decrease [%]
standard	2.5%	-21.61	$5.08 \cdot 10^{10}$	-
standard	50.0%	-3.94	$3.62 \cdot 10^9$	-
standard	97.5%	4.05	$7.59 \cdot 10^8$	-
actual	2.5%	-21.16	$5.09 \cdot 10^{10}$	-0.1
actual	50.0%	-3.85	$3.08 \cdot 10^9$	14.9
actual	97.5%	4.05	$4.97 \cdot 10^8$	34.5

Table F5: The consistency of the difference between calculation and measurement $\Delta L_{AE,c-m}$ over a range of wind speeds.

meteorological condition	quantile	constant [dBA]	residual [$dB A^2$]	residual decrease [%]
standard	2.5%	-17.31	$9.00 \cdot 10^{10}$	-
standard	50.0%	-3.12	$1.10 \cdot 10^{10}$	-
standard	97.5%	4.32	$3.68 \cdot 10^9$	-
actual	2.5%	-17.10	$8.57 \cdot 10^{10}$	4.7
actual	50.0%	-3.11	$9.69 \cdot 10^9$	12.2
actual	97.5%	4.23	$3.24 \cdot 10^9$	12.0

Table F6: The consistency of the difference between calculation and measurement $\Delta L_{AE,c-m}$ over a range of wind directions.

aircraft performance	quantile	constant [dBA]	residual [$dB A^2$]	residual decrease [%]
standard	2.5%	-21.16	$5.09 \cdot 10^{10}$	-
standard	50.0%	-3.85	$3.08 \cdot 10^9$	-
standard	97.5%	4.05	$4.97 \cdot 10^8$	-
derived	2.5%	-21.22	$7.29 \cdot 10^{10}$	-43.3
derived	50.0%	-3.52	$2.77 \cdot 10^9$	9.9
derived	97.5%	3.55	$5.13 \cdot 10^8$	-3.2

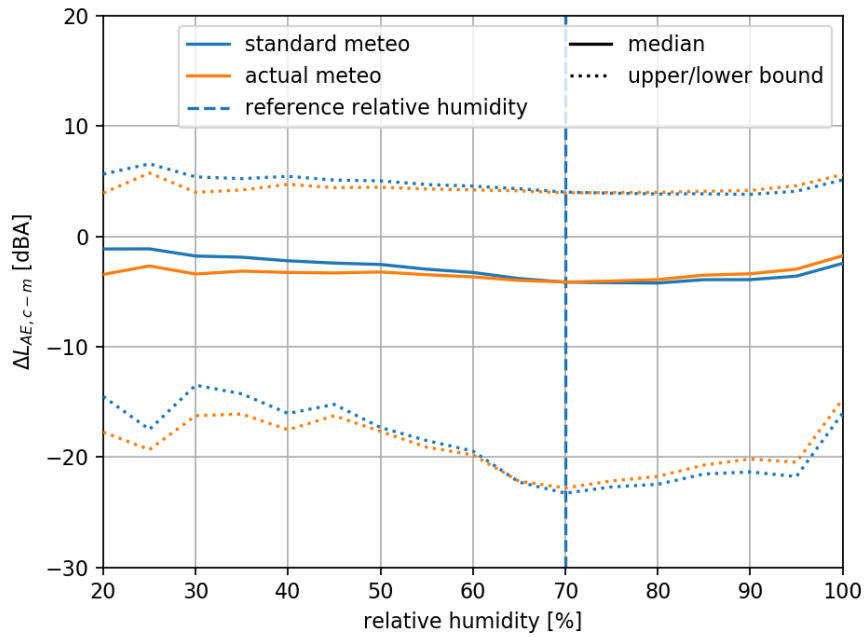


Figure E2: The 95% confidence bounds of the difference between the sound exposure level calculation and measurement $\Delta L_{AE,c-m}$ versus the relative humidity. Calculations using standard aircraft performance with both standard and actual meteorological conditions.

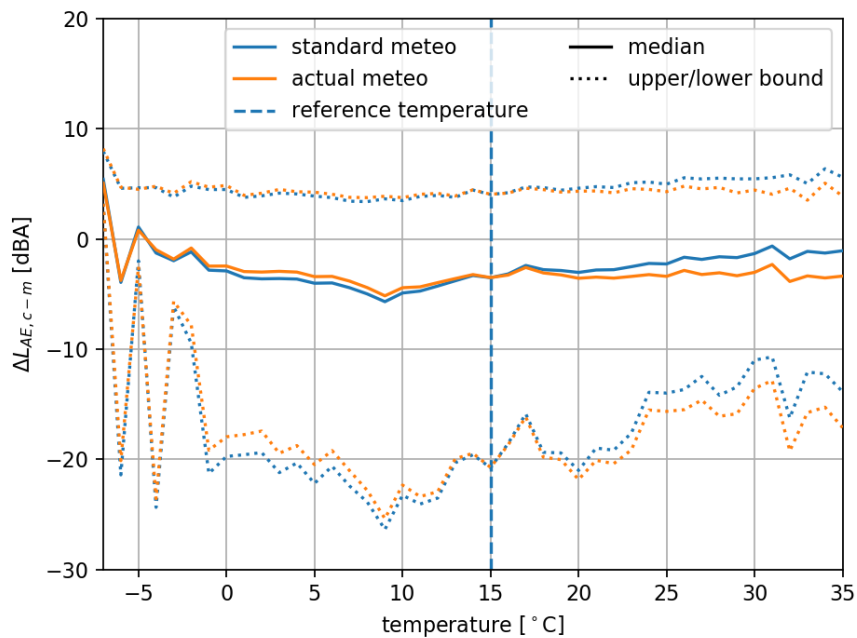


Figure E3: The 95% confidence bounds of the difference between the sound exposure level calculation and measurement $\Delta L_{AE,c-m}$ versus the temperature. Calculations using standard aircraft performance with both standard and actual meteorological conditions.

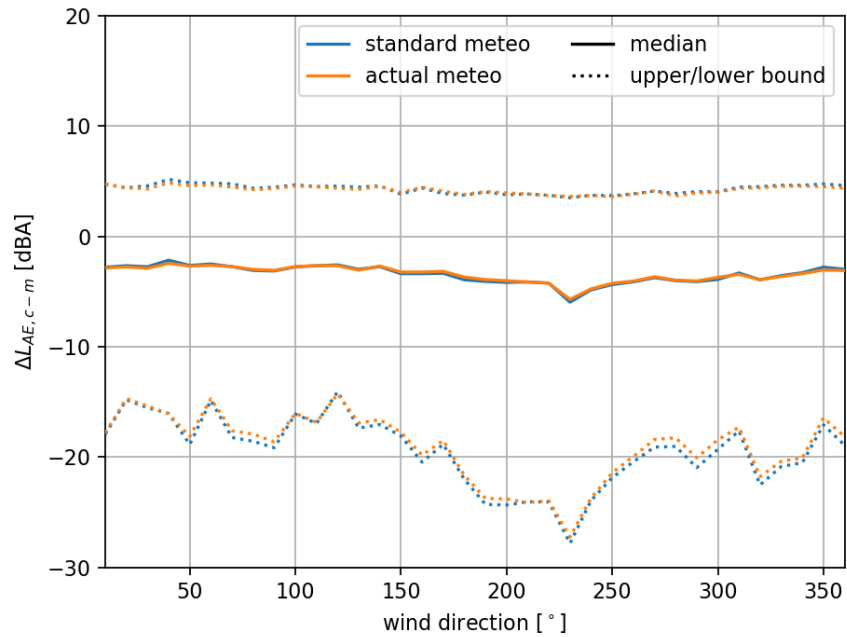


Figure E4: The 95% confidence bounds of the difference between the sound exposure level calculation and measurement $\Delta L_{AE,c-m}$ versus the wind direction. Calculations using standard aircraft performance with both standard and actual meteorological conditions.

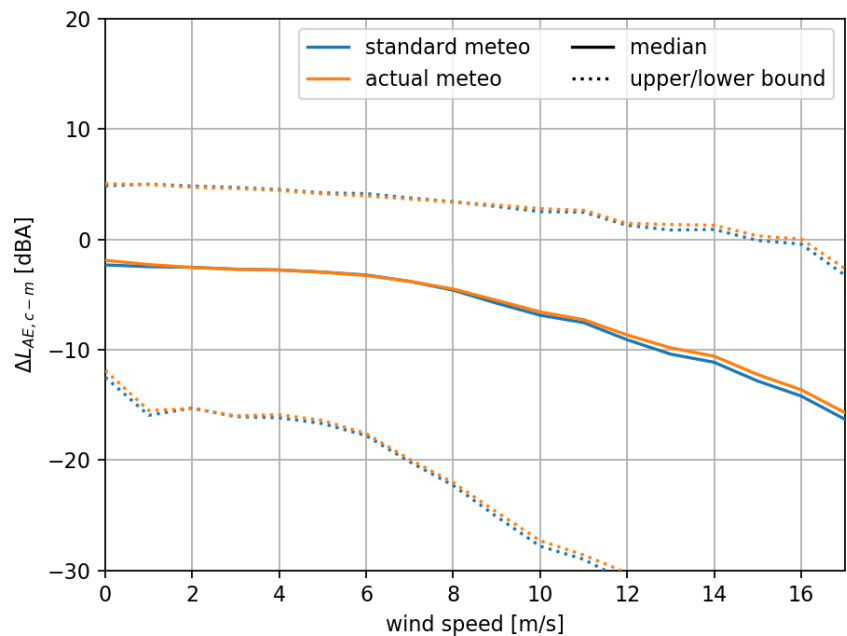


Figure E5: The 95% confidence bounds of the difference between the sound exposure level calculation and measurement $\Delta L_{AE,c-m}$ versus the wind speed. Calculations using standard aircraft performance with both standard and actual meteorological conditions.

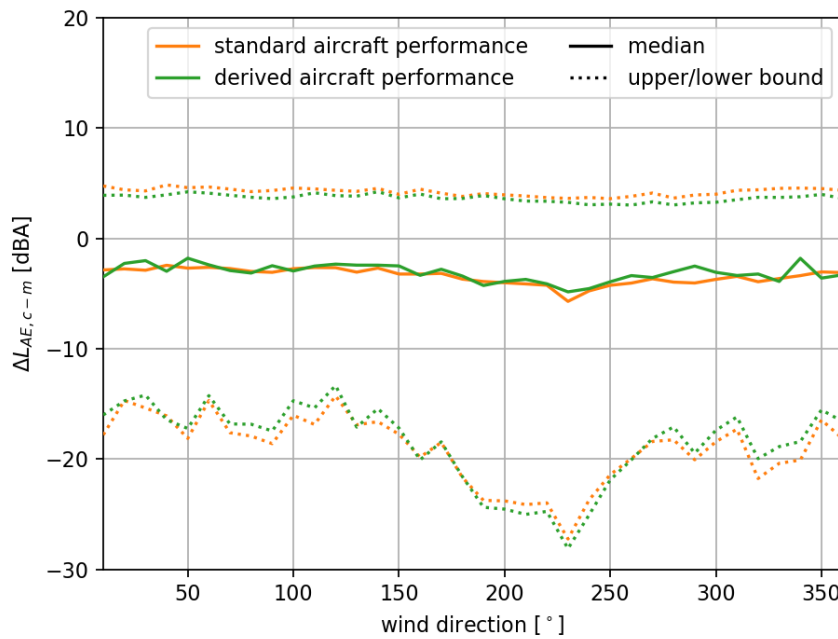


Figure E6: The 95% confidence bounds of the difference between the sound exposure level calculation and measurement $\Delta L_{AE,c-m}$ versus the wind direction. Calculations using standard and derived aircraft performance, both with actual meteorological conditions.

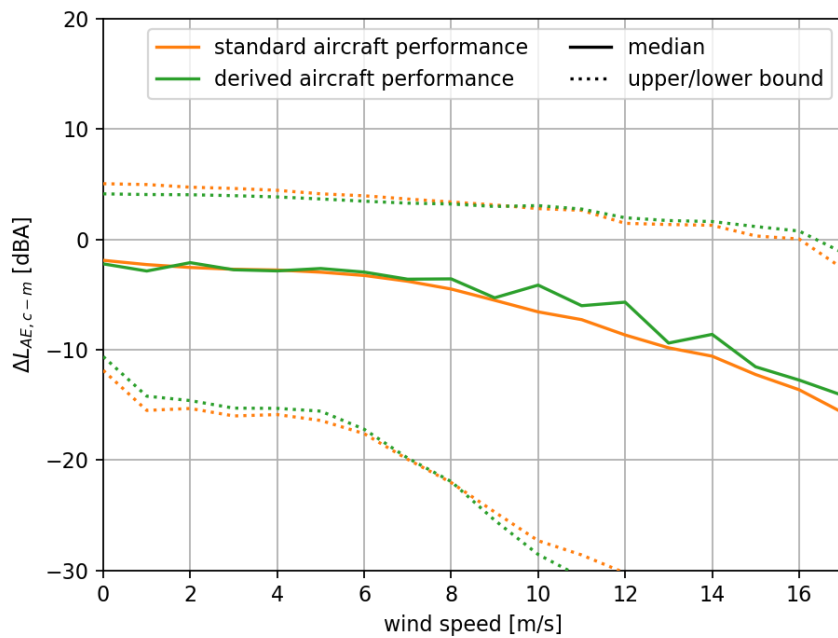


Figure E7: The 95% confidence bounds of the difference between the sound exposure level calculation and measurement $\Delta L_{AE,c-m}$ versus the wind speed. Calculations using standard and derived aircraft performance, both with actual meteorological conditions.

G

Derivation of BADA force balance equation

The two methods for the derivation of actual aircraft flight performance considered for this research are the force balance equation from ECAC Doc. 29 and Total-Energy Model from BADA. Although they are provided in different formats and using different units, the methods are almost equal. In order to compare them, the Total-Energy Model is rewritten such that it has the same format (and units) as the force balance equation provided in ECAC Doc. 29.

Take ECAC Doc. 29 as a starting point. The force balance equation provided in ECAC Doc. 29 [13] is:

$$\frac{F_n}{\delta} = W \frac{R \cos \gamma + \sin \gamma + \frac{a}{g}}{N \delta} \quad (\text{G.1})$$

where F_n is net thrust per engine in lbf, W is the aircraft weight in lb, R is the drag-to-lift ratio C_D/C_L , γ is the flight path angle, g is the gravitational acceleration of 9.81 m/s^2 in ft/s^2 , a is the average acceleration of the aircraft in ft/s^2 , N is the number of engines supplying thrust, and δ is the ratio of ambient air pressure at the aircraft to the standard air pressure at mean sea level.

The Total-Energy Model from BADA [11] is provided as:

$$(T - D)V_{TAS} = mg \frac{dh}{dt} + mV_{TAS} \frac{dV_{TAS}}{dt} \quad (\text{G.2})$$

where T is the thrust acting parallel to the aircraft velocity vector in N, D is the aerodynamic drag in N, m is the aircraft mass in kg, h is the altitude in m, g is the gravitational acceleration of 9.81 m/s^2 , V_{TAS} is the true airspeed in m/s, and d/dt is the time derivative in s^{-1} .

Rewriting the equation to keep only the thrust on the left-hand side of the equation, the following equation can be obtained:

$$T = D + mg \left(\frac{dh}{dt} \frac{1}{V_{TAS}} \right) + m \frac{dV_{TAS}}{dt} \quad (\text{G.3})$$

Since V_{TAS} is also a derivative in time (of the distance along the direction of the true airspeed), the term between the brackets can be simplified to a single fraction indicating the change in height over the change in distance, which is equal to the sine of the flight path angle γ .

$$\frac{dh}{dt} \frac{1}{V_{TAS}} = \frac{dh}{dt} \frac{dt}{ds_{TAS}} = \frac{dh}{ds_{TAS}} = \sin \gamma \quad (\text{G.4})$$

where ds_{TAS}/dt is the derivative of the travelled distance along the vector of the true airspeed in m/s and γ is the flight path angle.

In BADA the following definitions are provided for the drag and lift-coefficient, assuming the lift-coefficient for a flight path angle of zero.

$$D = \frac{C_D \rho V_{TAS}^2 S}{2} \quad (\text{G.5})$$

$$C_L = \frac{2mg}{\rho V_{TAS}^2 S \cos \phi} \quad (G.6)$$

where a lot of new variables are introduced. However, they are irrelevant since they are cancelled out when substituting $R = C_D/C_L$ and Equation G.6 in Equation G.5. Substitution of these equations leads to Equation G.7.

$$D = \frac{RC_L \rho V_{TAS}^2 S}{2} = \frac{Rmg}{\cos \phi} \quad (G.7)$$

Using Equation G.3, Equation G.4 and Equation G.7, the equation for the thrust is now known (Equation G.8). To obtain the corrected net thrust per engine, the thrust needs to be divided by the number of engines and the pressure ratio δ (Equation G.9). Furthermore, the dV_{TAS}/dt is the acceleration along the vector of the airspeed a_{TAS} .

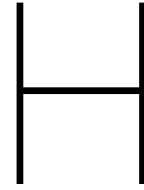
$$T = \frac{Rmg}{\cos \phi} + mg \sin \gamma + m \frac{dV_{TAS}}{dt} \quad (G.8)$$

$$\frac{F_n}{\delta} = \frac{T}{N\delta} \quad (G.9)$$

Combining Equation G.8, Equation G.9 and using a_{TAS} , the equation can be written as follows, which has the same format as Equation 2.25.

$$\frac{F_n}{\delta} = mg \frac{R \frac{1}{\cos \phi} + \sin \gamma + \frac{a_{TAS}}{g}}{N\delta} \quad (G.10)$$

Now, the units can be converted. To obtain the corrected net thrust in pounds force lbf, $m \cdot g$ should also be converted to lb. Furthermore, a_{TAS} and g can have any unit of acceleration (m/s^2 or ft/s^2) as long as they are consistent with each other. After applying the unit conversion, the Total-Energy Method is now in the same format as the force balance equation of ECAC Doc. 29.



Uncertainty quantification of long-term average noise levels

Aircraft noise model uncertainty has been assessed before in [2, 39], both using the "Guide to the expression of uncertainty in measurement (GUM)" [22]. This method assesses the uncertainty of all model and input elements individually to determine the overall uncertainty of the model. This research only the estimation of the total long-term average noise level uncertainty is required. This research uses a different approach to quantify the uncertainty of the long-term average noise level. A statistical bootstrapping method is used because it does not require any prior knowledge of the error distribution of both the model and the inputs. More specifically, case re-sampling using a Monte Carlo algorithm is used for this research.

A statistical bootstrapping method uses random sampling with replacement to construct new data sets that are based on the original data set. These new data sets are slightly different, because the method allows copies within the data set. So an entry in the original data set might be present multiple times in one of the new data sets, but absent in another. For each new and slightly altered data set, the long-term average noise level can be determined. When performing this procedure many times (hence the Monte Carlo algorithm), a large number of long-term average noise levels can be determined. Similar to the single event noise levels a probability density function can be constructed with these results.

10000 new data sets have been constructed for this research, all containing XX observations. Results of the uncertainty estimation can be found in Figure H.1. The long-term average noise level calculations as described in Equation 4.1 is heavily influenced by high single event noise levels. Because the noise levels of the derived flight performance calculations still contain outliers, all flights with single event noise levels above 120dBA were ignored. This creates a fair comparison between the results of various calculation methods and their differences with the long-term average noise level based on the measurements.

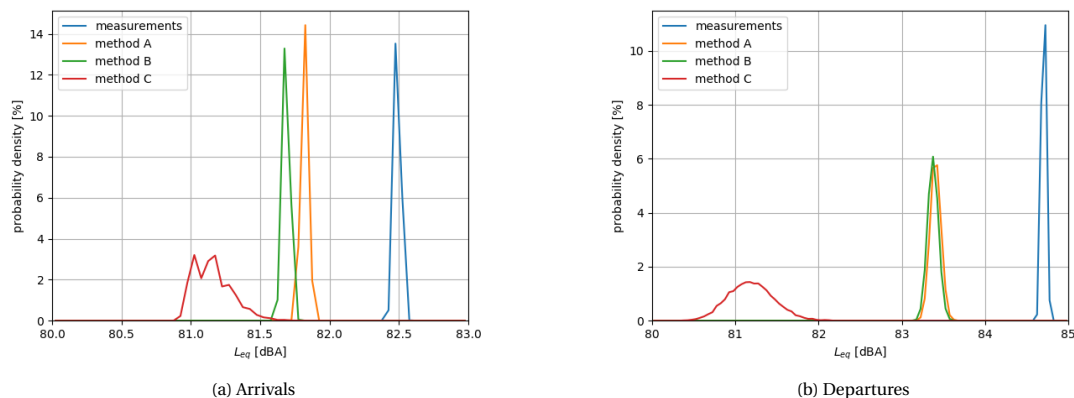


Figure H.1: Probability density of L_{eq} based on the bootstrapping results for the measurements and the three calculation methods. Definitions of the methods A, B, and C can be found in Table 4.2.

For each data set, the difference between calculated and measured long-term average noise level is determined. These differences are shown in Figure H.2. The results are further summarised in Table H.1. Although the results themselves will be further discussed in chapter 4 and chapter 5, these figures and the table already make clear that there are differences in the uncertainties of the various calculation methods that are valuable to address.

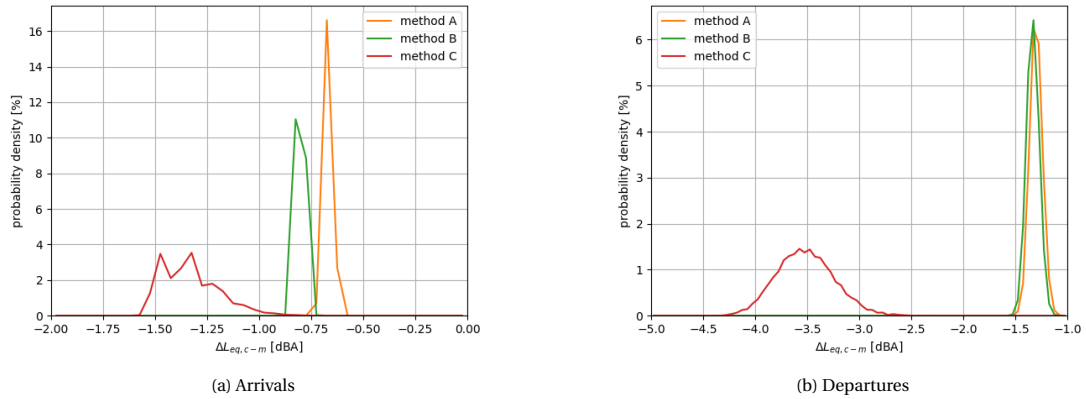


Figure H.2: Probability density of $\Delta L_{eq,c-m}$ based on the bootstrapping results for the three calculation methods. Definitions of the methods A, B, and C can be found in Table 4.2.

Table H.1: Uncertainty quantification of $\Delta L_{eq,c-m}$, the difference between the calculated and the measured long-term average noise level.

Method	Operation	Singular $\Delta L_{eq,c-m}$	Lower $\Delta L_{eq,c-m}$	Upper $\Delta L_{eq,c-m}$
A	arrival	-0.67	-0.73	-0.60
B	arrival	-0.80	-0.87	-0.74
C	arrival	-1.33	-1.57	-0.57
A	departure	-1.30	-1.54	-1.06
B	departure	-1.33	-1.57	-1.09
C	departure	-3.51	-4.36	-2.34

Bibliography

- [1] Features of the ANCON noise modelling process. <https://www.caa.co.uk/Consumers/Environment/Noise/Features-of-the-ANCON-noise-modelling-process/>. [Online; accessed 27-September-2019].
- [2] Douglas Allaire, George Noel, Karen Willcox, and Rebecca Cointin. Uncertainty quantification of an Aviation Environmental Toolsuite. *Reliability Engineering & System Safety*, 126:14–24, June 2014. ISSN 09518320. doi: 10.1016/j.res.2014.01.002. URL <http://linkinghub.elsevier.com/retrieve/pii/S0951832014000039>.
- [3] M. Arntzen and D.G. Simons. Modeling and synthesis of aircraft flyover noise. *Applied Acoustics*, 84:99–106, October 2014. ISSN 0003682X. doi: 10.1016/j.apacoust.2013.09.002. URL <http://linkinghub.elsevier.com/retrieve/pii/S0003682X13002181>.
- [4] Michael Arntzen, Sander J. Heblj, and Dick G. Simons. Weather-Dependent Airport Noise Contour Prediction Concept Based on Ray Tracing. *Journal of Aircraft*, 51(5):1351–1359, September 2014. ISSN 0021-8669, 1533-3868. doi: 10.2514/1.C032149. URL <http://arc.aiaa.org/doi/10.2514/1.C032149>.
- [5] C. Asensio, M. Recuero, and M. Ruiz. Aircraft noise-monitoring according to ISO 20906. Evaluation of uncertainty derived from the classification and identification of aircraft noise events. *Applied Acoustics*, 73(3):209–217, March 2012. ISSN 0003682X. doi: 10.1016/j.apacoust.2011.09.002. URL <http://linkinghub.elsevier.com/retrieve/pii/S0003682X11002477>.
- [6] Ingo U Borchers, Urban Emborg, Antonio Sollo, Elly H Waterman, Jacques Paillard, Peter N Larsen, Gerard Venet, Peter Goeransson, and Vincent Martin. Advanced study for active noise control in aircraft (asanca). In *Fourth Aircraft Interior Noise Workshop*, 1992.
- [7] Council of European Union. Council regulation (EU) no 2015/996, 2015. <http://data.europa.eu/eli/dir/2015/996/oj>.
- [8] W.H. Dalmeijer. Gebruiksprognose 2020 (Dutch). Technical report, Amsterdam Airport Schiphol, 9 2019.
- [9] Luc Dekoninck, Timothy van Renterghem, and Dick Botteldooren. Noise Contours around Brussels Airport for the Year 2017. Technical report, Ghent University, Department of Information Technology (INTEC) – WAVES Research Group, 4 2018.
- [10] EMS Brüel & Kjær. Airport Noise Monitoring and Management – ANOMS. <https://www.emsbk.com/anoms/>, 2019. [Online; accessed 28-October-2019].
- [11] Eurocontrol. User Manual for the Base of Aircraft Data (BADA) - Revision 3.6, 7 2004.
- [12] Eurocontrol. Aircraft Noise and Performance (ANP) Database. <https://www.aircraftnoisemodel.org>, 2018. [Online; accessed 01-October-2018].
- [13] European Civil Aviation Conference (ECAC). *Doc 29: Report on Standard Method of Computing Noise Contours around Civil Airports*, fourth edition, 12 2016. URL <https://www.ecac-ceac.org/ecac-docs>.
- [14] Andy Field and Graham Hole. *How to design and report experiments*. Sage, 2002.
- [15] Antonio Filippone. Aircraft noise prediction. *Progress in Aerospace Sciences*, 68:27–63, July 2014. ISSN 03760421. doi: 10.1016/j.paerosci.2014.02.001. URL <http://linkinghub.elsevier.com/retrieve/pii/S0376042114000311>.

- [16] Antonio Filippone, Lothar Bertsch, and Michael Pott-Pollenske. Validation strategies for comprehensive aircraft noise prediction methods. In *12th AIAA Aviation Technology, Integration, and Operations (ATIO) Conference and 14th AIAA/ISSMO Multidisciplinary Analysis and Optimization Conference*, Indianapolis, Indiana, September 2012. American Institute of Aeronautics and Astronautics. ISBN 9781600869303. doi: 10.2514/6.2012-5411. URL <http://arc.aiaa.org/doi/10.2514/6.2012-5411>.
- [17] Google. Google Maps. <https://www.google.com/maps>, 2019. [Online; accessed 28-October-2019].
- [18] S.J. Hebli. Toepassing ECAC Doc29 voor het bepalen van de geluidbelasting van het vliegverkeer van Schiphol - Methode zoals gevolgd bij de MER NNHS Schiphol (Dutch). Technical Report NLR-CR-2017-305, Netherlands Aerospace Centre (NLR), 2 2019.
- [19] Davey Hooijmeijer. Dutch aircraft noise model: Classification comparison with measurements. Master's thesis, Delft University of Technology, 7 2019. URL <http://resolver.tudelft.nl/uuid:8e5e3406-e2e5-4909-93a8-1998808746d4>.
- [20] International Civil Aviation Organization (ICAO). *Doc 9871: Technical Provisions for Mode S Services and Extended Squitter*, second edition, 2012.
- [21] International Civil Aviation Organization (ICAO). *Doc 9911: Recommended Method for Computing Noise Contours around Airports*, second edition, 2018.
- [22] International Organization for Standardization (ISO). *ISO/IEC Guide 98-3:2008: Uncertainty of measurement—Part 3: Guide to the expression of uncertainty in measurement (GUM: 1995)*, first edition, 2008.
- [23] International Organization for Standardization (ISO). *IEC 61672-1: Electroacoustics - Sound level meters - Part 1: Specifications*, second edition, 2013.
- [24] Michael C Lau, Christopher J Roof, Gregg G Fleming, Amanda S Rapoza, Eric R Boeker, David A McCurdy, and Kevin P Shepherd. Behind start of take-off roll aircraft sound level directivity study-revision 1. Technical report, United States Department of Transportation, 2015.
- [25] Roberto Merino-Martínez, Sander J Hebli, Dick HT Bergmans, Mirjam Snellen, and Dick G Simons. Improving aircraft noise predictions considering fan rotational speed. *Journal of Aircraft*, 56(1):284–294, 2018.
- [26] Roberto Merino-Martínez, Mirjam Snellen, and Dick G. Simons. Functional Beamforming Applied to Imaging of Flyover Noise on Landing Aircraft. *Journal of Aircraft*, 53(6):1830–1843, November 2016. ISSN 0021-8669, 1533-3868. doi: 10.2514/1.C033691. URL <http://arc.aiaa.org/doi/10.2514/1.C033691>.
- [27] Omgevingsraad Schiphol (ORS). Dashboard Internetconsultatie - Omgevingsraad Schiphol. <https://www.omgevingsraadschiphol.nl/consultatie/7023-2/>, 2018. [Online; accessed 18-November-2019].
- [28] Viktor R. Op de Woert. Improving aircraft noise modelling with radar-based flight profiles. Unpublished article from an Aerospace Engineering master student at Delft University of Technology, 2013.
- [29] Manon Raimbault and Danièle Dubois. Urban soundscapes: Experiences and knowledge. *Cities*, 22(5): 339 – 350, 2005. ISSN 0264-2751. doi: <https://doi.org/10.1016/j.cities.2005.05.003>. URL <http://www.sciencedirect.com/science/article/pii/S0264275105000557>.
- [30] Darren Rhodes and Eric R Boeker. Recommended Method for Computing Noise Contours Around Airports - Recent Updates to ICAO Doc 9911. *ICAO Environmental Report 2019*, pages 62–65, 2019.
- [31] SAE. *AIR1845: Procedure for the Calculation of Airplane Noise in the Vicinity of Airports*, 9 1995. URL <https://doi.org/10.4271/AIR1845>.
- [32] SAE. *ARP866B: Standard Values of Atmospheric Absorption as a Function of Temperature and Humidity*, 12 2012. URL <https://doi.org/10.4271/ARP866B>.
- [33] SAE. *ARP5534: Application of Pure-Tone Atmospheric Absorption Losses to One-Third Octave-Band Data*, 8 2013. URL <https://doi.org/10.4271/ARP5534>.

- [34] SAE. *AIR5662: Method for Predicting Lateral Attenuation of Airplane Noise*, 10 2019. URL <https://doi.org/10.4271/AIR5662>.
- [35] Abhishek K. Sahai, Mirjam Snellen, and Dick G. Simons. Objective quantification of perceived differences between measured and synthesized aircraft sounds. *Aerospace Science and Technology*, 72: 25 – 35, 2018. ISSN 1270-9638. doi: <https://doi.org/10.1016/j.ast.2017.10.035>. URL <http://www.sciencedirect.com/science/article/pii/S1270963816313773>.
- [36] Deniz Sari, Nesimi Ozkurt, Ali Akdag, Murat Kutukoglu, and Aliye Gurarslan. Measuring the levels of noise at the İstanbul Atatürk Airport and comparisons with model simulations. *Science of The Total Environment*, 482-483:472-479, June 2014. ISSN 00489697. doi: 10.1016/j.scitotenv.2013.07.091. URL <http://linkinghub.elsevier.com/retrieve/pii/S0048969713008735>.
- [37] Schiphol Nederland B.V. Over NOMOS. <http://noiselab.casper.aero/ams>, 2018. [Online; accessed 22-August-2018].
- [38] FH Schreutelkamp and GL Strang van Hees. Benaderingsformules voor de transformatie tussen rd-en wgs84-kaartcoördinaten. *NGT Geodesia, februari*, pages 64-69, 2001.
- [39] Beat Schäffer, Stefan Plüss, and Georg Thomann. Estimating the model-specific uncertainty of aircraft noise calculations. *Applied Acoustics*, 84:58-72, October 2014. ISSN 0003682X. doi: 10.1016/j.apacoust.2014.01.009. URL <http://linkinghub.elsevier.com/retrieve/pii/S0003682X14000280>.
- [40] Junzi Sun, Joost Ellerbroek, and Jacco M. Hoekstra. Aircraft initial mass estimation using bayesian inference method. *Transportation Research Part C: Emerging Technologies*, 90:59 – 73, 2018. ISSN 0968-090X. doi: <https://doi.org/10.1016/j.trc.2018.02.022>. URL <http://www.sciencedirect.com/science/article/pii/S0968090X18302626>.
- [41] H.W. Veerbeek and D.H.T. Bergmans. Verification of Heathrow Noise and Track Keeping Systems. Technical Report NLR-CR-2016-089, NLR, 7 2016.